الجمهورية الجزائرية الديمقراطية الشعبية
République Algérienne Démocratique et Populaire
وزارة التعليم العالي و البحث العلمي
Ministère de l'Enseignement Supérieur et de la Recherche Scientifique

المدرسة الوطنية المتعددة التقنيات
Ecole Nationale Polytechnique

Ecole Nationale Polytechnique

Département Génie Civil

Laboratoire de Génie Sismique et Dynamique des Structures

LGSDS

End-of-study project dissertation

for obtaining the State Engineer's degree in Civil Engineering

3D digitization of existing structure from a photogrammetric surveys in BIM environment for structural assessment

Realized by :
Mr. Abdelmalek HIGOUN
Mr. Mohamed Amine AMAMRA

Supervised by :
Mr. Nouredine BOURAHLA

Publicly presented and defended on the 6 th of July, 2023.

Jury members:

President	Mr. Abdelkrim BOURZAM	Pr	ENP
Supervisor	Mr. Nouredine BOURAHLA	Pr	ENP
Examiner	Mr. Abdelmadjid TADJADIT	MCB	ENP

ENP 2023

الجمهورية الجزائرية الديمقراطية الشعبية
République Algérienne Démocratique et Populaire
وزارة التعليم العالي و البحث العلمي
Ministère de l'Enseignement Supérieur et de la Recherche Scientifique

المدرسة الوطنية المتعددة التقنيات
Ecole Nationale Polytechnique

Ecole Nationale Polytechnique

Département Génie Civil

Laboratoire de Génie Sismique et Dynamique des Structures

LGSDS

End-of-study project dissertation

for obtaining the State Engineer's degree in Civil Engineering

3D digitization of existing structure from a photogrammetric surveys in BIM environment for structural assessment

Realized by :
Mr. Abdelmalek HIGOUN
Mr. Mohamed Amine AMAMRA

Supervised by :
Mr. Nouredine BOURAHLA

Publicly presented and defended on the 6 th of July, 2023.

Jury members:

President	Mr. Abdelkrim BOURZAM	Pr	ENP
Supervisor	Mr. Nouredine BOURAHLA	Pr	ENP
Examiner	Mr. Abdelmadjid TADJADIT	MCB	ENP

ENP 2023

الجمهورية الجزائرية الديمقراطية الشعبية
République Algérienne Démocratique et Populaire
وزارة التعليم العالي و البحث العلمي
Ministère de l'Enseignement Supérieur et de la Recherche Scientifique

المدرسة الوطنية المتعددة التقنيات
Ecole Nationale Polytechnique

Ecole Nationale Polytechnique

Département Génie Civil

Laboratoire de Génie Sismique et Dynamique des Structures

LGSDS

Mémoire de projet de fin d'étude

Pour l'obtention du diplôme d'Ingénieur d'État en Génie Civil

Numérisation 3D d'un ouvrage existant à partir d'un relevé photogrammétrique dans un environnement BIM en vue d'une expertise de structure

Réalisé par :
M. Abdelmalek HIGOUN
M. Mohamed Amine AMAMRA

Encadré par :
M. Nouredine BOURAHLA

Présenté publiquement et défendu le 6 juillet 2023.

Membres du jury :

Président	M. Abdelkrim BOURZAM	Pr	ENP
Promoteur	M. Nouredine BOURAHLA	Pr	ENP
Examinateur	M. Abdelmadjid TADJADIT	MCB	ENP

ENP 2023

Dedications

“

I dedicate this work to

My parents, may Allah protect them, who have always done everything for my success and education.

My beloved siblings, and all my family who has always supported me in my studies.

All my friends and colleagues

My partner ***Abdelmalek****, and to all those who contributed directly or indirectly to make this project possible.*

Thank you very much

”

- Amine

“

I dedicate this work to

My parents, who have been my primary source of support after Allah. Their unwavering efforts in raising, guiding, and assisting me have paved the way for my achievements.

My beloved sister and brothers, who have also provided me with support, celebrated my accomplishments, and offered moral backing.

My friends, words alone cannot express my gratitude to each and every one of them. However, I would like to acknowledge a few individuals here to convey my deep thanks and love. I am particularly grateful to my close friends ***Islam Haouas***, ***Ramzi Kecir***, ***Moussa Kaced***, ***Mohamed***, *my Sheikh* ***Ayman Hamidi*** *and the VIC president* ***Issam Gherib***. *May they all be blessed and protected by Allah.*

I would like to express special appreciation to ***Abdelmalek Atchi***, *without whom this project would not have been executed flawlessly.*

My great partner, ***Mohamed Amine***, *your collaboration has been invaluable.*

Lastly, I extend my sincere thanks to all those who have directly or indirectly contributed to the realization of this project.

Thank you sincerely to everyone.

”

- Abdelmalek

Acknowledgements

First and foremost, we thank Almighty Allah for giving us the strength and patience to complete this work.

We would like to express our special gratitude to our supervisor, Mr. Nouredine BOURAHLA, who placed his trust in us and provided unwavering support and guidance throughout our education and the completion of this thesis. We are grateful for his competent assistance, patience, and encouragement. His critical eye has been invaluable in structuring the work and improving the quality of its various sections. We extend our sincerest thanks to you, Mr. Nouredine BOURAHLA.

We also want to extend our sincere thanks to the jury members for taking the time to read and evaluate our work. Your recognition is truly an honor to us.

We would also like to express our appreciation to the educational and administrative team at ENP, particularly the civil engineering teachers, for their dedication in providing us with an excellent education.

Furthermore, we would like to express our deepest gratitude to our parents for their support and encouragement throughout these years of education. We send them all our love and gratitude.

Lastly, we want to acknowledge and thank everyone who has directly or indirectly contributed to the completion of this work.

ملخص

نظرا للتقدم التكنولوجي السريع ، اكتسبت تقنية التصوير القياسي مزيدًا من الاعتراف كتقنية متعددة الاستخدامات وفعالة من حيث التكلفة للحصول على نماذج ثلاثية الأبعاد رقمية من صور ثنائية الأبعاد.يمكن العثور على تطبيقاته في مختلف المجالات ، لا سيما في قطاعات البناء والهندسة المدنية ، خاصة مع الاستخدام الواسع النطاق لنمذجة معلومات البناء (BIM) التي سهلت العديد من التطبيقات في هذا المجال.

وتماشيا مع ذلك ، تهدف هذه الدراسة إلى توضيح مفهوم التصوير القياسي، وأساسياته ، واستخداماته ، وتحديد فوائده وتحدياته الرئيسية. في هذا السياق، قمنا باختيار تقييم دقة وصحة طريقتنا من خلال تطبيقها على عنصر مخبري بسيط، واستخراج فوائدها وقيودها استنادًا إلى اختبارات تشمل استخراج الاهتزازات الطبيعية باستخدام اختبار الاهتزازات المحيطة واختبار الانثناء بأربع نقاط لتحديد سلوك العنصر تحت تأثير القوى المطبقة.

بناءً على النتائج المستخلصة من العنصر المخبري، نعتزم استخدام طريقة التصوير القياسي عن طريق دمجها مع نتائج اختبار الاهتزازات المحيطة لتحديد خصائص المواد المستخدمة في المعالم الرومانية الموجودة في تيبازة بسبب تنوعها وتعقيد أشكالها. نهدف إلى معايرة خصائص المواد في النموذج الثلاثي الأبعاد الرقمي باستخدام خوارزمية جينية لتحقيق تشابه نسبي جيد بين الاهتزازات الطبيعية للمحاكاة والاهتزازات الحقيقية.

كلمات مفتاحية :

التصوير القياسي، نمذجة معلومات البناء (BIM) ، طريقة، عنصر مخبري، اختبار الاهتزازات المحيطة، خصائص المواد، الخوارزمية الجينية.

Résumé

En raison des avancées technologiques rapides, la photogrammétrie a gagné une reconnaissance croissante en tant que technique polyvalente et rentable pour obtenir des modèles tridimensionnels numériques à partir d'images bidimensionnelles. Ses applications peuvent être trouvées dans divers domaines, notamment dans les secteurs de la construction et du génie civil, en particulier grâce à l'utilisation généralisée de Building Information Modeling (BIM) qui a facilité de nombreuses applications dans ce domaine.

Dans le cadre de cette étude, nous visons à élucider le concept de photogrammétrie, ses fondamentaux, ses utilisations, et à identifier ses principaux avantages et défis. Nous nous concentrons spécifiquement sur le développement d'une procédure adaptée, fiable et efficace pour convertir des images en modèles tridimensionnels numériques afin de les utiliser dans l'évaluation des structures. Dans ce contexte, nous avons choisi d'évaluer l'exactitude et la validité de notre méthode en l'appliquant à un spécimen de laboratoire géométriquement simple, en extrayant leurs avantages et limitations basés sur des tests impliquant l'extraction des vibrations naturelles à l'aide du test de vibration ambiante et d'un test de flexion à quatre points pour déterminer le comportement de l'élément sous l'effet des forces appliquées.

Sur la base des résultats obtenus à partir du spécimen de laboratoire, nous avons l'intention d'employer la méthode de la photogrammetrie en combinant les résultats du test de vibration ambiante pour déterminer les propriétés des matériaux utilisés dans les monuments romains situés à Tipaza en raison de leur diversité et de leurs formes complexes. Nous visons à calibrer les propriétés des matériaux dans le modèle tridimensionnel numérique en utilisant un algorithme génétique pour atteindre une bonne similarité relative entre les vibrations naturelles simulées et les vibrations réelles.

Mots clés : Photogrammétrie, Building Information Modeling (BIM), Procédure, Spécimen de laboratoire, Test de vibration ambiante, Propriétés des matériaux, Algorithme génétique.

Abstract

Due to rapid technological advancements, photogrammetry has gained increasing recognition as a versatile and cost-effective technique for obtaining numerical three-dimensional models from two-dimensional images. Its applications can be found in various fields, particularly in the construction and civil engineering sectors, especially with the widespread use of Building Information Modeling (BIM) that have facilitated numerous applications in this field.

In line with this, The present study aims to elucidate the concept of photogrammetry, its fundamentals, uses, and identify its key benefits and challenges. We specifically focus on developing a suitable, reliable, and effective procedure for converting images into numerical three-dimensional models to be utilized in the evaluation and assessment of structures. In this context, we have chosen to evaluate the accuracy and validity of our method by applying it to geometrically simple laboratory specimen, extracting their benefits and limitations based on tests involving the extraction of natural vibrations using ambient vibration test and a four-point bending test to determine the behavior of the element under applied forces.

Based on the results obtained from the laboratory specimen, we intend to employ the photogrammtery method by combining it with ambient vibration test results to determine the material properties used in the Roman landmarks located in Tipaza due to their diversity and complex shapes. We aim to calibrate the material properties in the numerical three-dimensional model using a genetic algorithm to achieve a good relative similarity between the simulated natural vibrations and the actual ones.

Keywords : Photogrammetry, Building Information Modeling (BIM), Procedure, Laboratory specimen, Ambient vibration test, Material properties, Genetic algorithm.

Contents

List of Figures

List of Tables

General Introduction

This study has been conducted as part of a final year project proposed by the Earthquake Engineering and Structural Dynamics Laboratory (LGSDS) at the Civil Engineering Department. It focuses on the 3D digitization of an existing structure through a photogrammetric survey, utilizing a point cloud, within a Building Information Modeling (BIM) environment for structural expertise purposes.

Motivation and Scope

Advancements in photogrammetry technology have made it a versatile and cost-effective technique applicable to various domains. Its non-invasive nature, portability, and affordability make it an attractive choice for capturing detailed three-dimensional information. This study aims to explore the potential of photogrammetry within the construction industry, specifically in the context of structural assessment. By leveraging the capabilities of BIM, the study seeks to enhance the efficiency of design, construction, and preservation processes.

Objectives

The primary objective of this study is to develop a comprehensive procedure for utilizing photogrammetry to create accurate 3D models of existing structures within a BIM environment. The study focuses on the digitization process using photogrammetry techniques and subsequent utilization of the point cloud data for structural analysis and evaluation. Additionally, the study aims to assess the applicability of photogrammetry in laboratory conditions and its potential for historical monument preservation.

Outline of the dissertation

This report begins with a comprehensive introduction that provides an overview of the study, including its motivation, scope and objectives.

The first chapter presents a literature review on photogrammetry, covering its definition, principles, branches, and types. It explores the advancements of photogrammetry in the construction field and discusses its characteristics and limitations while proposing potential solutions. The chapter also discusses the relationship between photogrammetry and Building Information Modeling (BIM) and Historic Building Information Modeling (HBIM).

The second chapter outlines the photogrammetry process, explaining the steps involved in transforming image data into a simulation-ready 3D model. It covers image alignment, raw mesh generation, and mesh processing, and demonstrates the utilization of the 3D model in Finite Element Method (FEM) software. The chapter provides a detailed description of each processing step using a steel column as an illustrative example.

The third chapter explores the application of photogrammetry for analyzing lab specimens through two case studies conducted on RC beam specimens in a laboratory. The first case study focuses on modal analysis, while the second involves a four-point bending test. The objective is to assess the accuracy and usefulness of photogrammetry in generating precise 3D models for further investigations. The findings from these case studies are presented and analyzed, highlighting the strengths and limitations of photogrammetry in laboratory conditions.

The fourth chapter discusses the important application of photogrammetry in identifying material properties in existing structures, particularly historical monuments. It introduces a combined technique of photogrammetry and ambient vibration testing (AVT) to determine material properties, along with an optimization approach using artificial intelligence (AI) through genetic algorithms. The study specifically examines selected elements from the Tipaza historical site to validate the effectiveness of the photogrammetry procedure and optimization methodology.

The conclusion of the report summarizes the key findings and presents future research prospects that have emerged from the study.

Chapter 1

Photogrammetry and its applications

1.1 Introduction

Photogrammetry is gaining increasing recognition as a versatile and cost-effective technique that finds applications across various domains. Its portability, non-invasiveness, and affordability make it an attractive choice for capturing three-dimensional information [14]. In this chapter, we provide a comprehensive overview of photogrammetry, encompassing its definition, underlying principles, and the diverse branches and types it encompasses. Furthermore, we explore the recent advancements in photogrammetry technology, with a specific emphasis on its applications within the construction industry. We also acknowledge and thoroughly discuss the characteristics and limitations of photogrammetry, while proposing potential solutions. Additionally, we delve into the utilization of photogrammetry in Building Information Modeling (BIM) and Historic Building Information Modeling (HBIM), highlighting the significant benefits that arise from generating detailed 3D models of existing structures. This emphasis on efficiency enhancement in design, construction, management, and preservation.

1.2 Photogrammetry

1.2.1 Definition

Photogrammetry is the science of obtaining three-dimensional measurements of objects using photographs taken from different perspectives. The word "photogrammetry" is derived from three Greek words: photos (light), gramma (description), and metron (measurement). According to the American Society of Photogrammetry (ASP), the photogrammetry can be defined as **"the science, art, and techniques of obtaining reliable information about physical objects and the environment through a process of recording, measuring, and interpreting aerial and terrestrial photographs"** (American Society of Photogrammetry, 1980) [4].

The definition of photogrammetry has evolved significantly over time due to advances in science and technology, rendering the traditional definition inadequate. Nowadays, many researchers refer to photogrammetry as image-based reconstruction or modeling. This involves creating 3D models of an object from its 2D images, using various tools such as advanced software, high-resolution cameras, smartphones, and automated drones. Photogrammetry can be considered the opposite of photography, and it can be used to obtain an object's profiles, estimate its geometric properties, and monitor its changes over time, including its orientation, relative location, and geometry.

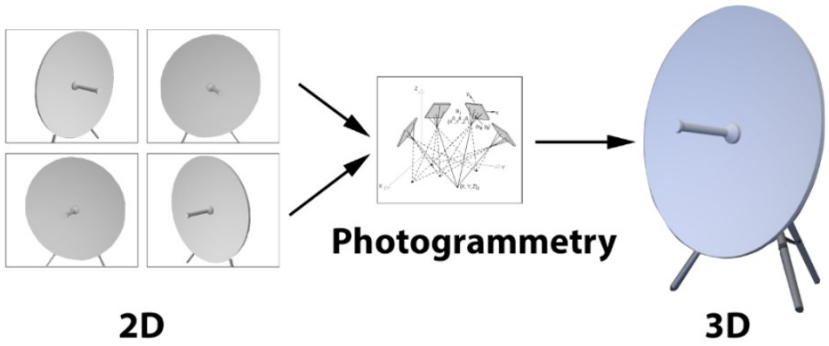

Figure 1.1: Photogrammetric process to convert 2D to digital 3D[19].

1.2.2 The concept

Photogrammetry is a technique that involves obtaining measurements from photographs. The method relies on trigonometry principles and involves taking overlapping pictures from various positions. These pictures establish different ”lines of sight” between the camera point and the object being studied. By triangulating the intersections of these lines, one can determine the 3D location of the object's points of interest [14].

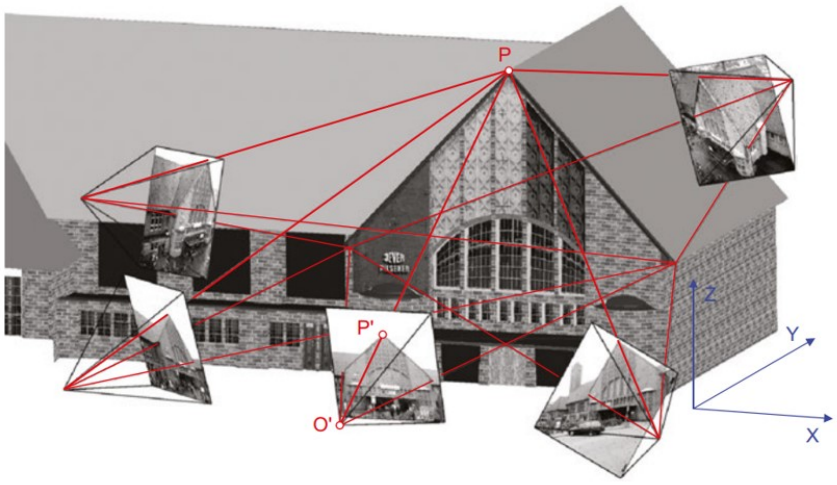

Figure 1.2: Principle of photogrammetric measurement [34].

Photogrammetry extracts geometric information from a two-dimensional image, akin to the two eyes of a human. To enhance precision, additional points of view are required, which can be equated to having more ”eyes”. In essence, the more pictures obtained of an object, the greater the accuracy achieved [36].

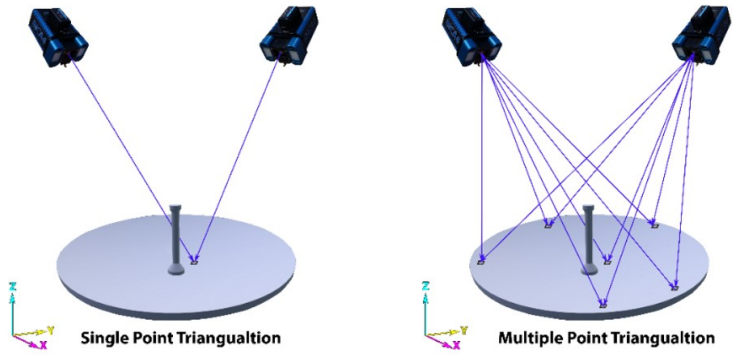

Figure 1.3: Single and multiple point triangulation[19].

Photogrammetric systems typically yield 3D coordinates of objects based on image measurements. This data can be used to obtain other characteristics like lines, distances, areas, and surface definitions, as well as quality information such as comparisons with design and machine control data. It's also possible to directly determine geometric elements like straight lines, planes, and cylinders without having to calculate point coordinates. The captured images themselves serve as objective documentation of the object's state during the time of capture, and they can be presented as corrected camera images, orthophotographs, or graphic overlays [34].

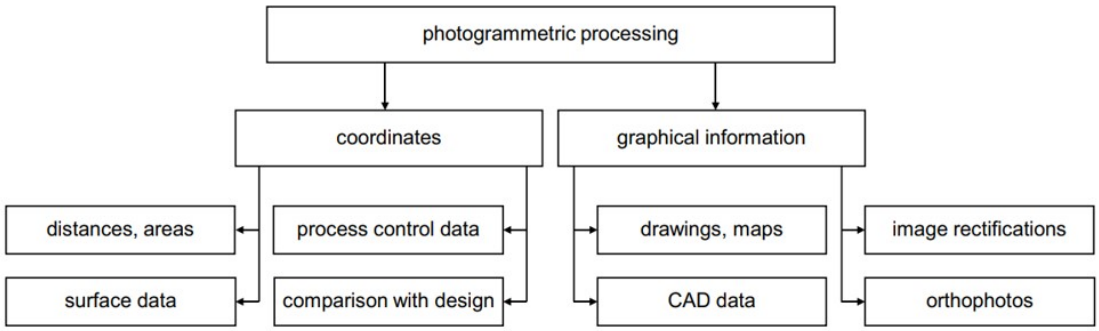

Figure 1.4: Typical photogrammetric products [34].

1.2.3 Branches of photogrammetry

Photogrammetry can be classified into two main branches [21]:

- **Metric Photogrammetry**

  It is used for precise measurements and calculations on photographs. It involves determining the size, shape, and position of photographic features and obtaining other information such as relative locations (coordinates) of features, areas, and volumes. These photographs are captured using a metric camera and are commonly used in engineering fields like surveying.

- **Interpretive Photogrammetry**

  It deals with recognizing and identifying photographic features on a photograph, such as shape, size, shadow, and pattern. This branch adds value and intelligence to the information seen on the photograph through annotation.

1.2.4 Types of photogrammetry

Photogrammetry is classified based on the properties of the object to be modeled, with the primary classification determined by whether the photographs are taken from the air or the ground [54]. Here are the three types of photogrammetry:

- **Aerial photogrammetry:** Aerial photogrammetry is a method used to generate two-dimensional (2D) or three-dimensional (3D) models using photographs taken from a high altitude, typically from an airplane. These images of the Earth are transformed into models by cartographers [3]. It involves taking photographs sequentially in the same flight path [32], with planes directed towards predetermined landmarks on a piece of land. The camera's speed is adjusted to match that of the aircraft, and the aircraft's altitude above the ground is measured [13]. These photographs are later processed using a stereo plotter to create topographic and thematic maps, as well as digital terrain models. They can also be used in automated processing [52].

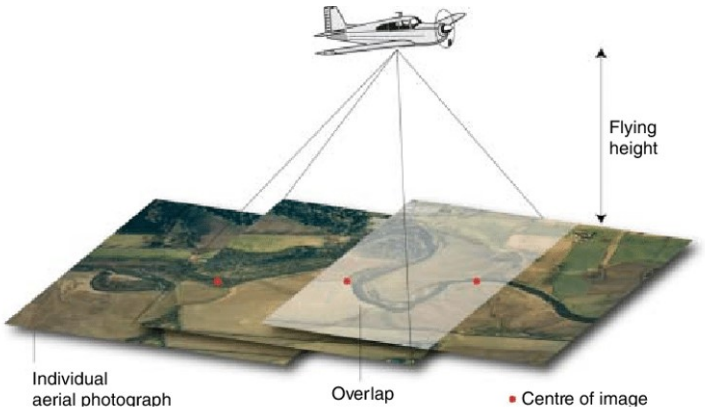

Figure 1.5: The principles of aerial photograph acquisition from an aircraft to allow subsequent photogrammetry and quantification of channel and floodplain topography [20].

- **Terrestrial photogrammetry:** Terrestrial photogrammetry refers to taking photos of objects from traditional tripods positioned on the ground. By capturing multiple overlapping photographs, it is possible to obtain stereoscopic measurements of objects in three dimensions [51]. This technique of photogrammetry demands comparatively lower investments and technical skills [22]. Terrestrial photogrammetry, also known as close-range photogrammetry, involves capturing images from a stationary position on the ground, either handheld or fixed, with the camera axis parallel to the Earth's surface. The camera's coordinates and other data are collected when the photo is taken, and theodolites are commonly used instruments

for this technique. Unlike aerial photogrammetry, terrestrial photogrammetry is non-topographic and not related to the physical arrangement of the area's features. Drawings, 3D models, and measurements are the output of terrestrial photogrammetry, which can be used for modeling buildings, engineering structures, stockpiles, and film sets [59].

Figure 1.6: Terrestrial photography [60].

- **Spatial photogrammetry:** Satellites are utilized to capture images in this photogrammetry discipline. The progress in satellite technology has facilitated the acquisition of high-quality data with high resolution and global coverage within a shorter timeframe [50].

1.3 History of photogrammetry

Throughout the evolution of photogrammetry, the advancement of the science and art has been made possible by the contributions of several professionals from diverse fields. These individuals include geodesists, physicists, surveyors, photographers, and software engineers who have played a crucial role in the development process of photogrammetry.

According to [57], Leonardo da Vinci's contribution to the field of photogrammetry is significant because he was among the pioneers to explain the concept of perspective, which is a crucial aspect in photogrammetry. He wrote about perspective in 1480: "Perspective is nothing else than the seeing of an object behind a sheet of glass, smooth and quite transparent, on the surface of which all the things may be marked that are behind this glass. All things transmit their images to the eye by pyramidal lines, and these pyramids are cut by the said glass. The nearer to the eye these are intersected, the smaller the image of their cause will appear" This idea laid the foundation for later developments in photogrammetry, which uses photographs (or digital imagery today) to measure and analyze objects from different perspectives. While Leonardo da Vinci did not directly contribute to the development of photogrammetry as we know it today, his work helped establish the basic principles that underlie this field.

Photogrammetry and photography both emerged in the mid-19th century [15], it has come a long way since then, progressing from analog to optical-mechanical to mathematical-

analytical methods, and ultimately to soft-copy photogrammetry or digital 3D models [57]. Konecny [29] identified various development cycles in the historical evolution of photogrammetry, each lasting about 50 years and marked by an earlier invention that enabled photogrammetry to move to the next phase. Kondratjew's economic theory was the basis for Konecny's development cycles [57].

The four development cycles of photogrammetry are as follows:

- The first cycle, called **Plane table photogrammetry (1850-1900)**, involved transferring directions from exposed photos onto map sheets oriented on a plane table. Notable figures during this period include Dominique François Jean Arago, who in 1837, was credited with the discovery of the principle of stereoscopic vision, and Carl Pulfrich, who in 1890, designed the first workable stereo-comparator. The individual credited with coining the term "Photogrammetry" is Dr. Albrecht Meydenbauer. He established the Royal Prussian Photogrammetric Institute and was its director until 1909. Dr. Meydenbauer gained recognition for conducting architectural surveys using photogrammetry techniques.
- The second cycle, called **Analog "Classical" Photogrammetry (1900-1960)**, utilized mechanical and/or optical methods to extract information from analog photographs, which were taken by film-based cameras. This cycle took advantage of aerial photography, made possible by the development of airplanes in 1903. Noteworthy figures during this period include C.W. Wright and F.E. Wright, who utilized a panoramic camera to capture ground photos during their Alaska survey in 1904. Additionally, Eduard Dolezal developed the first analytical plotter in 1936, making significant contributions to the field.
- The third cycle, called **Analytical Photogrammetry (1960-2000)**, utilized mathematical processes performed by computers to reconstruct camera positions. Prominent contributors during this period include Helmut Baerwald, who developed one of the earliest digital image processing systems for photogrammetry in 1968, and Franz Leberl, who created an automated system for aerial triangulation in 1976.
- The fourth cycle, called **Digital Photogrammetry (2000-Present)**, processes digital photographs using similar mathematical principles as analytical photogrammetry. Nowadays, digital photogrammetry utilizes advanced technologies and innovations, such as automated drones, high-resolution cameras, and smartphones, to reconstruct 3D models of objects accurately and with high quality.

Figure 1.7 demonstrates the primary inventions that caused a change in phase, which are further explained.

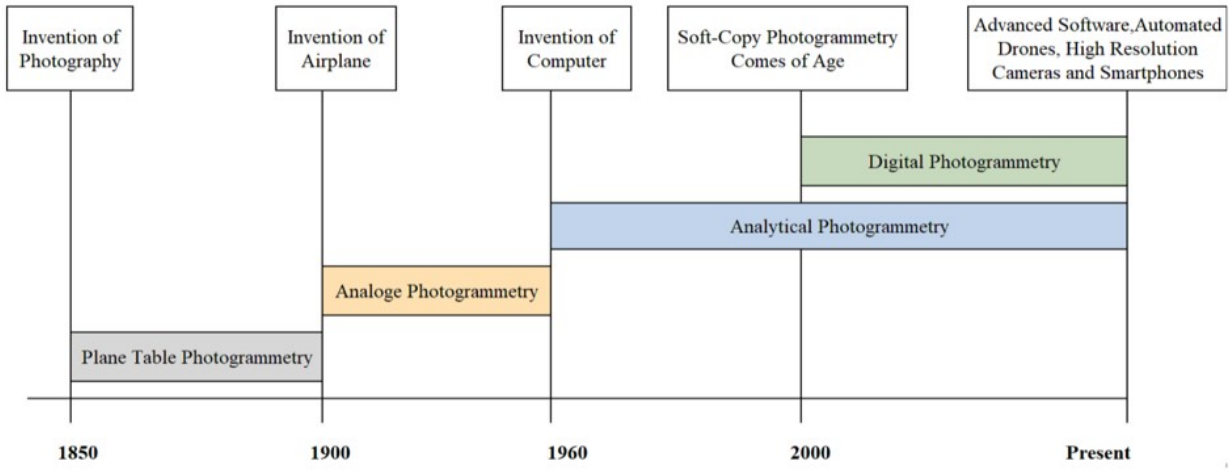

Figure 1.7: Photogrammetry development timeline [49].

Each cycle comes with a unique set of technological advancements that break down specific barriers. These barriers include expertise levels and the required means to produce a scene. The accuracy of the plot relies on various factors such as the precision of the rendering instrument, the quality of the image, stereoscopic acuity, the accuracy of georeferencing, image resolution, and the stereo configuration of the pair [2].

1.4 Current developments in photogrammetry

The significant progress in automatic digital image analysis has expanded the potential applications of photogrammetry and made it more accessible to a wider range of users who do not possess specialized knowledge in the field.

The advancements in 3D measurement technologies are being driven by trends such as Industry 4.0, building information modelling (BIM), and the digital transformation. High-end systems and low-cost sensors are both benefiting from this advancement. With the rise of new technical challenges such as unmanned aerial vehicles (UAV) and autonomous driving, innovative sensor systems are in demand, along with more extensive maps and environment models. To tackle these challenges, modern approaches like simultaneous localization and mapping (SLAM), visual odometry, and structure from motion (SfM) are now being combined with classical photogrammetric methods [33].

In recent years, there have been several exciting developments in photogrammetry that have improved its accuracy, efficiency, and versatility.

One major advancement is the use of new sensors, such as synthetic aperture radar (SAR), flash lasers, mobile Lidar, 3D and multispectral cameras, that can capture high-resolution data in various domains. Another development is the implementation of dense matching techniques that can generate high-density 3D point clouds from images, allowing for more detailed analysis of objects and environments [28].

Machine learning techniques have also been incorporated into photogrammetry, en-

abling automatic image orientation, surface reconstruction, scene analysis, change detection, classification, and information extraction. UAV photogrammetry has emerged as a new field, utilizing unmanned aerial vehicles as platforms for carrying sensors and performing automated flight missions [28].

Lastly, there has been significant progress in the development of photogrammetric image processing software that can handle large-scale data sets, support various sensor models, provide geometric and radiometric corrections, and offer user-friendly interfaces. All these advances in photogrammetry promise to open up new possibilities for research, planning, and decision-making across a wide range of industries and applications [33].

In the construction industry, photogrammetry has made significant advancements, with the use of UAVs to capture high-resolution aerial images of buildings, roads, bridges, and other structures for inspection, monitoring, planning, and documentation. Dense matching techniques are employed to create high-density 3D point clouds that can generate orthophotos, contour maps, and digital surface models. Photogrammetric data is combined with other sources such as GPS, laser scanning, and radar for creating precise 3D models used in design, analysis, simulation, and visualization. Photogrammetric software has been developed to handle extensive data sets, offer user-friendly interfaces, and provide geometric and radiometric corrections for efficient processing, editing, and exporting of photogrammetric products [25].

1.5 Application of photogrammetry in construction field

Photogrammetry is utilized across various scientific and technological domains. It finds applications in geodesy and cartography, aiding in construction and architecture by capturing images of significant historical sites. In the realms of astronomy and cosmonautics, photogrammetry is employed to ascertain the positions of celestial bodies and create planetary maps. Additionally, it plays a role in military engineering [55].

In construction, Photogrammetry plays a significant role in construction by serving various purposes [26]. The following are some essential applications [55]:

- **Deformation analysis and control:** It is utilized to accurately determine the deformations of engineering structures and ensure the precise installation of large-panel buildings.
- **Study of engineering structures:** Photogrammetry is employed to study the models of engineering structures. The photogrammetric method allows for the analysis of deformations occurring in the plane, while the stereo-photogrammetric method enables the examination of three-dimensional deformations.
- **Calculation of earthworks and route selection:** Photogrammetry facilitates the calculation of earthwork volumes and aids in selecting the most suitable road routes.

- **Land management and cadastral registration:** In the context of land management and cadastral registration, photogrammetry plays a crucial role in aerial surveying, topographic and geodesy measurements, and boundary surveying.
- **Visualization and spatial analysis:** Through the creation of digital 3D terrain models, orthophoto-maps, and relief models, photogrammetry enables comprehensive territory visualization and supports spatial analysis for various applications.
- **Architectural design and restoration:** It is utilized in architectural design, allowing for accurate measurements of structures, creation of projections, and the study of architectural monuments. It is particularly valuable in restoration efforts, encompassing the reconstruction of both visible and invisible parts of a structure using indirect signs.
- **Preservation of historical and cultural monuments:** Photogrammetry plays a vital role in the documentation, research, and preservation of historical and cultural monuments. It facilitates inventory management, enables the study of monument conditions (including deformations), restoration of drawings, and the establishment of archives. Additionally, it contributes to the promotion of national monuments through exhibitions and expositions.

1.6 Photogrammetry characteristics and limitations

Photogrammetry is a powerful technique that has transformed the way we capture and analyze the world around us, but like any technology, it has its characteristics and limitations.

1.6.1 Photogrammetry characteristics

These are some of the main characteristics of photogrammetry [1]:

- **3D scanning capabilities:** Photogrammetry serves as a valuable technique for 3D scanning, applicable to objects of varying sizes. It enables the capture of buildings and landscapes that would otherwise be difficult to scan. The software used in photogrammetry can automatically generate 3D models from images, providing a more convenient and affordable scanning method compared to other alternPhotogrammetry allows for the creation of accurate and permanent photographic records of specific locations or objects. These images possess metric properties, ensuring a highly precise and reliable record for various projects.
- **Ease, speed, and affordability:** Compared to traditional methods, photogrammetry offers a simpler, faster, and more cost-effective approach to obtaining measurements and other information. It requires minimal fieldwork, and the same photogrammetry images can be utilized for multiple analyses.
- **Access to challenging locations:** Aerial photogrammetry is particularly useful for surveying locations that are inaccessible or pose risks to personnel. By using

aerial platforms, photogrammetry allows for accurate data collection while minimizing potential hazards for surveying crews.

- **Reduced disruption:** Photogrammetry enables surveying and analysis of areas such as roads and cities with minimal disturbance. This means that much of the analysis can be conducted remotely from an office environment, reducing the need for extensive ground-based work.
- **Simplified analysis:** The coordinates of each point within the mapped area can be easily evaluated with minimal effort and cost. Photogrammetry produces full-color models and point clouds that are visually rich and straightforward to interpret. This makes it ideal for effectively presenting information to the public, government agencies, or organizations.

1.6.2 Photogrammetry limitation

Several limitations associated with the use of photogrammetry are discussed in [48][46]. These limitations include the following:

- **Light dependency:** Photogrammetric surveys require adequate light for accurate photography, and low light conditions can make it difficult to capture photographs effectively.
- **Visibility constraints:** Factors like rain, fog, or dense vegetation can obstruct the camera's line of sight or limit the amount of light available for clear photography. Poor weather conditions can also impact image quality.
- **Flight height and overlap:** The accuracy of measurements in photogrammetry heavily relies on the flight height. It is essential to have proper overlap between images to ensure adequate coverage and capture different perspectives.
- **Image pixel quality and matching algorithm:** High-quality image pixel resolution is necessary for precise photogrammetry results. The matching algorithm used for stereo image pairs can be challenging, requiring careful consideration.
- **Photography skills and observation environment:** Terrestrial photogrammetry requires skilled operators with photography expertise. Additionally, specific environmental conditions, such as illumination, rainfall, cloud cover, and fog, need to be taken into account.
- **3D-scan cleanup and scaling:** After creating a 3D model with photogrammetry, additional post-processing is often required to remove imperfections. Furthermore, photogrammetric models lack inherent scaling and require the use of a measuring stick in each scan for later adjustment.

Despite the challenges associated with photogrammetry, there are available solutions to overcome them. These solutions encompass the use of a suitable camera with high resolution and minimal distortion, adjustment of camera settings for clear image capture,

adoption of a tripod or stabilizer to ensure stable shots, establishment of a controlled environment with uniform lighting to mitigate shadow and glare problems, incorporation of markers or targets to improve the reconstruction of smooth surfaces, implementation of a scale bar or reference object for accurate scaling, and utilization of software to correct camera calibration and address other potential distortions [8].

1.7 Use of photogrammetry in BIM and HBIM

Over the last few decades, Building Information Modelling (BIM) has emerged as a highly important technology in the Architecture, Engineering, and Construction (AEC) industries. BIM is being increasingly used in various fields, including but not limited to transport infrastructure, 3D city modelling, economic systems, and the mechanical, electrical and plumbing (MEP) industries [47]. And because BIM is a comprehensive approach that involves the creation and management of information for a constructed asset by utilizing an intelligent model and a cloud-based platform [7], photogrammetry has the potential to produce precise 3D models of buildings and structures for use in BIM. Its integration with, can assist civil engineers in generating more precise and comprehensive models of structures and buildings that can serve various objectives, including design, construction, and maintenance [11].

Photogrammetry is a technique that utilizes cameras or drones to capture images for creating precise and intricate 3D models of buildings and structures in BIM and HBIM [61][35]. The use of photogrammetry enables the extraction of various types of information, such as geometric, semantic, material, and temporal data, about building components and their evolution over time [38]. Furthermore, photogrammetry facilitates the creation of parametric objects that can be seamlessly integrated into BIM and HBIM platforms [38][37].

BIM and HBIM are methodologies that incorporate 3D models augmented with data to facilitate the planning, building, supervision, and preservation of edifices. BIM is predominantly employed for contemporary constructions, whereas HBIM is utilized for historical or cultural landmarks that possess both material and non-material significance [37]. BIM and HBIM can benefit from photogrammetry in various ways, such as:

For **documentation**, it can be used to record the current conditions and attributes of the buildings, including their cultural and historical significance. As for **presentation**, photogrammetry enables the creation of realistic and immersive visualizations of the buildings, which can help to promote and convey their value and relevance. For **enhancement**, photogrammetry can be applied to enhance the functionality, accessibility, sustainability, and overall worth of the buildings. For **interpretation**, it can be utilized to study and comprehend the architectural and constructive features of the buildings, as well as their development and alterations throughout time [38][37]. In terms of **conservation**, it can aid in evaluating the state of the structures and the degree of deterioration, as well as in designing and overseeing restoration work. In the case of **maintenance**, it can be used to monitor and optimize the performance and operation of the buildings [61].

1.8 Conclusion

In conclusion, this chapter has provided a comprehensive overview of photogrammetry, including its principles, branches, and advancements. The limitations of the technique have been acknowledged and potential solutions discussed. The application of photogrammetry in Building Information Modeling (BIM) and Historic Building Information Modeling (HBIM) has demonstrated its capacity to enhance various industry aspects. The upcoming chapter will delve into the practicality and benefits of utilizing photogrammetry for creating scanned models in laboratory settings, further emphasizing its relevance in the field

Chapter 2

Photogrammetry procedure

(From images to simulation-ready 3D model of a Steel column Element)

2.1 Introduction

This chapter focuses on the photogrammetry procedure, from image data acquisition to building a simulation-ready 3D model. The process includes image alignment and raw mesh generation, mesh processing, and finally, model exploitation in FE software.

In the first part of the chapter, we discuss the importance of image data collection and its best practices to avoid errors after the fact. We then move on to the alignment of images, this process is followed by raw mesh generation, where the point cloud is converted into a mesh.

After discussing the initial steps, we delve into mesh processing, which involves refining and cleaning up the mesh to prepare it for FEM software. Finally, we discuss how the 3D model can be imported and used in FEM software to simulate physical behavior and analyze various properties such as stresses, deformations. A simple steel column element is chosen to illustrate the different steps of the procedure.

2.2 Image data collection

2.2.1 Photography

To generate a 3D model using photogrammetry, it is necessary to have a substantial collection of images that accurately depict the entire target object from a fixed distance and consistent angles to guarantee overlap. This set of images should cover the target object entirely. To capture as much detail as possible, this procedure can be repeated at multiple fixed distances to produce a dataset with more comprehensive coverage.

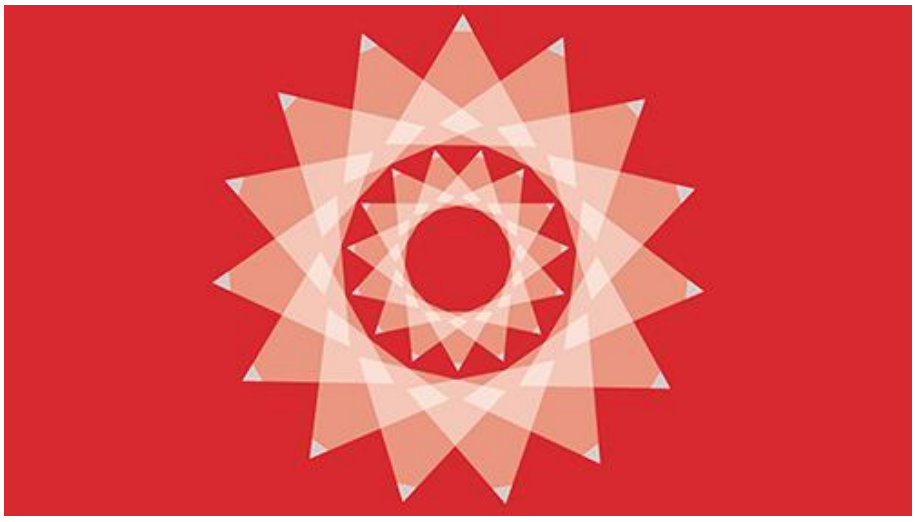

Figure 2.1: Photography technique for dataset capture [27].

2.2.2 Photogrammetry criteria

Photos used in photogrammetry must be taken in a specific way and must meet a certain set of criteria:

- **The number of photos:** which depend on the size, shape and the amount of details the target object has, and more images is always better than not enough, usually a set of 40 photos is a good starting point.
- **Photographs overlap:** photogrammetry software relies on points identified in multiple photos to construct models. Therefore, having overlapping photos is crucial for the software to identify and use these points accurately, photos taken in sequence should overlap by at least 60% [31].

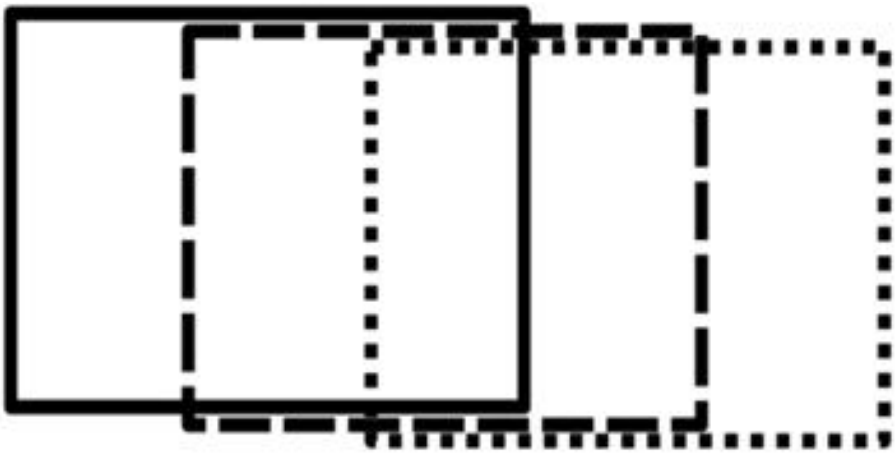

Figure 2.2: Overlapping consecutive images.

- **Multi-rotations capture:** multiple rotations or passes of taking photos around an object are necessary to acquire the best quality models, those rotations allow the software to interpret and include obscured parts of the object.

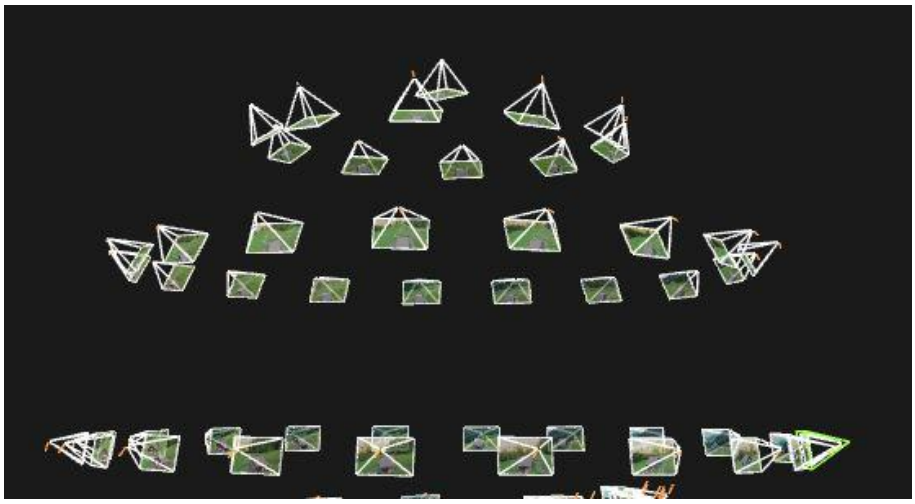

Figure 2.3: Three passes (levels) of rotations.

- **Adequate lighting:** Lighting is very essential when it comes to photogrammetry, too bright or too dark images might result in a bad model construction, shadows can also confuse the software as they are not static, to avoid that, lighting has to be consistent in the entire object and across all the dataset, that is why it is advised to pick an overcast day to shoot outdoors and use light diffusers indoors.
- **Capturing device:** Although the use of a professional DSLR camera is the best option for getting the most detail out of the object, and the user can adjust the amount of light permitted to the sensor using the aperture and ISO controls, the use of smartphone cameras is totally fine especially for relatively small objects, for this steel column structure we used both a smartphone as well as a Nikon D3200 DSLR camera.

Figure 2.4: A sample from the captured image dataset.

2.3 Model Generation

2.3.1 RealityCapture

RealityCapture is a fully featured photogrammetry software that automates the process of creating virtual reality scenes, textured 3D meshes, orthographic projections, and other visual representations from images and/or laser scans [17], and it was our software of choice for this step for its simple interface and straightforward workflow.

2.3.2 Image alignment

Image alignment in photogrammetry is the process of aligning multiple images of an object or scene in a common coordinate system. It involves identifying common features in the images and using mathematical algorithms to calculate the necessary geometric transformations. In our case we only used automatic alignment of images as our photo acquisition was mostly good, but manual intervention must be expected in case of poor data collection or the impossibility of redoing the photography. The alignment process creates only a sparse point cloud, which provides a rough representation of the object. The user can then reduce the area of calculation by using a bounding box to cover only the area of interest, thereby ignoring unnecessary parts.

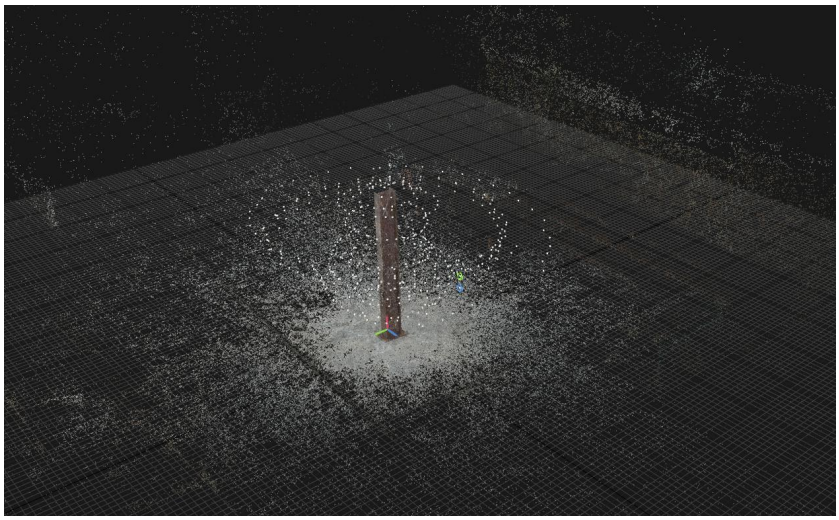

Figure 2.5: Sparse point cloud after alignment.

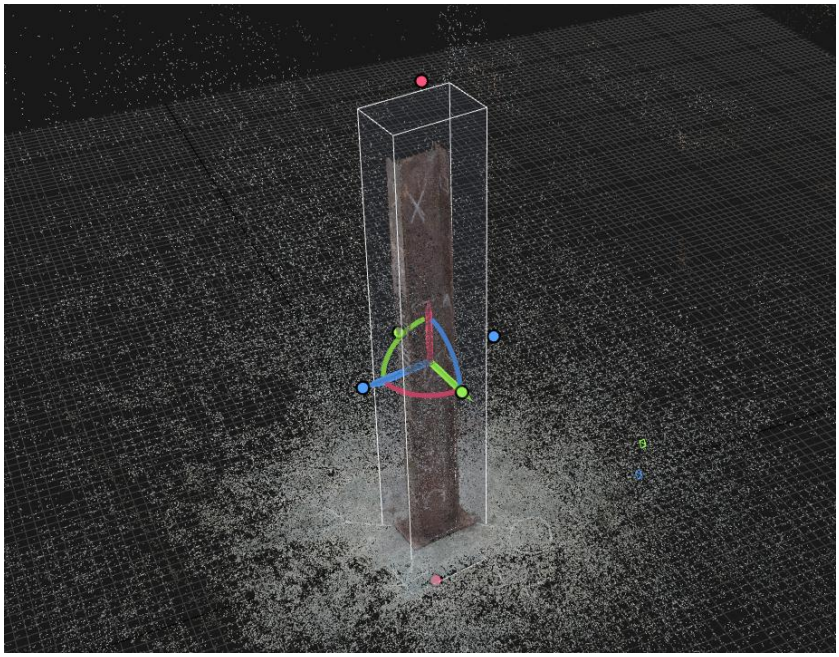

Figure 2.6: Bounding box adjustment.

2.3.3 Mesh generation

Moving to the mesh generation step, where after the alignment the algorithm creates a more dense point cloud under the hood which then uses to create the mesh of the model, after that the mesh can be exported as is or it can be decimated a little bit using the simplify tool to make the exported file smaller in size, RealityCapture support exporting to a lot of formats, we chose **.OBJ** as it is supported by Houdini, which is the software that will be used for meshing as described below.

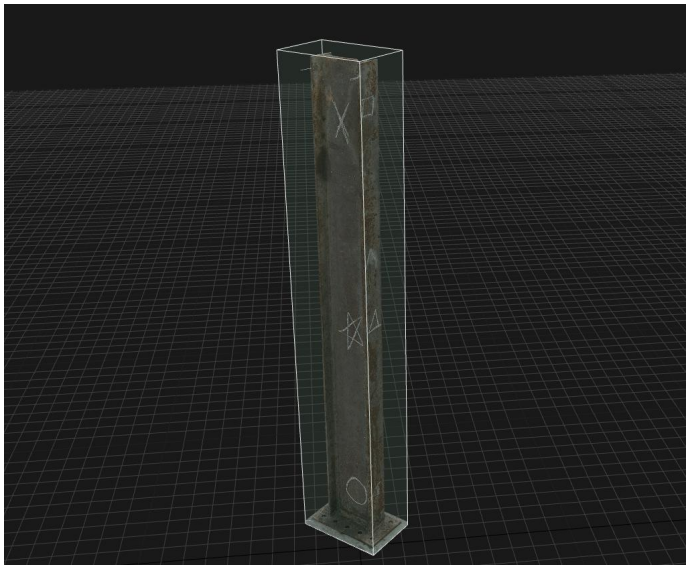

Figure 2.7: Dense point cloud.

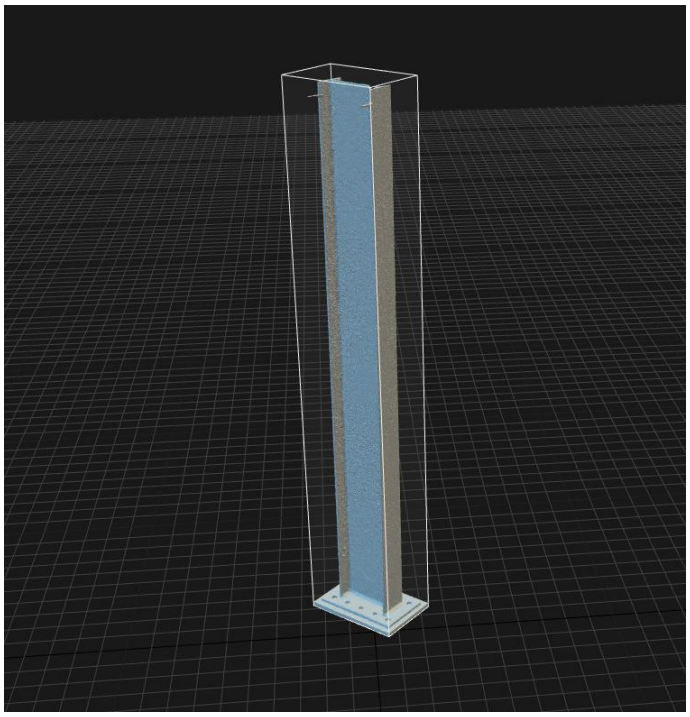

Figure 2.8: Finale RealityCapture Mesh.

2.4 Mesh Processing

2.4.1 Importing the model

After performing the model calculations and the mesh generation in RealityCapture, and exporting the model in the appropriate format, it is imported into Houdini. Houdini is a node-based 3D software that is widely used in Film and Video Game industries and is developed by Side Effects [53], It is a highly regarded software thanks to its procedural non-destructive workflow which makes it the perfect tool for doing a semi-automated mesh processing, and it also supports all the available formats whether it be importing from a 3d scanning/photogrammetry environment or exporting to simulation and analysis one, the **File** node is used to locate the model and importing it into the scene.

Figure 2.9: File node.

2.4.2 Model Decimation

The first step of processing the mesh would be decimating it into a reasonable and workable number of polygons as the exported one from RealityCapture is too heavy to render in the Houdini viewport and for that we use the PolyReduce node, which gives an option of the percentage of the polygons to keep with respect to the initial number, and anything below 600k polygons is a good middle-ground.

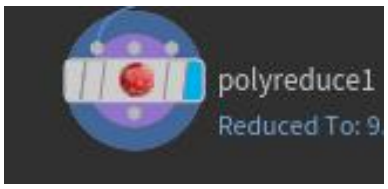

Figure 2.10: PolyReduce node.

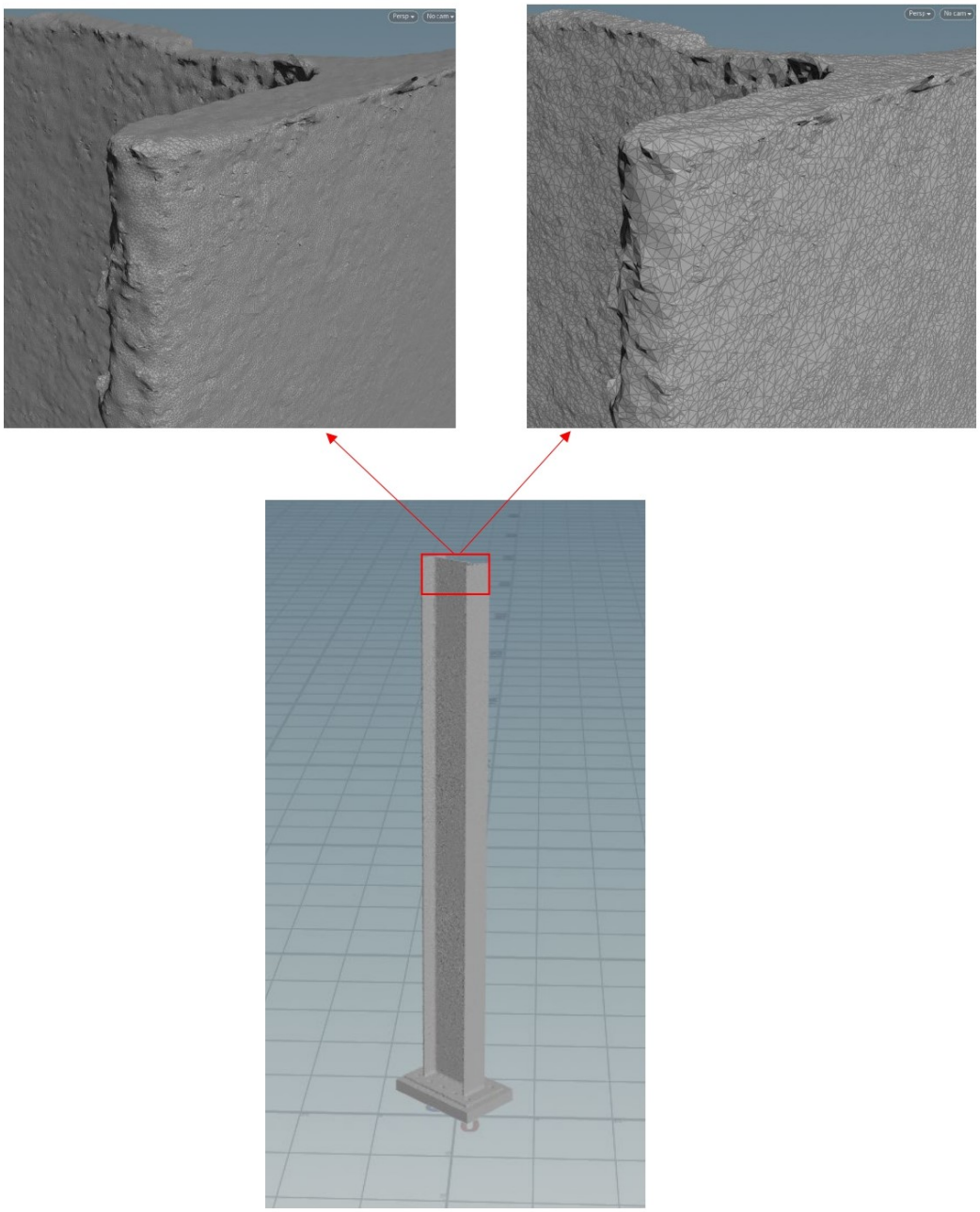

Figure 2.11: Model before (left) and after (right) Decimation.

2.4.3 Mesh Clean-up and smoothing

The process of photogrammetry can sometimes leave the generated mesh with a lot of imperfections that the real object didn't necessarily have and that is due to a lot of factors such as poor lighting or lack of some capturing angles, in addition to some attached unwanted objects such as supports or in our case the floor that needs to be removed.

2.4.3.1 Extra-polygons removal

To remove unwanted attachments there are many different techniques like the **Clip** or the **Boolean**, both tools let the user either cut the model using a bounding-box or subtracting another geometry like a sphere or a custom built object using Boolean operations, which are more suitable for relatively simple geometries like in our example, and for more complex geometries manual selection of the unwanted polygons is a must as it provides much more control over the removed mesh.

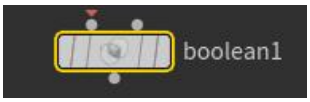

Figure 2.12: Boolean node.

Figure 2.13: Clip node.

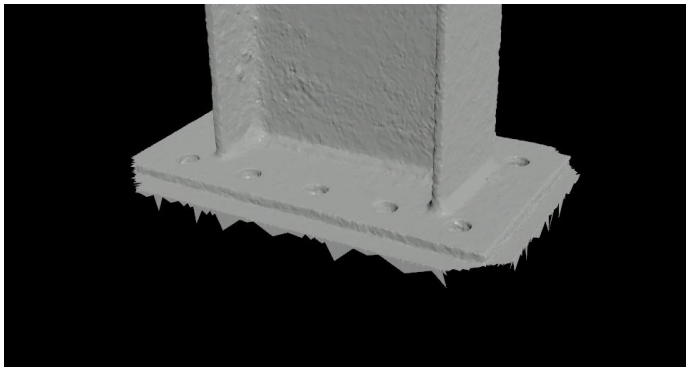

Figure 2.14: Model before clean-up.

2.4.3.2 Closing the model

Performing Boolean operations and cutting on the geometry leaves the model with some gaps and openings that need to be patched in order to create a water-tight* mesh, and to do that we used the **PolyFill** node which takes care of the majority of the gaps in the model.

Figure 2.15: PolyFill node.

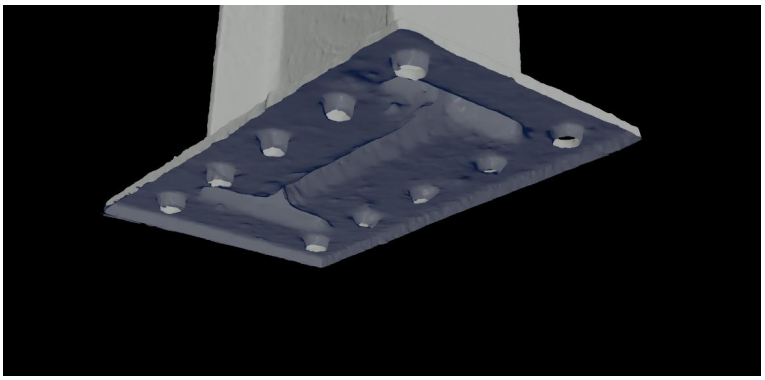

Figure 2.16: Open mesh.

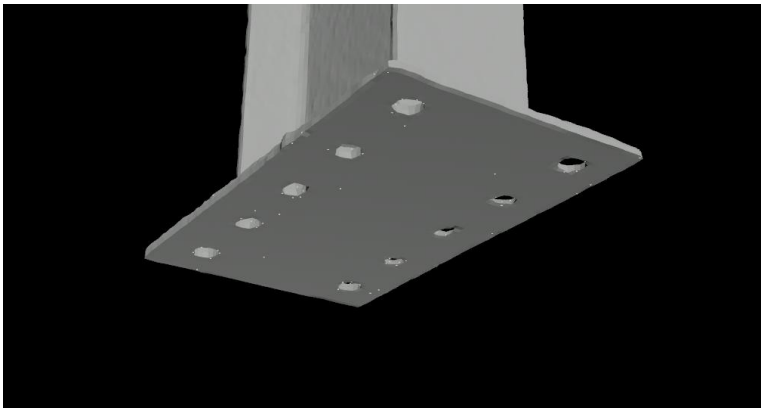

Figure 2.17: Water-tight mesh.

2.4.3.3 Mesh smoothing

Mesh smoothing in Houdini is very straightforward like any other software, but in order to remove the noisy areas that can cause calculation problems in FE software the smoothing value has to be increased substantially, but with a high value of smoothness the model will lose its convex and concave features as well as the right angles that were present in the real specimen, and to work around this problem, Houdini possesses a robust **Measure** tool that not only calculates volumes and areas but also the geometry curvature and outputs it as an attribute to be used in creating points or polygonal groups, which helped us create groups around the areas that have a high amount of convexity/concavity, so they can be excluded from the selection set in the **Smooth** node and in that way only the planar areas get extensively smoothed out leaving the specimen features untouched. After that a couple of re-meshing operations where applied to both give the model a uniform distribution of polygons as well as reducing the overall number of surface elements to something below 30k elements which can be easily imported by a simulation program.

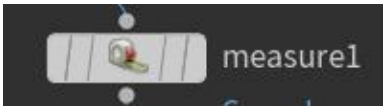

Figure 2.18: Measure node.

Figure 2.19: Smooth node.

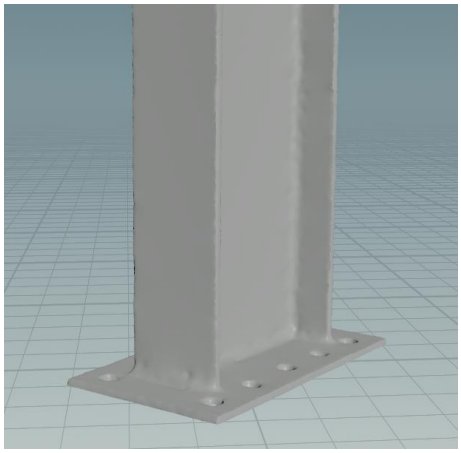

Figure 2.20: Smoothed mesh.

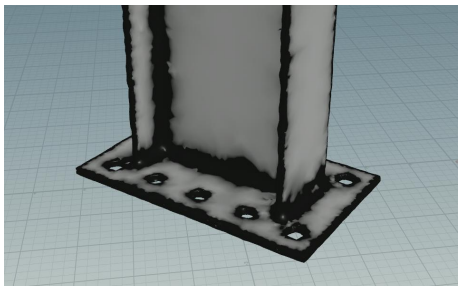

Figure 2.21: Curvature based grouping visualization.

2.4.4 Model calibration

Calibrating the model is a very important step as photogrammetry unlike 3d scanning doesn't provide any measurement data, but because all the dimensions are unchanged only one measurement from the specimen is required to calibrate the model, and to do that we measured the height of the specimen, and in Houdini we used the distance function that measures the distance between two points and from its output we either uniformly scale up or down the model until we roughly land on the desired measurement, and we can check that other dimensions of the specimen are kept approximately intact and most of the differences are due to the clean-up, axial calibration has to be taken care of as well as it is important down the line when we do the modal analysis, and for that the only thing we did was to use the orthographic view mode to try and get the planar surfaces of the model as parallel as possible to the 3 principle planes (xoy) (xoz) (yoz), It is worth mentioning that after every step of the cleanup and the smoothing the outputted models were compared with each other area and volume wise to ensure minimal change to the original model.

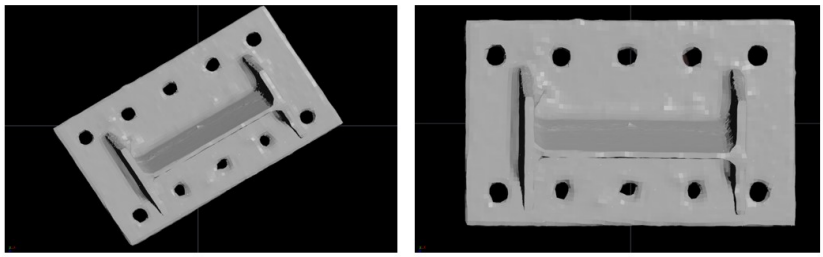

Figure 2.22: Model before (left) and after (right) axial calibration.

Figure 2.23: Model before (left) and after (right) scale calibration (Length of the bottom rectangular base).

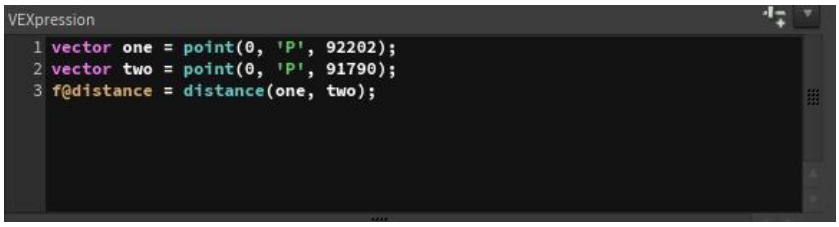

Figure 2.24: The distance function.

2.4.5 Model Export

The last step of the pre-processing phase is to export it to the FE software, and for that we used the Houdini **ROP Geometry Output** node which provides a variety of exporting options and formats, in our case we are only interested in two which are **.STL** and **.PLY**, both formats are compatible with the software we used in the analysis with PLY being favored as it occupies less disk space.

2.5 Constitution of the FE Model

2.5.1 COMSOL Software overview

COMSOL Multiphysics is a versatile numerical simulation software that uses the finite element method for analyzing and solving physics and engineering problems. It is especially useful for simulating coupled or multi-physics phenomena, offering user-friendly interfaces and the ability to model systems of partial differential equations (PDEs). COMSOL provides an integrated development environment (IDE) and unified workflow for various applications [40]. These features makes it a first choice in all the applications of the present work.

2.5.2 Model Import

As we stated before, the software is capable of importing both .STL and .PLY formats, so after creating a 3d component and choosing the solid mechanics physics type, we imported the model from the geometry section. Comsol automatically divides the object based on the elements normal to create planar surfaces, this under the hood operation makes it easier to apply forces and boundary conditions afterwards. It is worth noting that this type of import ignores the mesh coming from Houdini but it allows for geometry modifications such as boundary partitioning and further preprocessing. Alternatively the user can import and use the Houdini mesh for simulations at the expense of geometry modifications, and that can be done from the mesh section import.

2.5.3 Final simulation mesh

- **Surface Mesh**

  The need for some geometry modification in Comsol requires the ignorance of the mesh from Houdini. Therefore, a new surface mesh has to be created in the Mesh section of the component. The **Free Triangular** tool is used to create an adaptive triangular mesh with a non-uniform distribution. Then, the Adapt option is performed to obtain a uniform distribution. To avoid singularities, the size of the elements could be adjusted with a feedback window to control the number of elements that have been created.

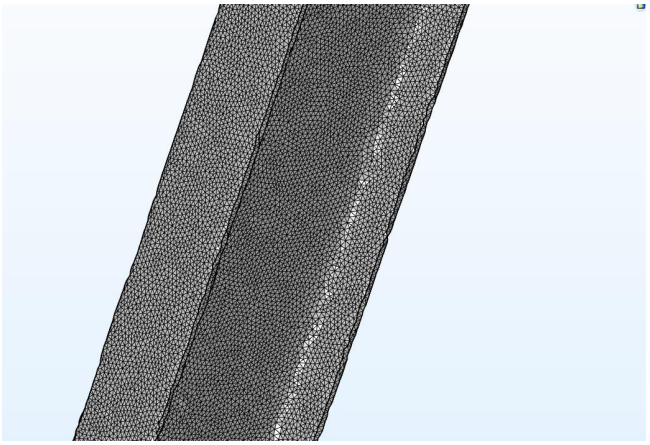

Figure 2.25: Surface mesh.

- **Volume Mesh**

  The volume mesh is then created based on the surface one with **Free Tetrahedral tool**. The mesh is composed of adjustable tetrahedral elements with a size node. The volume mesh can then be visualized with a mesh plot and an element filter to inspect it further.

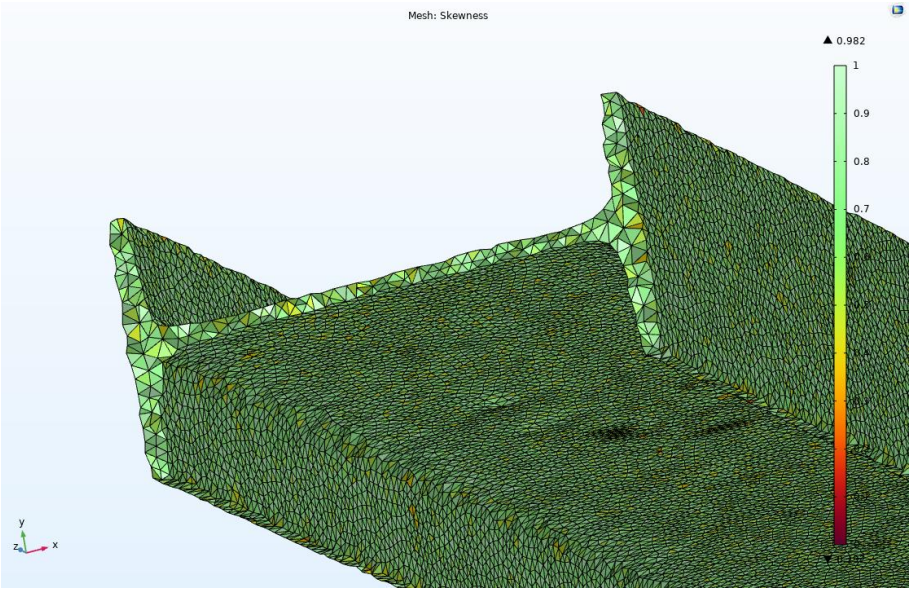

Figure 2.26: Volume tetrahedral mesh visualized using a mesh plot.

2.5.4 FE model analysis

At this phase the FE model is ready for further processing, such as imposing boundary conditions, material properties, loading assignment etc. For this model, we created a CAD replica of the specimen with the help of COMSOL modeling tools, the dimensions were as close as possible to the real ones, we chose the bottom face as a fixed constraint, for the material for both models we used the default COMSOL Structural Steel material as we wanted to study the geometrical effects on the specimen frequencies, for the analysis we ran an Eigen-frequency study to compare the first three modes of the two models.

For all the figures down below the results on the left belong to the CAD specimen, and the right ones belong to the digitized specimen.

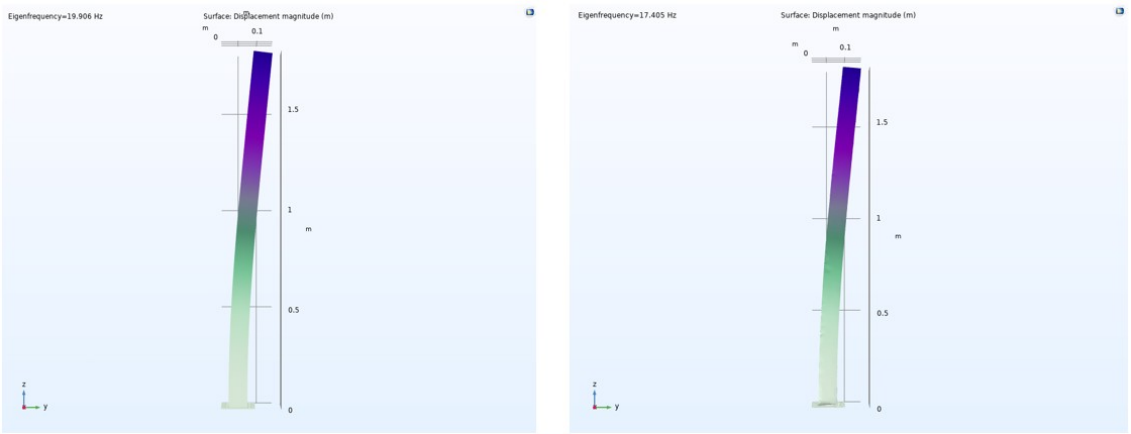

Figure 2.27: First mode scanned model (left) CAD model (right).

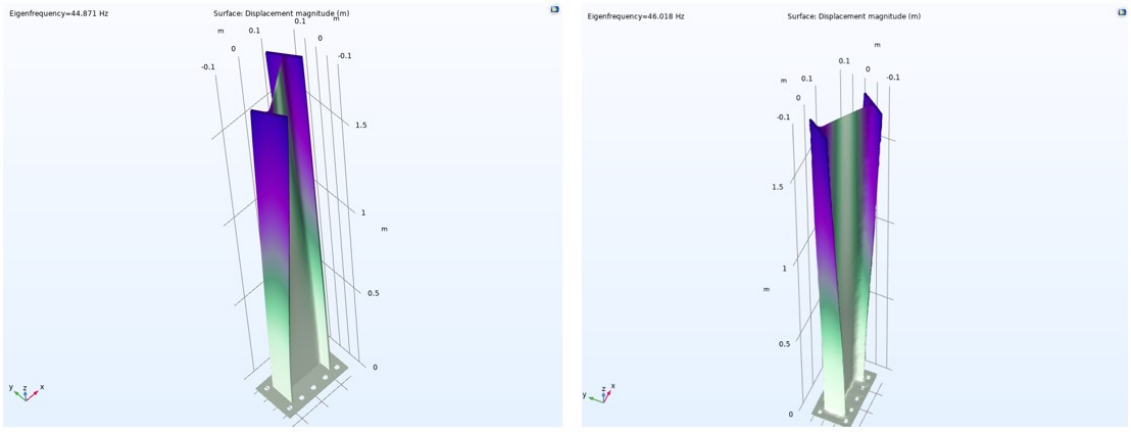

Figure 2.28: Second mode scanned model (left) CAD model (right).

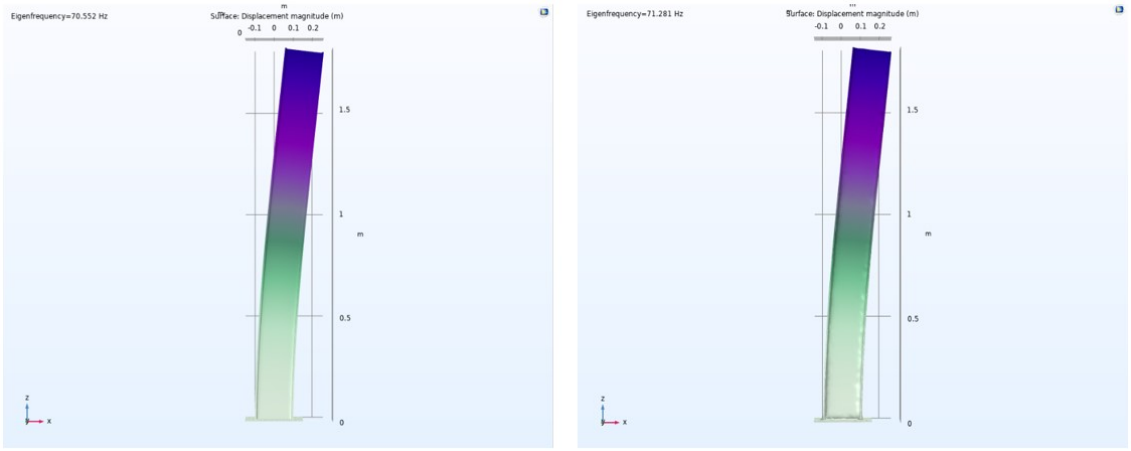

Figure 2.29: Third mode scanned model (left) CAD model (right).

Table 2.1: Comparison between frequencies of digitized specimen and CAD model

Mode	CAD Model (Hz)	Digitized Model (Hz)	Difference (%)
01	19.91	17.41	12.55
02	44.87	46.02	2.56
03	70.55	71.28	1.03

The discrepancies shown in the modal analysis can be attributed to the geometric and alignment differences in the models.

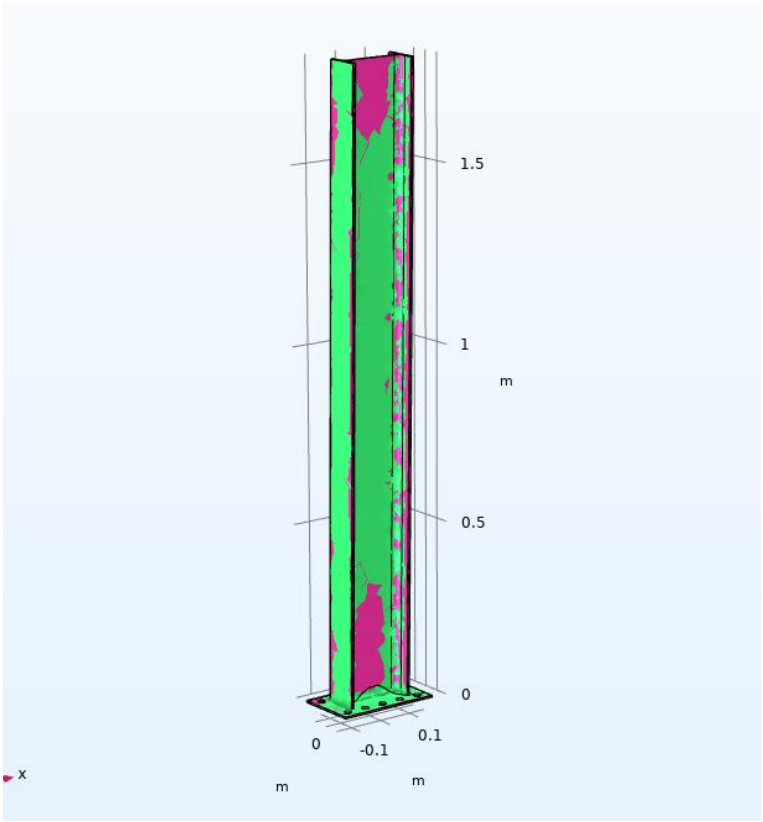

Figure 2.30: Overlap of the CAD model (green) and scanned model (pink).

Volume:	0.0053887 m^3	Volume:	0.0058773 m^3
Surface area:	1.4613 m^2	Surface area:	1.4233 m^2

Figure 2.31: Volume and area measurement, scanned model (left) CAD model (right).

The flowchart presented below mentions all the aspects mentioned earlier about the photogrammetry process, including the materials used and the software utilized in each step, providing a clear overview.

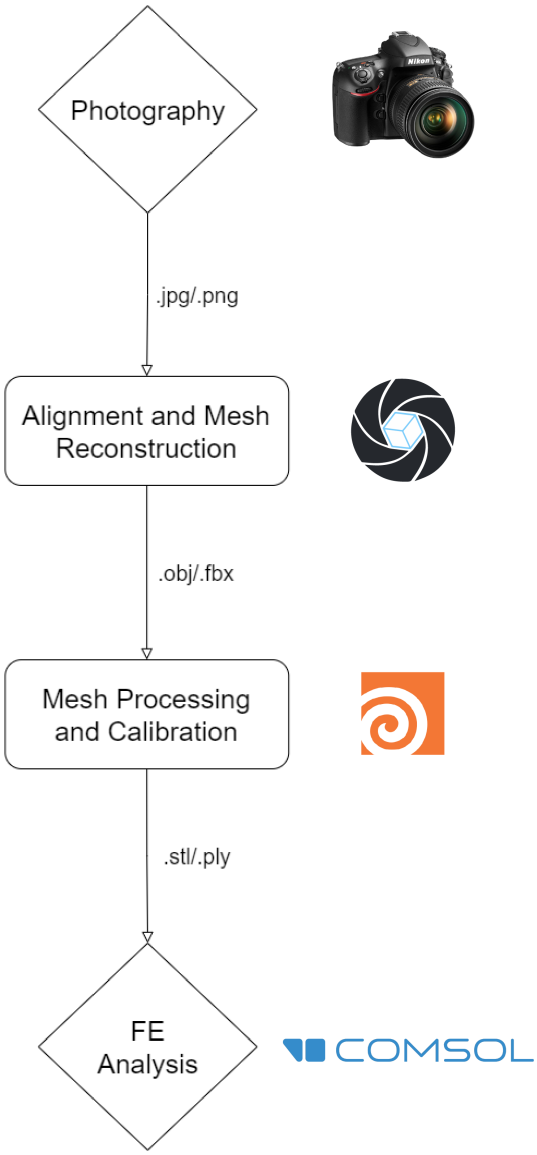

Figure 2.32: Flowchart Scheme of the Photogrammetry Process.

2.6 Conclusion

This chapter provides a comprehensive overview of the photogrammetry procedure and its importance in creating a simulation-ready 3D model. Step-by-step instructions on how to perform a photogrammetry scan are provided through an example of a steel beam segment in the laboratory. The tools and software used in the process are also described in detail. The resulting 3D model was converted into an FE model and subjected to modal analysis. The mode shapes and frequencies of the FE model were then compared to those of a CAD model. Differences in frequencies ranged from 1.03% to 12.55%, which were attributed to geometric and alignment mismatches. By following the steps outlined in this chapter, researchers and practitioners can obtain accurate 3D models from images and use them in simulations and analysis software with confidence.

Chapter 3

Laboratory tests

(Reinforced Concrete Beam)

3.1 Introduction

This chapter delves into the potential of utilizing photogrammetry technique for analyzing the behavior of lab specimen by conducting two case studies on RC beam specimen in the laboratory. The first case study focuses on a modal analysis study performed on a digitized RC beam specimen, while the second case study involves four-points bending test study. The main objective of these studies is to assess the efficacy of photogrammetry technique in helping getting precise 3D models for further analyses and investigations. The findings obtained will be presented and analyzed, providing crucial insights into the merits and the limits of the photogrammetry technique in laboratory conditions.

3.2 Specimen description

3.2.1 Beam description

In this study, a simply supported reinforced concrete beam was used, which had dimensions of 2.2 m in length, 0.12 m in width, and 0.22 m in height. The beam was supported by two steel supports at each end, which allowed it to vibrate freely in the vertical direction. The distance between supports is equal to 2 m.

Figure 3.1: simply supported RC beam.

3.2.2 Beam characteristics

The beam is a reinforced concrete (RC) beam intended for ambient vibration testing and will then be subjected to a four-point bending test.

The concrete's compressive strength, as well as the steel's Young's modulus and yielding stress, were all obtained from laboratory identification tests (tensile and compressive), while the concrete's modulus of elasticity and tensile strength were obtained using empirical formulations.

The table 3.1 presents the properties of the RC beam specimen used in our case studies, obtained from laboratory experiments.

Table 3.1: Material properties used in the study cases.

Concrete			
Average compressive strength	f_{cm}	17.11	MPa
Modulus of elasticity	E_{ci}	28.34	GPa
Tensile strength	f_{tm}	1.62	MPa
Steel bar (HA)			
Diameter	ϕ	12	mm
Modulus of elasticity	E	196	GPa
Yield strength	f_y	480	MPa

For the beam steel stirrups, a total of 20 stirrup with 11 cm even spacing, and a cross section of 8 mm in diameter was used.

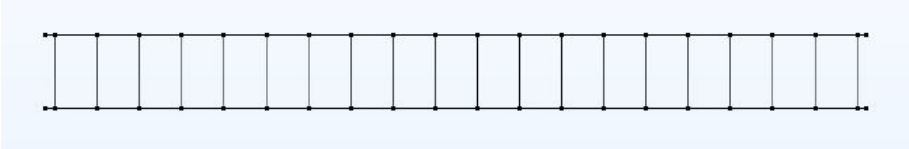

Figure 3.2: Steel stirrups distribution.

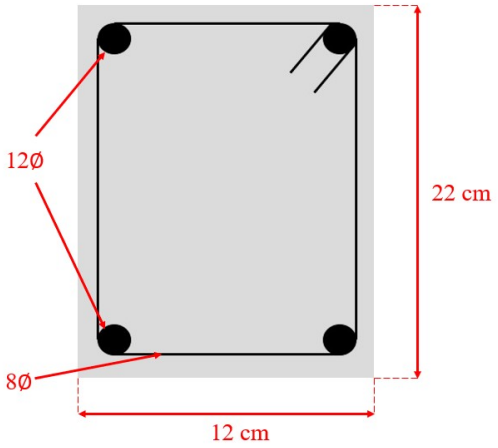

Figure 3.3: RC Beam cross section.

3.3 Scanned model process description

In order to obtain a scanned 3D model of our RC beam specimen, we will be applying the process outlined in Chapter 2. This scanned model will then be used in our case studies to analyze the behavior of the RC beam. Here briefly the process:

3.3.1 Image Data Collection

The first step of the photogrammetry-based FE modal analysis of the RC beam specimen involves the collection of high-resolution image data. This is achieved using a digital camera, and the images are taken from multiple angles around the beam to capture its entire geometry. To ensure accurate image stitching during the processing stage, sufficient overlap is ensured between the images.

3.3.2 Model Generation

The second step in the process is to use RealityCapture software to process the collected image data and create a 3D model of the RC beam. The software converts the images into a 3D point cloud and then generates the 3D model using this point cloud.

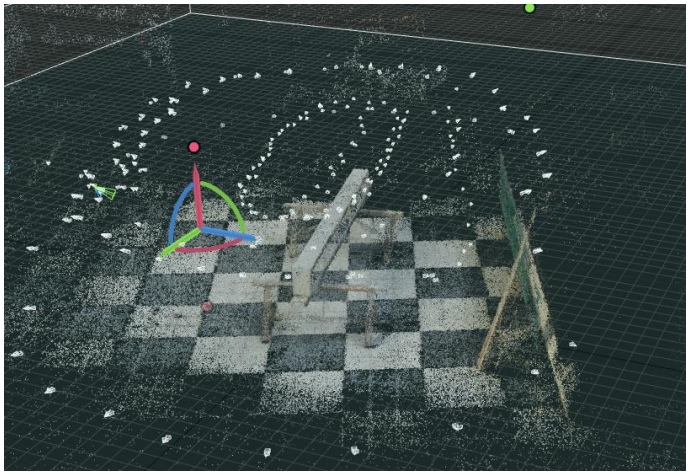

Figure 3.4: 3D Point Cloud Model of RC Beam Obtained from RealityCapture Images.

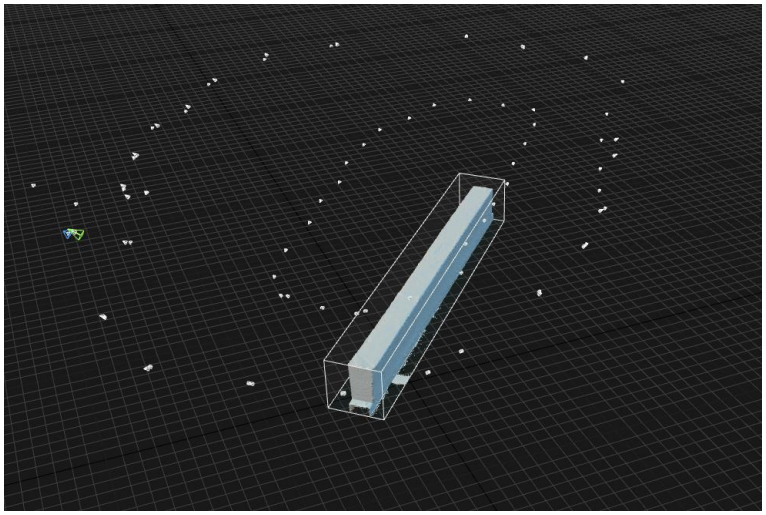

Figure 3.5: 3D Point Cloud Model of RC Beam Obtained from RealityCapture Images.

3.3.3 Mesh Processing

The next step in the process involves using Houdini software to create a mesh model for finite element analysis. The software applies algorithms to generate a mesh that accurately represents the surface of the 3D model with small and regularly-shaped elements. The mesh model is also refined to decrease the element size in complex geometries and areas where high stress concentrations are expected. This step ensures that the results of the FE analysis are accurate and reliable.

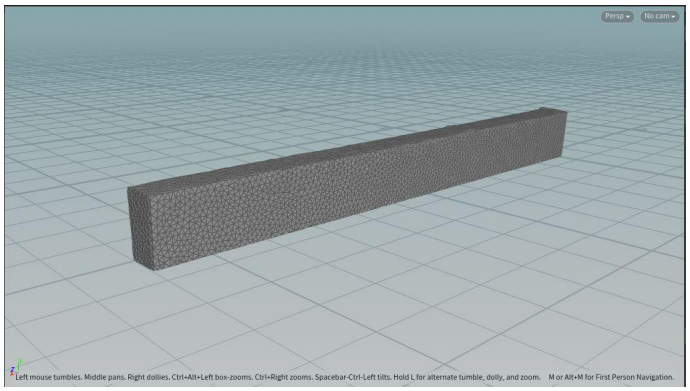

Figure 3.6: Optimized Mesh Model of RC Beam Using Houdini Software.

3.3.4 Constitution of the FE Model

The next step is to construct the Finite Element (FE) model for the RC beam specimen using COMSOL multiphysics analysis software. The FE model is a numerical representation of the physical system and is used to simulate the behavior of the beam under different loading conditions. The FE model includes the mesh generated in the previous step and is further enhanced by assigning material properties to the different elements of the mesh. These properties include Young's modulus, Poisson's ratio, and density.

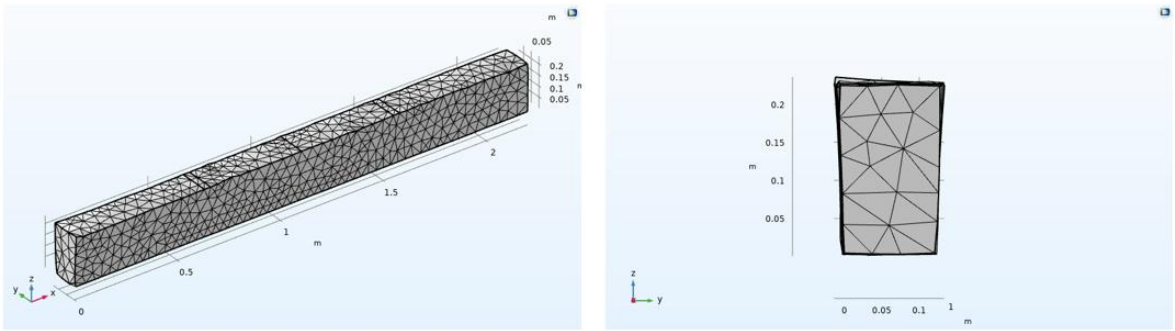

Figure a. 3D view **Figure b. Plan YZ view**

Figure 3.7: FE Model Construction of the scanned RC Beam Specimen using COMSOL Multiphysics.

3.4 Case 1: Modal analysis study on digitized lab specimen

The dynamic behavior of structures is of great importance in ensuring their safety, efficiency, and durability. This part examines the experimental and numerical techniques used for analyzing the dynamic characteristics of lab specimen. We will begin by discussing the ambient vibration experiment and the process of frequency extraction. This non-destructive testing method allows us to measure the natural frequencies of structures under ambient conditions. We will then delve into the use of finite element modal analysis for both a photogrammetry-scanned specimen and a modeled specimen. This numerical technique enables us to simulate the dynamic behavior of structures. Finally, we will present a comparative analysis between the experimental, scanned, and modeled methods of dynamic analysis.

3.4.1 Ambient vibration Experiment and frequency extraction

3.4.1.1 Ambient vibration test

Ambient vibration "Output Only" is the vibration of structures resulting from natural causes such as wind, traffic, human actions, and seismic activity. These vibrations are typically small in amplitude and can be used to determine the dynamic properties of civil engineering structures. The analysis of ambient vibrations can help extract critical information like natural frequencies, damping ratios, and mode shapes of these structures [39].

The technique is a quick and relatively uncomplicated process that can be carried out without causing any disruption to the normal functioning of a structure [30]. The process of ambient vibration testing involves recording the vibrations in real-time and analyzing the recordings. This technique for testing structures relies on detecting the minor vibrations that occur due to ambient forces [10]. Thus, the ambient vibration measurement can be a useful method for accurately determining the dominant natural vibration periods of structures [6]. One of the main benefits of this method is the ability to obtain real-time records and perform rapid nondestructive analyses [12].

Ambient vibration test consists of two main steps: Data acquisition and data analysis. **Data acquisition** involves measuring the vibration signals at different locations on the structure using sensors such as accelerometers, seismometers, or displacement sensors. Sensors are devices that can transform mechanical vibrations into electrical signals [5]. **Data analysis** requires the utilization of various techniques such as frequency domain methods, time domain methods, or stochastic methods to extract the modal parameters [24].

3.4.1.2 Experimental study

3.4.1.2.1 Measurement points

In conducting an ambient vibration test on a simply supported beam, it is crucial to consider the appropriate placement of the sensor. The sensor should be positioned at locations that effectively capture the predominant modes of vibration and oriented based on the expected direction of dominant vibration signals. In the present study, three measurement points were taken on the top surface of the reinforced concrete beam, specifically at the mid-span point, the quarter-span point, and the support point. By selecting these locations, it was possible to capture the necessary data required to analyze the behavior and characteristics of the beam under ambient vibration.

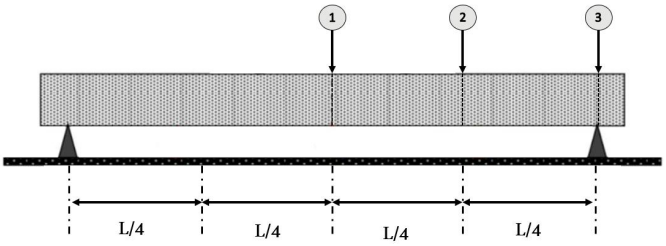

Figure 3.8: Sensor's measurement points.

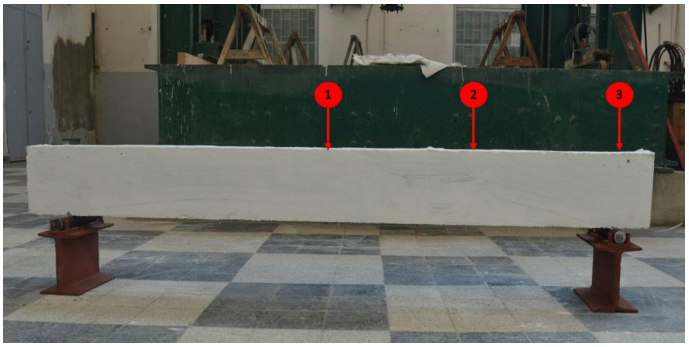

Figure 3.9: Measurement Points on RC Beam.

3.4.1.2.2 Instrumentation

In this study, several ambient vibration tests were conducted on a simply supported RC beam to investigate its dynamic behavior. The City Shark II data acquisition system was used in conjunction with a three-degree-of-freedom sensor (seismometer) type Lennartz electronic (Le3Dlite) to collect the necessary data. The seismometer used in this study was placed at three measurement points along the beam to capture the vibrations present at different locations. To ensure accurate measurements, the seismometer was securely mounted on the beam and calibrated before and after each test. This was necessary to ensure that the recorded data was reliable and could be used for subsequent analysis.

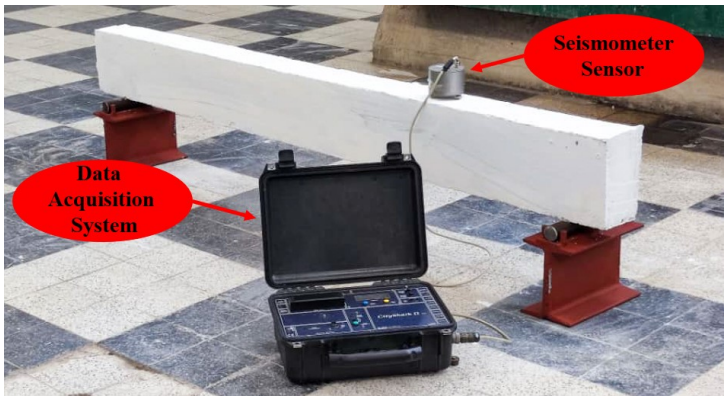

Figure 3.10: Ambient vibration recording equipment.

It should be noted that the seismometer used in this study had to be mounted securely to prevent any motion between the sensor and the beam. Any motion between the two would have resulted in inaccurate measurements, and hence the seismometer was firmly mounted in place using suitable clamps and fixtures.

3.4.1.2.3 Acquisition station

The City Shark II data acquisition system was chosen for its ability to accurately measure and record the signals generated by the seismometer. The system was able to convert the analog signals generated by the sensor into digital format and record them at a high sampling rate. This allowed for the precise measurement of the vibrations present in the beam and provided accurate data for further analysis. The recordings were set to last for 2 minutes each and sampled at a rate of 400 Hz. As the signals can vary considerably due to random excitations like wind and micro vibrations, the gain setting can be adjusted to ensure the signals remain usable and not oversaturated.

Figure 3.11: Ambient vibration test during recording.

3.4.1.2.4 Acquisition and signal processing software

To extract the recorded signal data from the PCMCIA card and transfer it to a computer, the ReadCity software is utilized. The downloaded file contains all the information of the recorded signals, which are represented as velocity versus time.

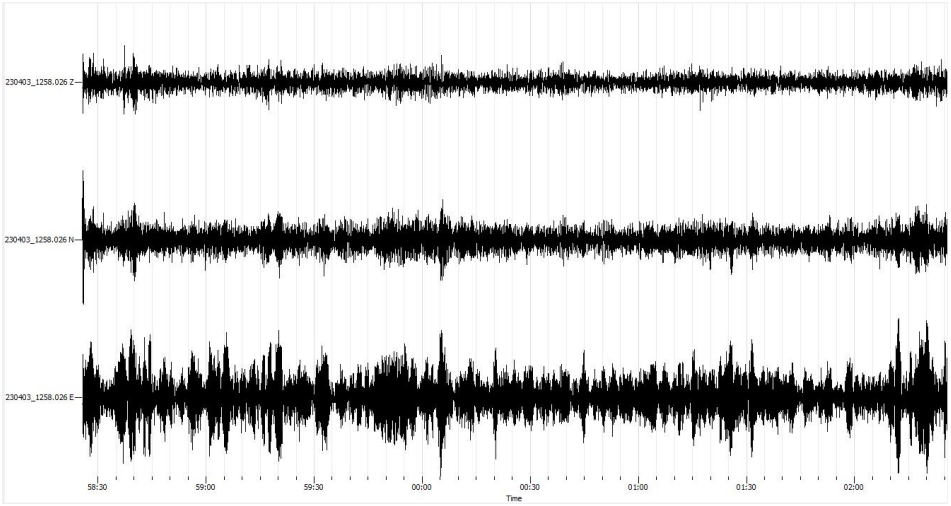

Figure 3.12: Example of RC beam response (velocity versus time) from software GEOPSY.

For analysis of the ambient vibration data, the Geophysical Signal Database for Noise Array Processing (Geopsy) software is used. This software is capable of performing a wide range of signal processing operations to perform modal identification of structures exposed to ambient vibrations.

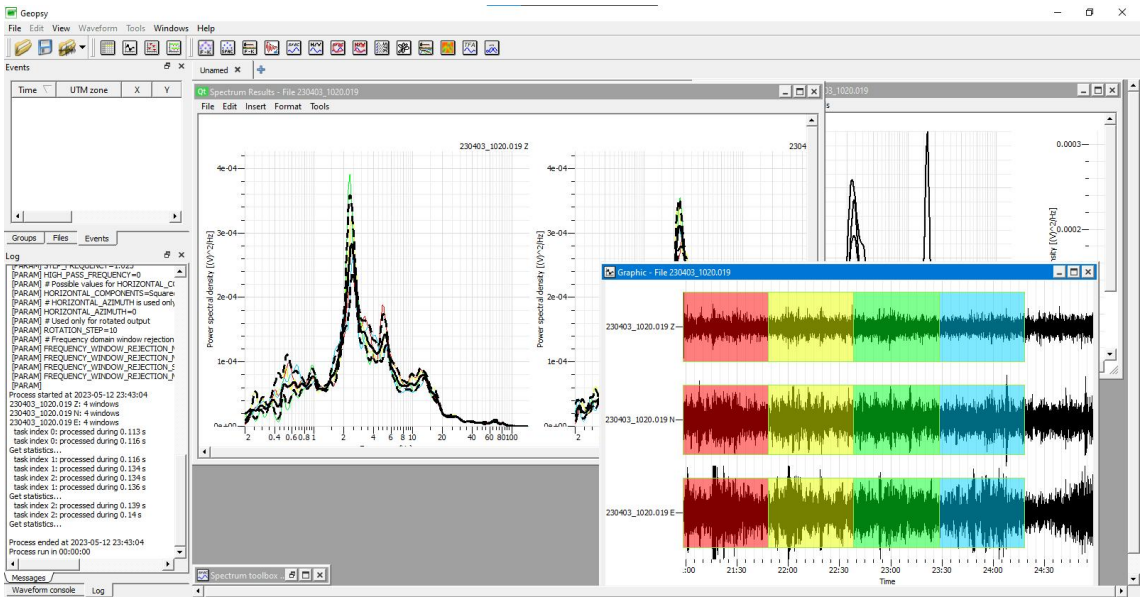

Figure 3.13: Signal processing software GEOPSY.

3.4.1.2.5 Frequency Analysis of Ambient Vibration Data

To extract eigenfrequencies from a measurement signal, it is necessary to convert the signal from the time domain to the frequency domain. The Fourier transform (Baptiste Joseph Fourier 1807) was utilized to achieve this conversion [5].

The Fourier transform is a mathematical procedure that changes a function from its primary domain, typically time or space, into a form in the frequency domain and conversely. The Discrete Fourier Transform (DFT) is used to convert a discrete signal, obtained by sampling a continuous signal at equidistant time intervals, into a frequency domain representation [58]. This digital processing technique is necessary because processing of signals in computers requires discrete data. The Discrete Fourier transform can be computed efficiently using an algorithm called the fast Fourier transform (FFT) [16].

The frequency domain representation of a time signal, known as the Fourier spectrum, shows the distribution of frequencies present in the signal, and the vibration modes are indicated by peaks.

3.4.1.2.6 Ambient vibration test procedures

The ambient vibration testing carried out on the RC beam described earlier involved several procedures, which are mentioned below:

- Preliminary testing analysis and instrumentation scheme preparation.
- Recording of the structure's response using City Shark II equipment.
- Processing of the recorded signals using Geopsy software.
- Identification of the beam's natural frequencies of vibration through experimentation.

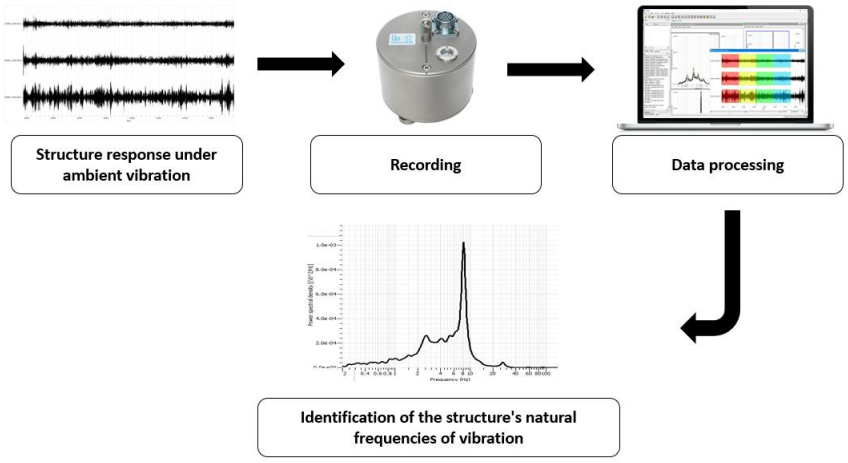

Figure 3.14: Ambient vibration test procedures scheme.

3.4.1.3 Experimental results

The Geopsy software is utilized to process signals and generate Fourier spectrum response curves for both horizontal and vertical directions. It is significant to mention that the identification of natural frequencies in the curves starts from 30 Hz because the preceding peaks represent the ambient vibration frequencies of the ground. This conclusion was reached after an additional measurement was taken on the ground.

The Fourier spectrum curves of the vertical (Z) and horizontal (N) vibrations measured at different locations on the beam are shown in figures 3.15, 3.16, and 3.17. Specifically, figure 3.15 corresponds to the mid-span (L/2), figure 3.16 to the quarter-span (L/4), and figure 3.17 to the support point.

By observing the frequency at which the Fourier spectrum curve's amplitude reaches its maximum value, it is possible to determine the natural frequency.

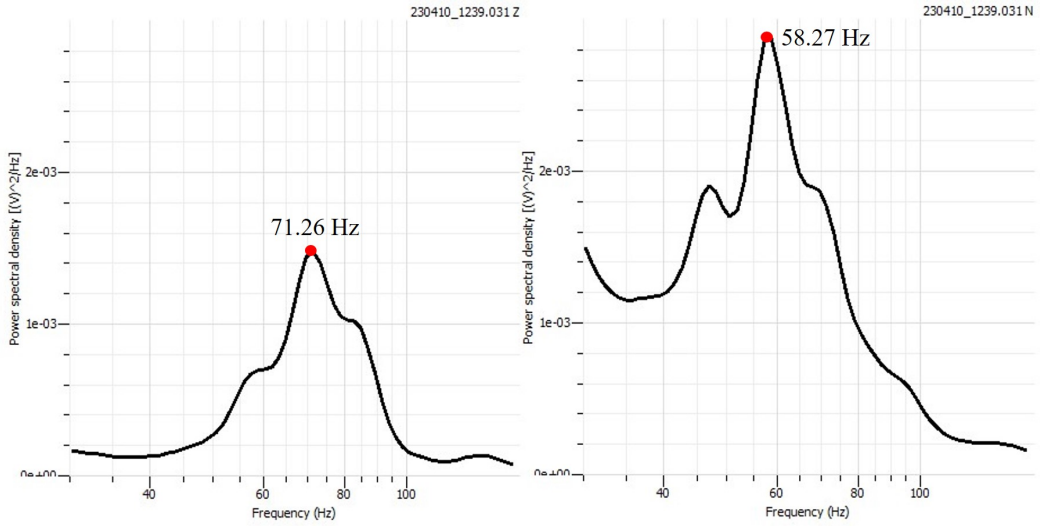

Figure 3.15: The measured Fourier spectrum curves of mid-span (L/2).

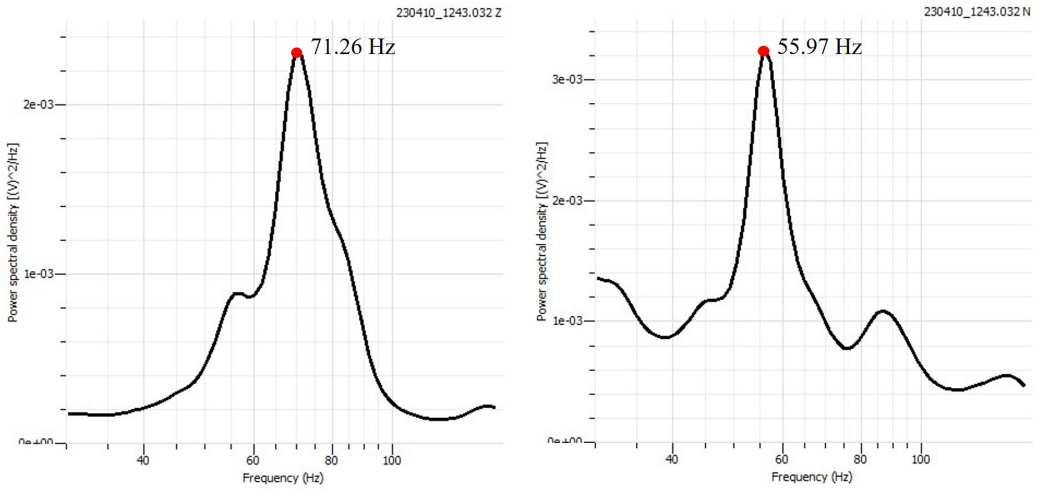

Figure 3.16: The measured Fourier spectrum curves of quarter-span (L/4).

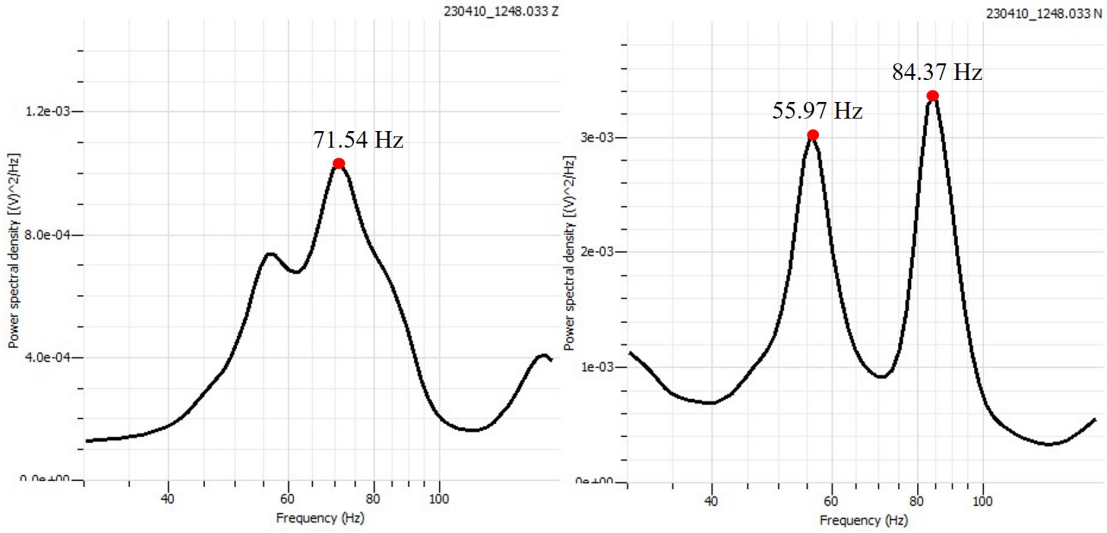

Figure 3.17: The measured Fourier spectrum curves of the support point.

It was found that the fundamental frequency of the RC beam was 58.27 Hz in the horizontal direction (N), while the second mode frequency was 71.26 Hz. Despite the presence of multiple peak frequencies in other curves, such as 55.97 Hz and 58.27 in the horizontal direction (N). Due to the high rigidity of the specimen, it becomes highly sensitive to support instability and other interferences, leading to the presence of numerous peaks that are unrelated to the specimen's mode shapes. Consequently, identifying the frequencies that correspond to the model mode shapes becomes challenging. In such situations, it becomes necessary to depend on numerical frequencies to determine the corresponding experimental ones.

The values of the natural frequencies obtained from the analysis are presented in Table 3.2.

Table 3.2: The experimental natural frequencies

No	Mode shape	Frequency (Hz)
1	Horizontal flexion	58.27
2	Vertical flexion	71.26

3.4.2 FE Modal analysis of the photogrammetry scanned specimen

The main objective of this part of the study is to determine the natural frequencies of the earlier described reinforced concrete (RC) beam scanned specimen using photogrammetry technique to compare these frequencies with the experimental results to assess the accuracy of the photogrammetry scanning process in determining the dynamic characteristics of the RC beam specimen. For this purpose, the methodology outlined in Chapter 2 will be employed. This involves the photogrammetry scanning process for generating 3D models of the RC beam specimen, followed by finite element (FE) analysis to determine its natural frequencies.

3.4.2.1 Modal Analysis

Utilizing the previously obtained scanned model depicted in Figure 3.7, we conduct a modal analysis to determine the natural frequencies of the RC beam specimen. The FE model is subjected to a small displacement, and the resulting vibration is analyzed to determine the natural frequencies and mode shapes of the beam.

The table below presents the properties of the RC beam specimen in our case study, obtained from laboratory experiments and a manual matching of the fundamental frequencies. A very low modulus of elasticity has been found to match the lowest frequency. This can be attributed to uncertainties of the supports which were found to be loose.

Table 3.3: Material Properties of Reinforcement Steel and Concrete used in the Study

Material	**Modulus of Elasticity (E)**	**Poisson's ratio**	**Density**
Steel	196 GPa	0.3	7850 kg/m^3
Concrete	28.34 GPa	0.2	2300 kg/m^3

3.4.2.2 FE Modal analysis results

The presented results are obtained from the FE modal analysis of the scanned model using the photogrammetry process. The figures 3.18 and 3.19 illustrate the first and second mode shapes, respectively, obtained from the modal analysis of the scanned model.

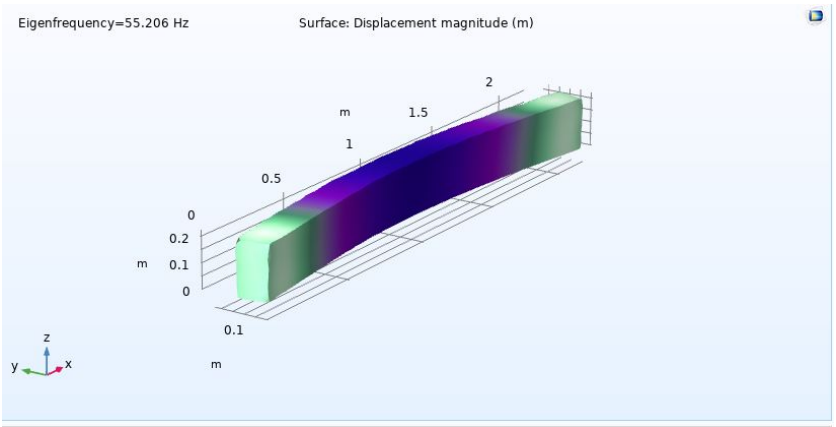

Figure 3.18: First Mode Shape of the scanned RC Beam.

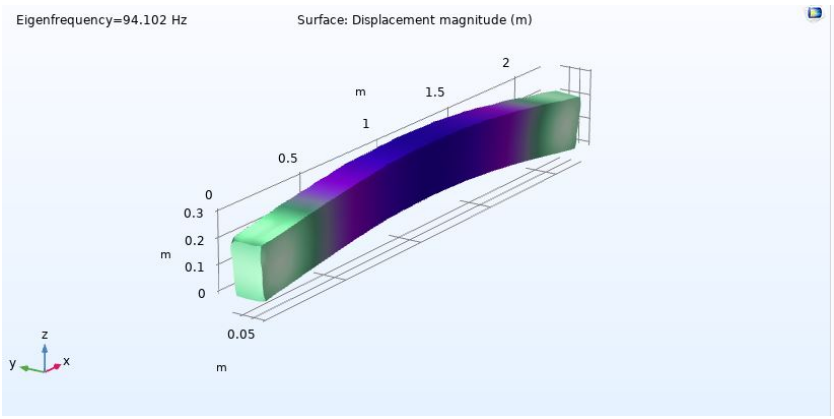

Figure 3.19: Second Mode Shape of the scanned RC Beam.

The results of the modal analysis conducted on the scanned model of the RC beam revealed that the first mode shape corresponds to a flexion in the horizontal (y) direction with a fundamental frequency of 55.21 Hz, whereas the second mode shape corresponds to a flexion in the vertical (z) direction with a frequency of 94.10 Hz.

The natural frequency values obtained from the analysis are presented in Table 3.4.

Table 3.4: Natural frequencies of the scanned specimen

No	Mode shape	Frequency (Hz)
1	Horizontal flexion	55.21
2	Vertical flexion	94.10

3.4.3 FE Modal analysis of the modeled specimen

In this part, a finite element (FE) model of the RC beam is created using COMSOL Multiphysics software. The model is based on the geometry and material properties of the physical beam specimen. The concrete is modeled using the elasto-plastic material model with isotropic hardening, while the steel reinforcement is modeled using the linear elastic material model. The FE model is meshed using tetrahedral elements, and a convergence study is carried out to ensure that the element size is appropriate for accurate results.

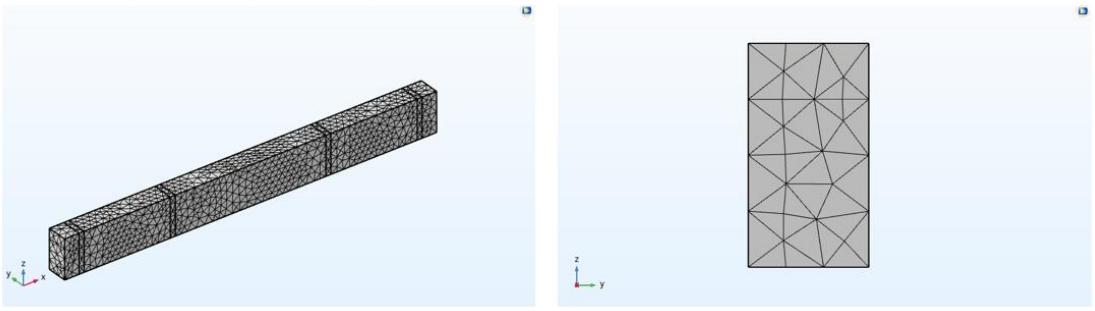

Figure a. 3D view

Figure b. Plan YZ view

Figure 3.20: FE Model Construction of the modeled RC Beam Specimen using COMSOL Multiphysics.

After the FE model is generated, a modal analysis is conducted to determine the natural frequencies and corresponding mode shapes of the beam. The analysis is carried out using the eigenfrequency solver in COMSOL Multiphysics software.

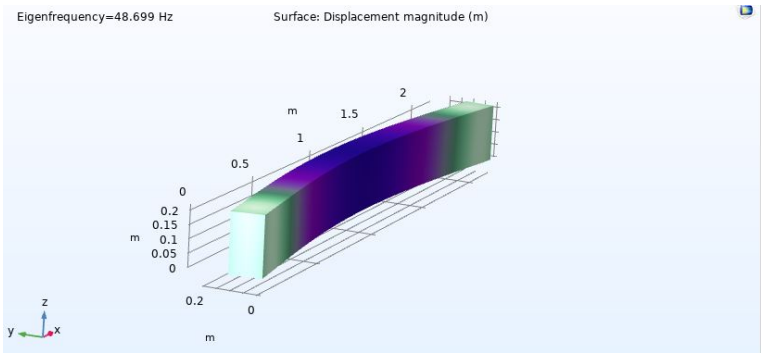

Figure 3.21: First Mode Shape of the modeled RC Beam.

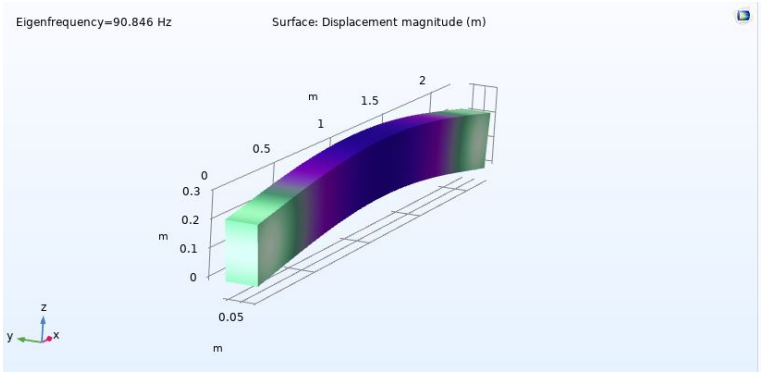

Figure 3.22: Second Mode Shape of the modeled RC Beam.

The results of the modal analysis are presented in Table 3.5, which shows the first and the second natural frequencies and corresponding mode shapes of the modeled RC beam.

Table 3.5: Natural frequencies of the scanned specimen

No	Mode shape	Frequency (Hz)
1	Horizontal flexion	48.70
2	Vertical flexion	90.85

3.4.4 Results and discussions:

As discussed previously, the natural frequencies of the RC beam were determined using ambient vibration testing as well as scanned and modeled analyses. The table below presents a comparison of the results obtained from these different methods.

Table 3.6: Comparison of the natural frequencies obtained from the three different methods

No	Mode shape	Ambient Vibration Frequency (Hz)	Scanned specimen Frequency (Hz)	Modeled specimen Frequency (Hz)	Scanned specimen Difference (%)	Modeled specimen Difference (%)
1	Horizontal flexion	58.27	55.21	48.70	5.25	16.42
2	Vertical flexion	71.26	94.10	90.85	32.05	27.49

In this study, the ambient vibration test (AVT) was used as a reference, and the material properties were determined to match the frequencies of the scanned beam and modeled beam analyses. The natural frequencies of the FE modal analysis and AVT are shown in table 3.6.

As mentioned before, the low elastic modulus could be attributed to various factors, such as external factors that affect ambient vibration testing accuracy. However, what seems to be even more important are the support conditions. It was observed that the beam was not firmly supported on the steel supports, and moreover, the supports themselves were resting on uneven ground, creating a loose connection between the supports and the beam.

The results revealed also that the scanned specimen showed a closer agreement with the AVT results for the first mode shape, while the modeled specimen had better agreement for the second mode shape. Furthermore, it is essential to note that the modeled specimen had a perfect geometry, while the scanned specimen had a geometric approximation of the real structure, which could be a factor in the observed differences between the two approaches.

3.5 Case 2: Four-points bending test

The four-points test is a widely used experimental procedure to evaluate the structural behavior and strength of reinforced concrete (RC) beams. In this second part of the chapter, a reinforced concrete beam specimen was subjected to a four-points bending experiment in the laboratory. Furthermore, a scanned counterpart of the beam was utilized for a numerical bending experiment. The primary goal of these analyses is to compare the experimental results with the numerical ones and to gather additional information about deformation through the application of photogrammetry. Additionally, these analyses aim to predict the damage and cracking patterns that may occur in the reinforced beam.

3.5.1 Laboratory experiment

3.5.1.1 Four-points bending experiment

A reinforced concrete (RC) beam is a structural element that is designed to resist bending and shear forces. The four-point bending test is a common method used to determine the flexural strength of RC beams [41]. In this test, the beam is supported at two points and loaded at two other points. The test is performed until the beam fails or reaches its maximum load capacity.

3.5.1.2 Used equipment

In order to perform force measurements and distribute loads, several equipment pieces are commonly utilized. These include a displacement comparators, force comparator, a force distributor, beam supports, and a loading mechanism, such as a jack.

Figure a. Load Comparator

Figure b. Displacement Comparator

Figure c. Supporting pin

Figure d. Load distributor

Figure 3.23: Four-points bending test equipment.

3.5.1.3 Progress of the experiment

In the reinforced concrete four-points bending experiment, the following steps are typically followed. Firstly, the reinforced concrete (RC) beam is positioned on top of the supports, ensuring that a distance of 10 cm is maintained between each end of the beam and the adjacent support. Subsequently, a (1m between two pins) load distributor is carefully placed on the beam, precisely in the middle. To measure the behavior of the beam under load, a force comparator is positioned between the load distributor and the beam, while three displacement comparators are positioned beneath each quarter of the distance between the two supports. The experiment then commences by gradually increasing the load applied to the beam, while simultaneously recording the corresponding load and displacement values. This process continues until the load reaches a point of failure, resulting in the destruction of the beam.

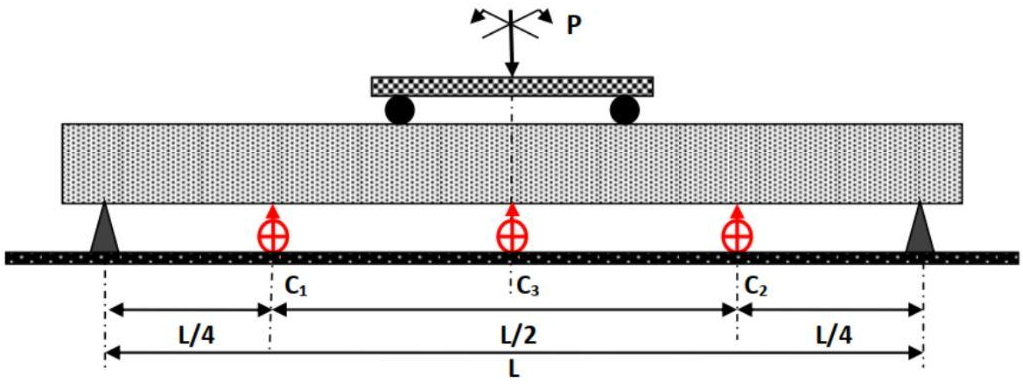

Figure 3.24: Beam positioning and comparators distribution (Displacement comparators in red).

NB: The specimen has to be photographed at different stages of the experiment, and this image data purpose is to compare between the real experimental model and the numerical simulation when it comes to the elasto-plastic behavior of the beam as well as the positioning of the cracks that appear and their distribution along the surface of the beam.

3.5.1.4 Experimental results

Based on the test results, load-displacement curve was generated using a force comparator and a displacement comparator. This curve provides valuable information about the behavior and response of the beam under applied loads.

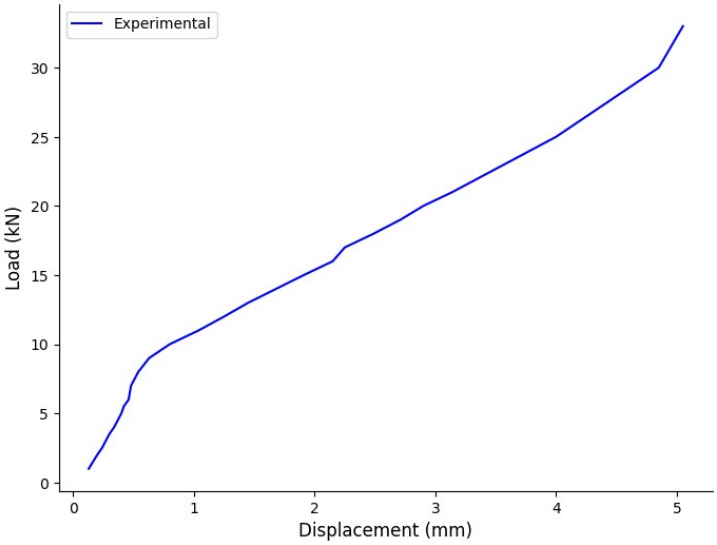

Figure 3.25: Experimental Load-Displacement curve.

Figure 3.26: Beam after reaching failure.

3.5.2 Deformation capture using photogrammetry

In order to conduct a comprehensive analysis of the beam element and assess the effectiveness of photogrammetry, we captured the beam at three specific stages: the undeformed stage, a stage where a residual displacement of 1.35mm was applied, and a stage with an unknown deformation. The primary objective of this data capture was to compare and evaluate how well photogrammetry captures residual displacements.

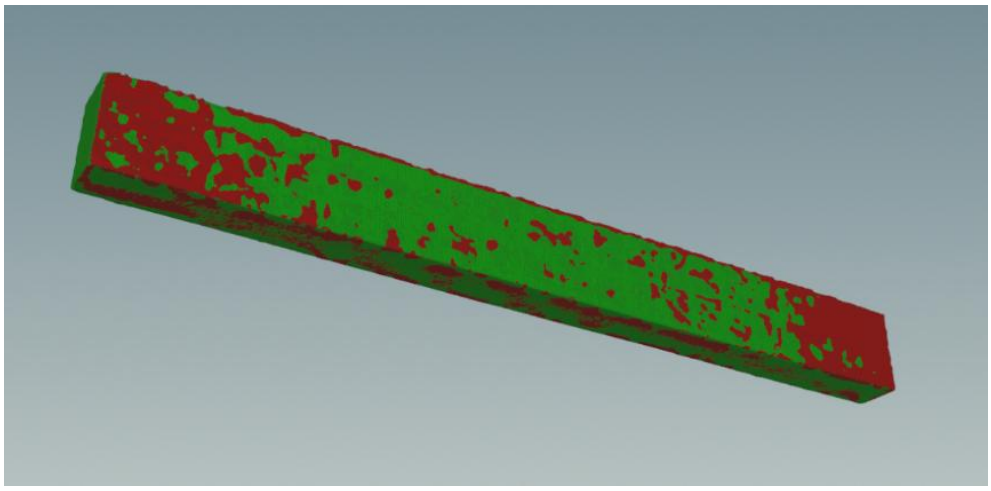

Figure 3.27: Non-deformed beam (red) and deformed beam (green) overlap.

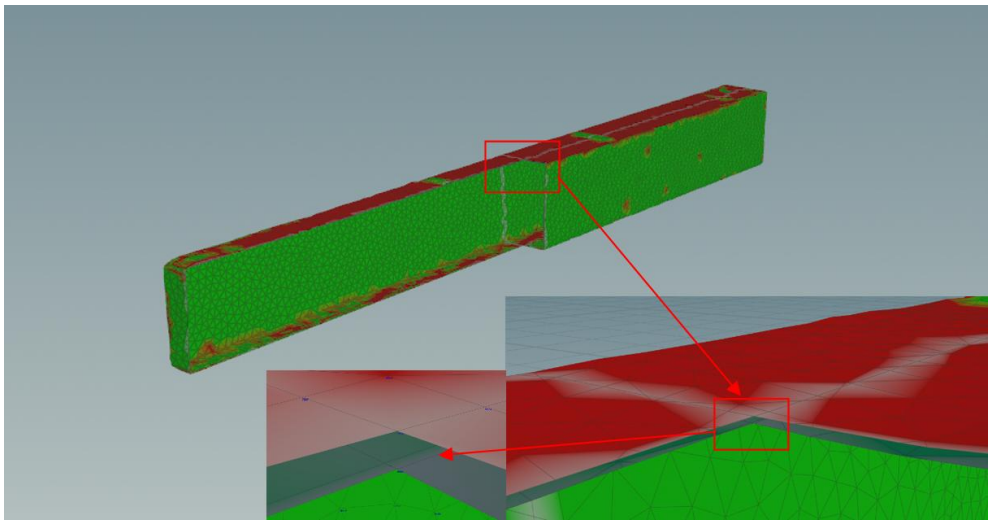

Figure 3.28: Residual displacement.

```
1 vector one = point( 0, 'P', 5477);
2 vector two = point( 0, 'P', 8803);
3 f@dist = distance( one, two);
```

dist
0.00136951

Figure 3.29: Distance measuring function and Measured distance.

For the first captured deformation the experimental residual displacement was **1.35mm** where the numerical model value was **1.37mm**.

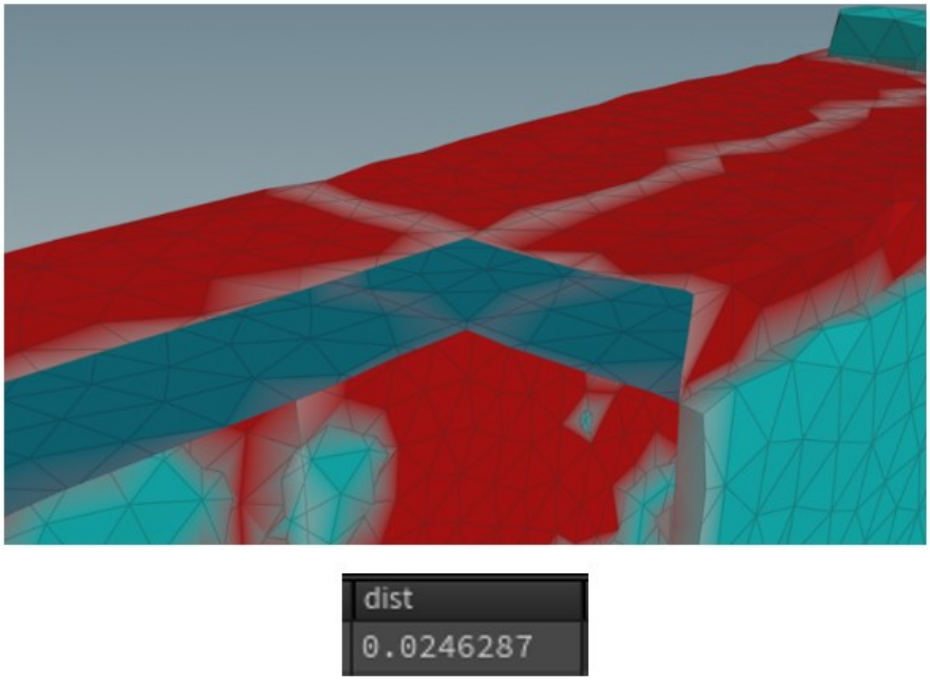

Figure 3.30: Residual displacement from another capture and its Measured distance.

As for the second capture the residual experimental displacement was not measured but the numerical value for it was **24.6mm**, which confirms that the photogrammetry is capable of capturing small deformation.

3.5.3 Numerical Analysis

In order to perform the four-point bending test numerically, we will utilize the scanned model obtained through our process. However, it is crucial to mention that calibration of the material properties is required to ensure the accuracy of the simulation results.

3.5.3.1 Concrete plasticity model

Due to the intricate nonlinear behavior exhibited by concrete materials, numerous theories regarding the representation of plasticity models in finite element method (FEM) analyses have been documented in existing literature. Among the plasticity models the Ottosen's failure criterion[43] [42] [44], and it is a four-parameter failure criterion proposed for short-time loading of concrete, and this model was chosen due to its simplicity and its low input parameters, especially in our case where the only information about concrete behavior we have is its compressive strength, it is also perfect in our case because its availability as we are using COMSOL which integrates this model directly in its interface.

3.5.3.2 Ottosen model parameters

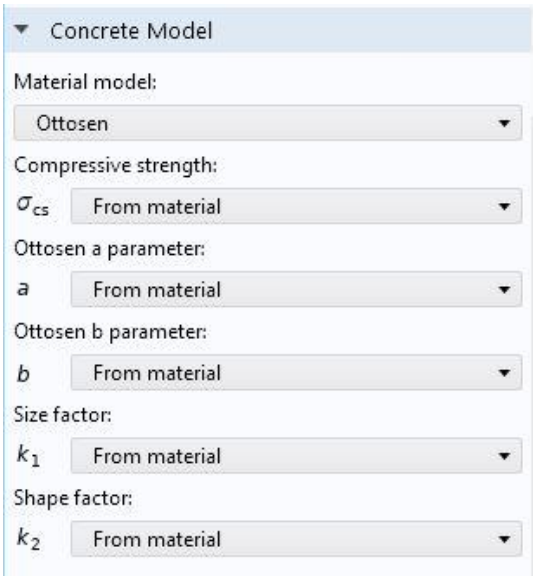

Figure 3.31: Concrete model tab (Ottosen parameters).

We stated before that we have the ultimate compressive strength of the concrete $f_c = 17\,\text{MPa}$, as for the other parameters they can be calculated directly from the model's equations, or they can be deduced from the parameters table and their dependence on σ_t/σ_c ratio [43].

σ_c: ultimate compressive strength of the concrete.

σ_t: ultimate tensile strength of the concrete ($f_t = 1.62\,\text{MPa}$ in our case).

Table 3.7: Typical parameter values for Ottosen failure criterion.

σ_t/σ_c	**a**	**b**	k_1	k_2
0.08	1.808	4.096	14.486	0.991
0.10	1.276	3.196	11.736	0.980
0.12	0.922	2.597	9.911	0.965

We used the first row of the table as it has the same ratio as our concrete's tensile/-compressive strengths ratio: $\sigma_t/\sigma_c = \frac{1.62}{17} = 0.08$

Figure 3.32: Inserted Ottosen parameters.

3.5.3.3 Steel reinforcement

3.5.3.3.1 Reinforcement modeling

For the steel rebars and stirrups, the elements were modeled as simple polygon lines and a Truss interface has been added to encompass those elements. A Multiphysics coupling node is added after that to apply the connection between the concrete and steel as a rigid embedment.

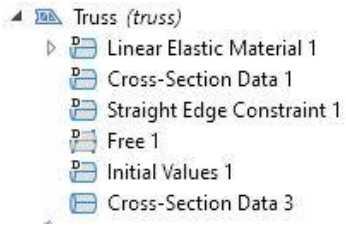

Figure 3.33: Truss interface.

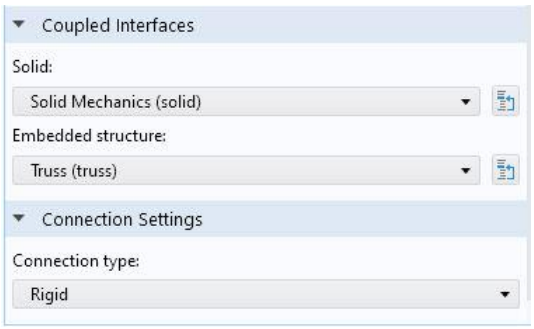

Figure 3.34: Embedded reinforcement interface.

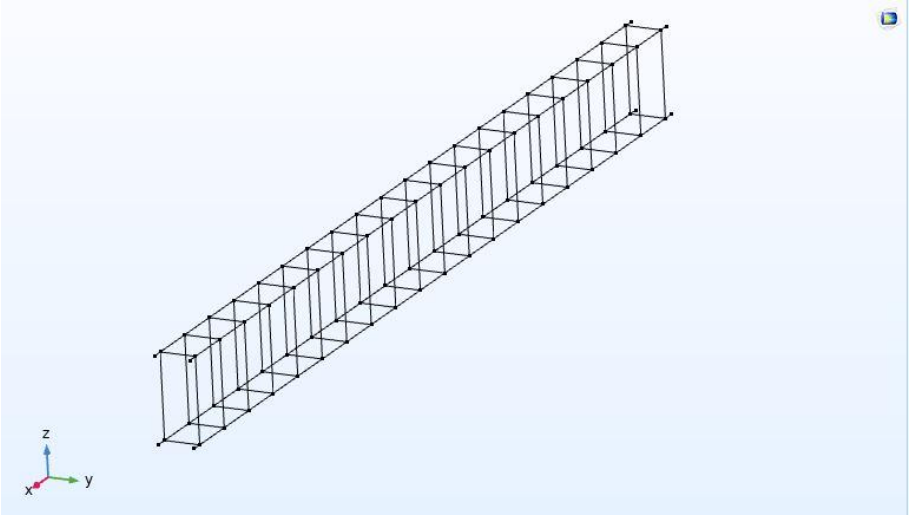

Figure 3.35: View of the steel reinforcement.

3.5.3.3.2 Plasticity model

Same as concrete, steel reinforcement bars also exhibit a non-linear behavior after reaching the yield stress, there are several constitutive models that describe the elasto-plastic behavior of steel but COMSOL by default uses the von mises yield criterion in its Truss interface, with different hardening laws to choose from, and what we found is that the linear hardening law works just fine with 3% of the elastic modulus for the isotropic hardening model.

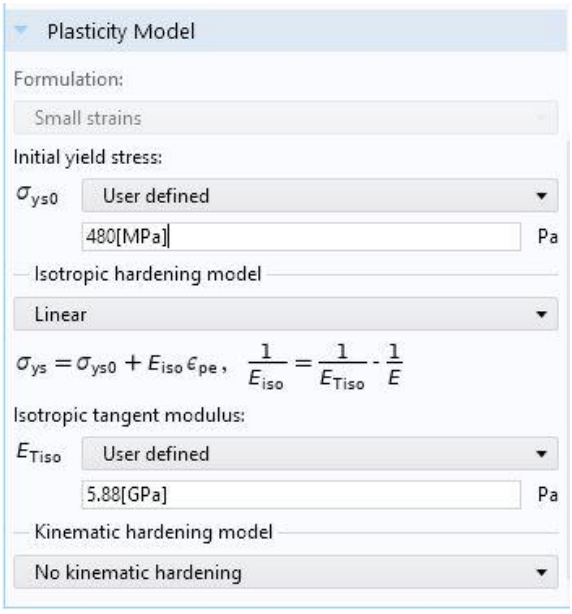

Figure 3.36: Plasticity model for the steel reinforcement.

3.5.3.4 Analysis settings

For analyzing the plastic behavior of the concrete, a Time Dependent study was used, with 0.05s time step and a total of 200 steps, a linear function of time was created in the definitions tab in order to control the load or the displacement applied on the beam.

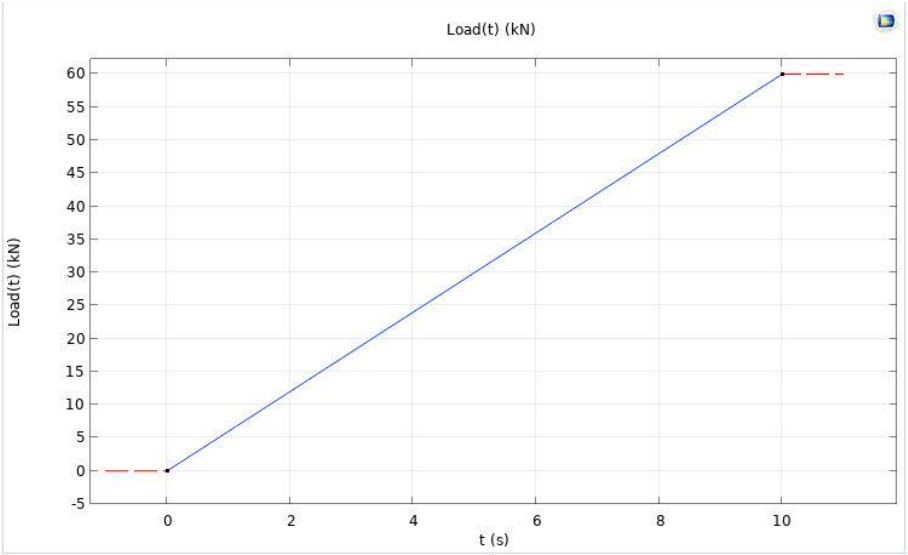

Figure 3.37: Applied load function.

As for the mesh part, the steel rebars were meshed each with 25 1D elements, and 8778 tetrahedral elements for the concrete block, a linear discretization was used to have lower CPU times but a quadratic one can always be selected for more precise results.

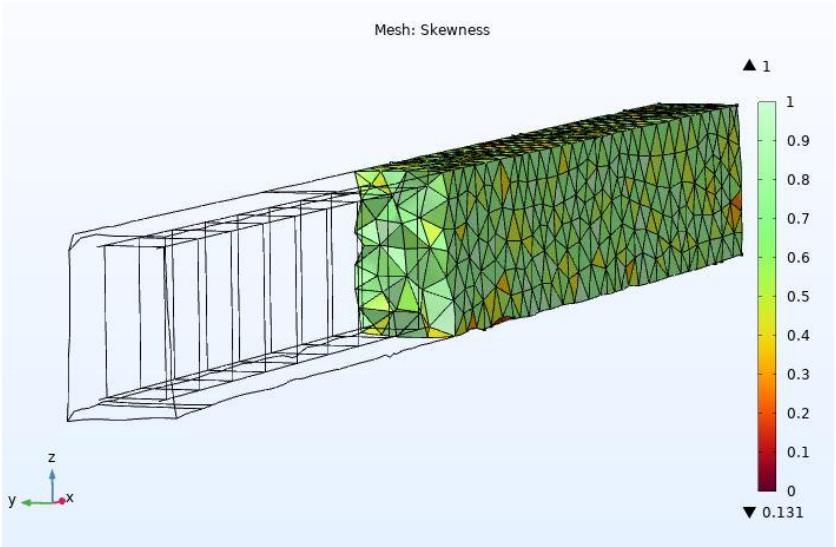

Figure 3.38: RC beam simulation mesh.

3.5.3.5 Numerical results

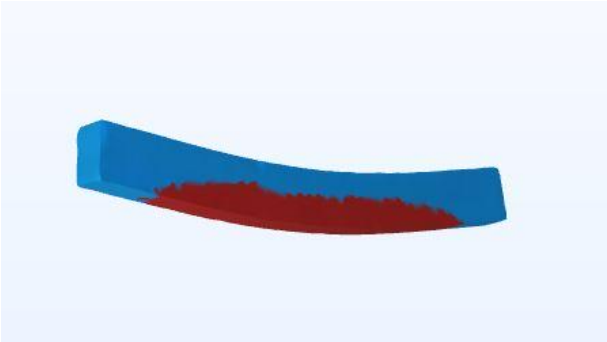

Figure 3.39: Plastified region.

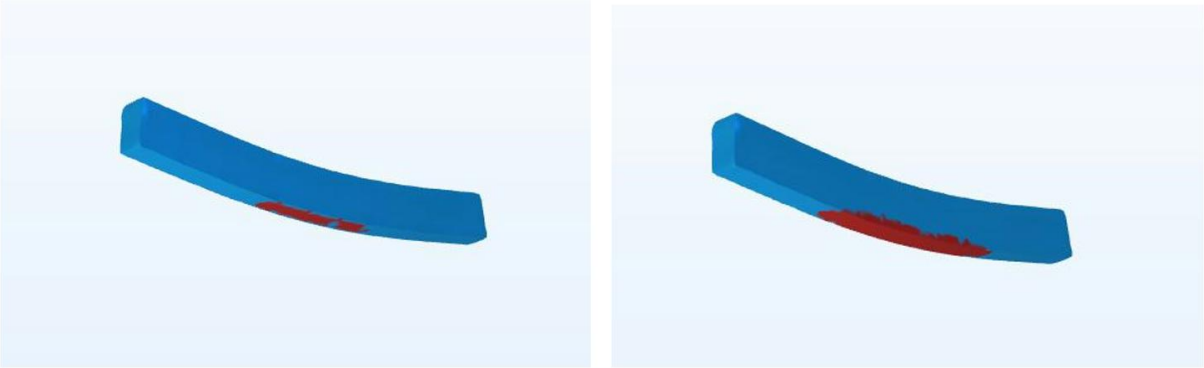

Figure 3.40: Plastified region in 6kN (left) and 9kN (right) of applied load.

We can notice that in the numerical model the beam started to show plastic strains at around 6 to 9 kN of applied force which agrees with the experimental result where at 7 kN residual displacement started to appear when unloading the beam.

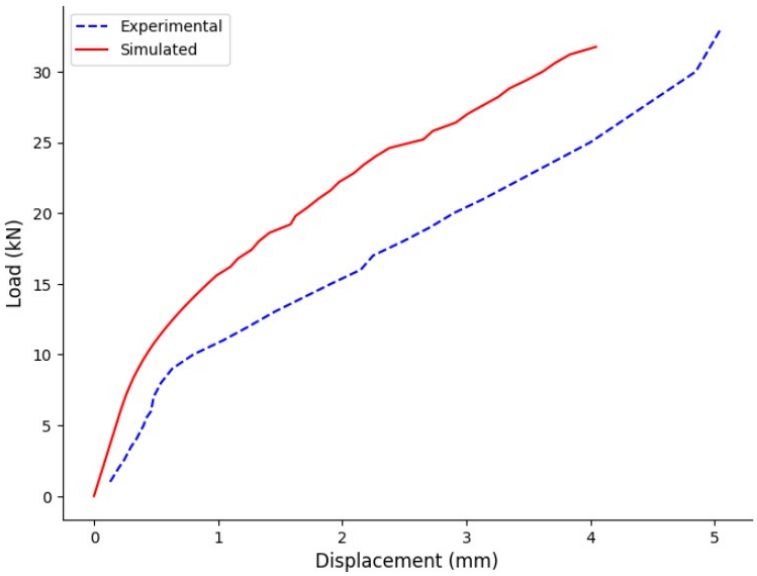

Figure 3.41: Comparison of Load-displacement curves simulation and experiment.

The force-displacement curve also shows a decent agreement between the experimental and simulated models especially in the elastic phase, as for the non-linear phase the differences are a bit more significant, the discrepancies present here can be attributed to a lot of different factors starting from the errors introduced in the photogrammetry and calibration process, to the uncertain nature of the non-linear behavior of reinforced concrete, It is worth mentioning that the displacement sensors used were rudimentary ones and more sensitive ones are required for more precise results.

3.5.4 Damage and cracks prediction

For the last section of this chapter, we wanted to predict the behavior of the digitized concrete beam after reaching its elastic limit, and see if the fracture pattern as well as its distribution matches that of the real specimen. For that, the default scalar damage model in Comsol was used as it only requires the tensile strength which we already have, and the fracture energy that can be derived from the tensile stress-strain curve. However, since we have not performed the tensile test, the energy is calculated from Equation (3.1) in the fib code [18]. It is worth noting that this model does not take into account the compressive damage; that's why the crushing effects did not appear in the simulated model. A better model would be that of Mazars [45], which calculates both the compressive and tensile damage. However, it has not been used in our case due to the lack of its input data.

$$G_F = 73 \cdot f_c^{0.18} \tag{3.1}$$

A fracture energy of 120 J/m^2 was used.

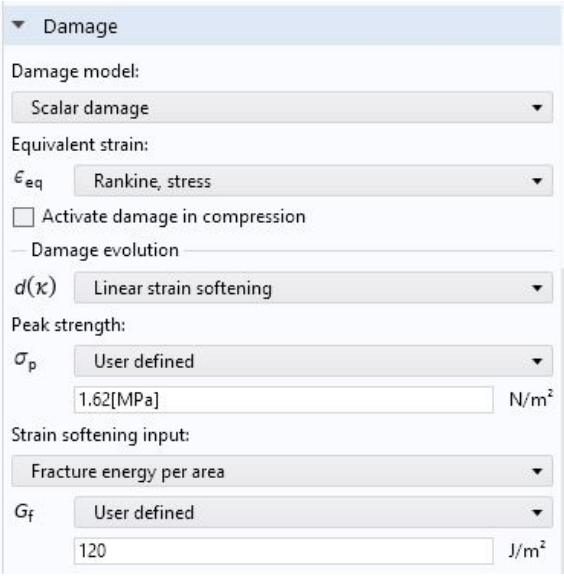

Figure 3.42: Damage model parameters.

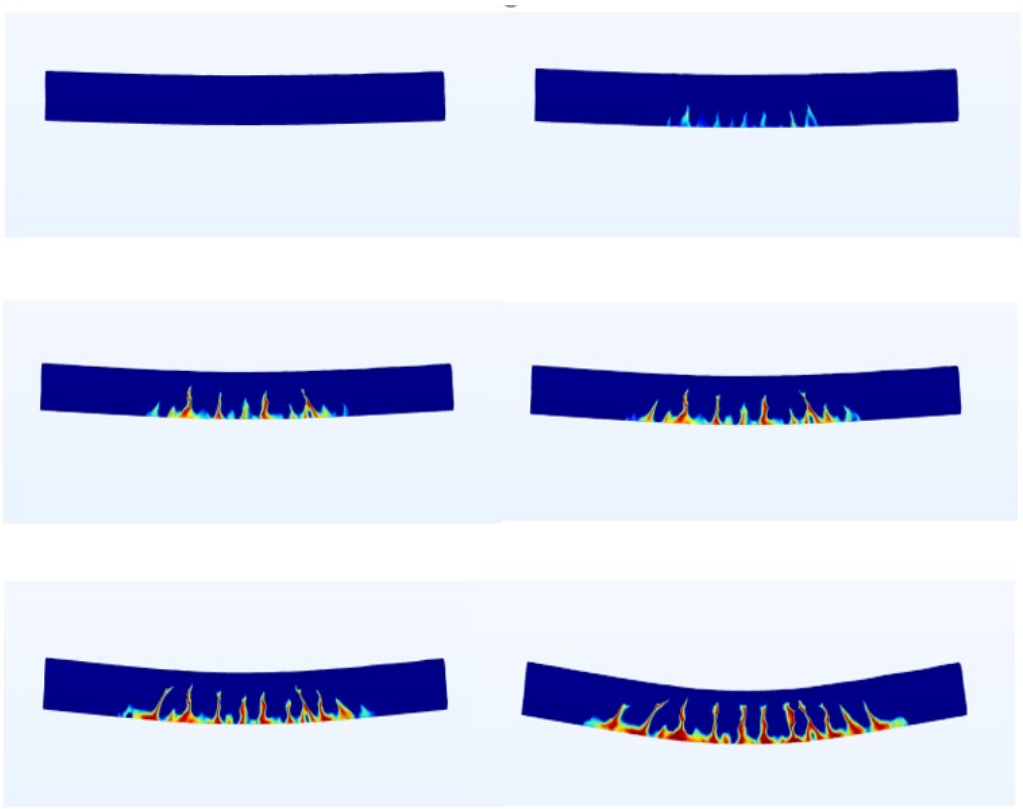

Figure 3.43: The evolution of damage.

NB: For all the figures containing a deformed beam from Comsol, the scale factor for those deformations was set to 10 for visualization purposes only.

Figure 3.44: Comparison between simulated and experimental cracking pattern.

In the numerical model the cracks start appearing at around 16.5 kN while in the real one the cracks appear after applying 15 to 16 kN of force, and the cracking pattern and Its distribution along the beam element in the simulated model looks to be matching the one in the real specimen.

3.5.4.1 Results and discussions

The photogrammetry process demonstrated its effectiveness as a reliable tool for capturing deformations and residual displacements. This non-contact measurement technique proved valuable in accurately documenting the structural behavior and changes in the beam during testing.

The Ottosen concrete plasticity model showcased its reliability in describing the nonlinear behavior of concrete. Despite the presence of factors that contribute to the uncertainty of concrete behavior, the model provided a satisfactory representation of the material's behavior.

While there may be other damage models available, the scalar damage model employed in Comsol showcased its capability in predicting the initiation of cracks in the concrete beam, as well as their pattern. This indicates that the model successfully captured the development of damage within the structure.

Despite inherent differences between the numerical analysis and the physical test, the results indicate that the scanned beam four-point bending analysis yielded reasonable estimates and results when compared to the reel test.

3.6 Conclusion

In conclusion, the photogrammetry technique proves to be a valuable tool for developing 3D models. While the benefits of this technique may not be fully demonstrated in the current specimen, which has a regular shape, accurate 3D models can still be obtained using photogrammetry for modal and potentially structural analysis. The true advantages of this technique will be showcased in the next chapter, where the specimens exhibit complex shapes.

Chapter 4

Photogrammetry application on a historical monument

4.1 Introduction

This chapter addresses an important application of photogrammetry as a tool to identify global material properties in existing structures which holds significant importance in the field of civil engineering, particularly in the domain of historical monuments. Obtaining accurate information regarding the global material properties of these structures is crucial for conducting expert analysis and ensuring their preservation. In this chapter, we present a technique that utilizes photogrammetry and ambient vibration testing (AVT) to determine the global material properties of a historical site. Furthermore, we propose an optimization approach based on artificial intelligence (AI) to refine the obtained results. Our study focuses specifically on selected elements from the Tipaza historical site, aiming to validate the effectiveness of the photogrammetry process developed in the previous chapters and the optimization methodology.

4.2 Site presentation

4.2.1 Historical Site Description

The Tipaza historical site, located on the Mediterranean coast of Algeria, represents an exceptional archaeological treasure with significant relevance to civil engineering. This UNESCO World Heritage Site preserves the remains of civilizations from the 6th century BC to the 6th century AD, including the Phoenicians, Romans, early Christians, and Byzantines. Comprising two archaeological parks adjacent to the urban complex and the Royal Mauritanian Mausoleum on the Sahel plateau, the site spans approximately 60 hectares. Notably, the Tipaza archaeological park is divided into three primary sections: the eastern necropolis, the central urban area, and the western religious complex [56].

This site offers civil engineers an opportunity to explore an impressive range of structures, such as an amphitheater, temples, a forum, a fourth-century basilica, baths, and remarkable mosaic artworks. These architectural marvels showcase the innovative use of materials, including stone, mortar, mosaic, marble, and wood, providing insights into ancient construction techniques and design ingenuity [9].

Figure 4.1: The archaeological park of Tipaza.

From this site, we have selected three elements for our work. The first element we have chosen is the column, which represents a simple architectural component. The second element, the wall, possesses a medium level of complexity. Lastly, we have selected arches, which are large and intricate structures for our analysis. The figures below represent the three selected elements chosen.

4.2.2 Elements description

4.2.2.1 Column description

The selected column for analysis in this study is characterized by being fixed at its base and possesses a height of 1.35 m. The column's section, measured at a specific height, exhibits dimensions of 0.55 m by 0.59 m. This configuration highlights the column's structural stability and integrity, with the fixed base providing a solid foundation. Notably, the column features multiple openings, suggesting the presence of voids within its structure.

Figure 4.2: Chosen Column from Tipaza Historical Site.

4.2.2.2 Wall description

The selected wall for analysis in this study has a height of 3.20 m. The dimensions of the wall section are 0.45 m by 1.50 m. It is constructed using a type of stone and rubble masonry. However, upon examination, it is evident that the wall has undergone significant deterioration. Crumbling sections and missing portions are notable features of the damaged wall.

Figure 4.3: Masonry Wall in the Tipaza Historical Site.

4.2.2.3 Arches description

The chosen arch in the Tipaza Historical Site is a relatively simple architectural structure composed of four interconnected arches. These arches are connected with a damaged wall, imparting a distinct character to the overall composition. With a maximum height of 3.50 m and a length of 13 m, the arches command attention within the site. The damaged wall, measuring 5.50 m at its base, provides stability and reinforces the structure. The arches exhibit a harmonious fusion of architectural brilliance and structural strength. Despite the damaged wall, the arches retain their shape and visual impact. The incorporation of diverse materials enhances their aesthetic appeal and reflects the resource diversity of the historical period.

Figure 4.4: The arches.

4.3 Identification Methodology

In this study, we aim to identify the material properties, including Young's modulus, density, of three distinct structures within the Tipaza Historical Site: a column, a wall, and arches. To achieve this, we propose a combined approach utilizing AVT (Ambient Vibration Testing) results and photogrammetry methods.

Initially, the AVT technique will be employed to determine the natural frequencies of each structural element. Subsequently, the photogrammetry approach will be utilized to capture images and create a scanned model of the structure. The material properties will be calibrated to obtain simulated frequencies that closely match the real frequencies obtained from AVT.

To enhance the effectiveness of our analysis, we will employ a genetic algorithm. This algorithm will search for the optimal combination of material properties for each structure. By considering factors such as minimizing the error between simulated and actual frequencies and satisfying constraints related to material behavior, the algorithm will assist in achieving the most accurate representation of the material properties for each structure.

By implementing this methodology through the utilization of an API (Application Programming Interface) code in the Python programming language, we aim to gain a comprehensive estimation of the material properties of the selected structures.

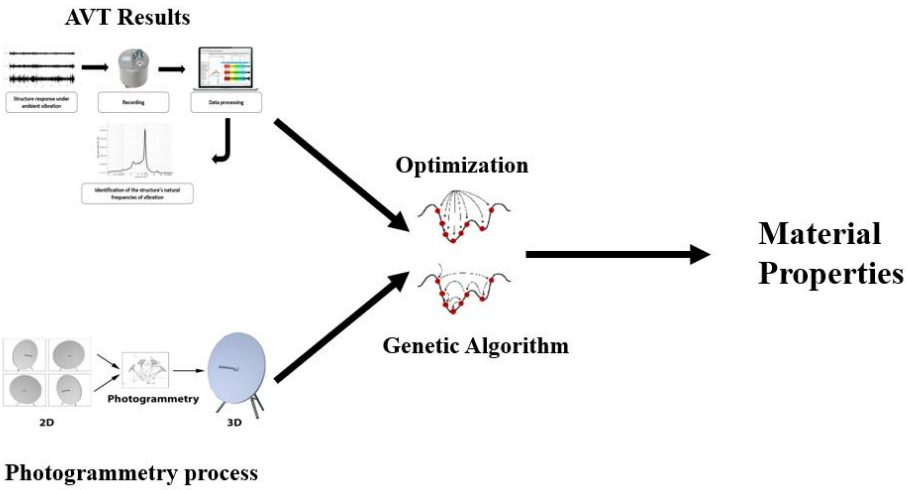

Figure 4.5: Methodology scheme.

4.4 Ambient vibration test and frequency extraction

In this section, the methodology outlined in Chapter 3 will be applied to extract the eigenfrequencies of each historical structure using ambient vibration testing (AVT). The following steps will be followed:

4.4.1 Experiment study

4.4.1.1 Measurement points

To conduct the AVT test effectively, it is crucial to strategically place the sensors at the measurement points that capture the predominant modes of vibration and align them with the expected direction of dominant vibration signals. In our study, we placed the sensors at the top of each structure.

Figure 4.6: Measurement Points on the column.

Figure 4.7: Measurement Points on the wall.

Figure 4.8: Measurement Points on the arches.

4.4.1.2 Instrumentation

In order to investigate the dynamic behavior of each element, a series of ambient vibration tests were performed in this study. The data acquisition system employed for this purpose was the City Shark II, which allowed for the collection of accurate and reliable data. To capture the vibrations, a three-degree-of-freedom sensor, specifically a seismometer of the Lennartz electronic (Le3Dlite) type, was utilized.

4.4.1.3 Acquisition station and measure

The City Shark II data acquisition system was selected for its precise measurement capabilities and its suitability for recording the signals obtained from the seismometer. Each recording was configured to last for a duration of 2 minutes, with a sampling rate of 150 Hz. It is important to note that the signals being measured can exhibit significant variation due to random excitations, such as wind and micro vibrations. To address this, the gain setting of the system can be adjusted to ensure that the signals remain within a usable range and are not oversaturated.

Figure 4.9: Ambient vibration test during recording on Tipaza historical site.

During the recordings, certain challenges were encountered, such as the presence of strong winds. These environmental factors can introduce additional noise and disturbances into the measurements. However, efforts were made to minimize these inconveniences and ensure that the recorded data remained as reliable and accurate as possible.

4.4.2 Experimental results

The Geopsy software was employed for signal processing and analysis in this study. Fourier spectrum response curves were generated for both the north and east directions for each selected structural element.

The figures below illustrate the Fourier spectrum response curves obtained for the column, wall, and arches. These curves provide a graphical representation of the frequency content and response amplitudes of the vibrations observed in each structural element.

4.4.2.1 The column

For the column, the figure illustrates the Fourier spectrum response curves, captured in both the north and east directions. The selection of these directions was based on the column's known behavior, which exhibits two distinct flexion shape modes in its fundamental state.

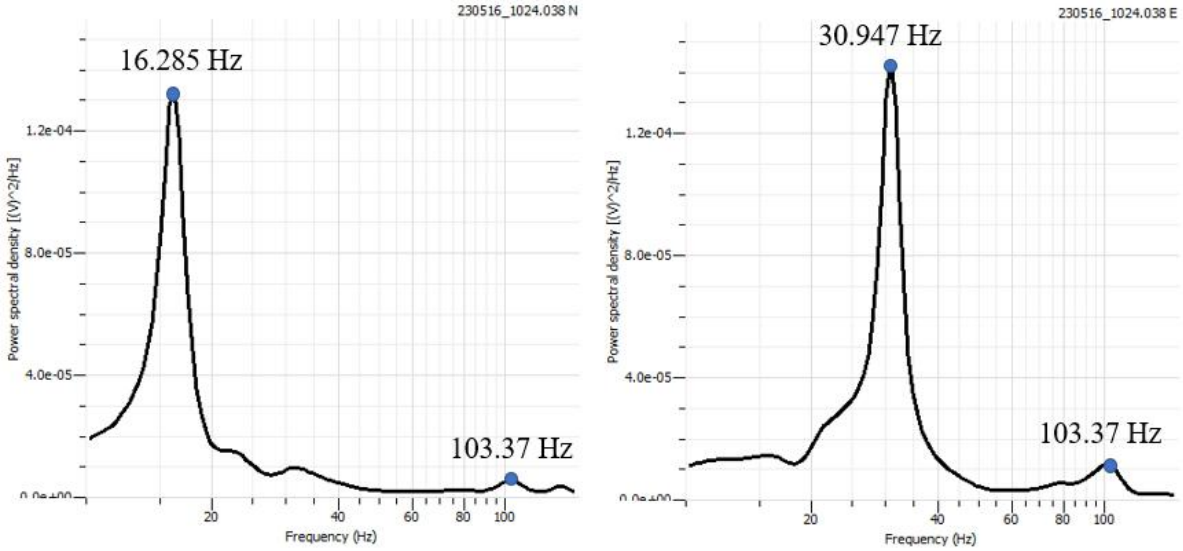

Figure 4.10: The measured Fourier spectrum curves of the column.

Our observation and analysis of the Fourier spectrum response curves for the column were conducted starting from a frequency range above 10 Hz. We made this assumption based on the understanding that peaks observed before 10 Hz are more likely to be attributed to ground and wind effects rather than the inherent structural dynamics of the column.

Upon analyzing the obtained Fourier spectrum response curves, it was observed that the first significant frequency for the column is in the north (N) direction, with a value of 16.285 Hz. The second frequency, measured in the east (E) direction, is 30.947 Hz. However, the observed value for the first frequency does not align with our initial expectations for a square, rigid column. Typically, we would anticipate the first and second frequencies to be very close in value. The deviation between the values may be attributed to the presence of multiple openings in the column, suggesting the possible existence of voids within its structure. Additionally, the partially fixed boundary conditions of the column can introduce slight variations in the observed frequencies. Further analysis and consideration of these factors will be necessary to gain a better understanding of the column's dynamic behavior.

Additionally, it was observed that both the north and east directions exhibit a peak at the same frequency of 103.37 Hz. This peak may indicate the presence of a torsion mode in the column, suggesting rotational vibrations around its central axis. The identification of this mode provides valuable insights into the dynamic behavior and structural response of the column.

4.4.2.2 The wall

The spectrum response curves for the wall are represented in the figure below, the north (N) and the east (E).

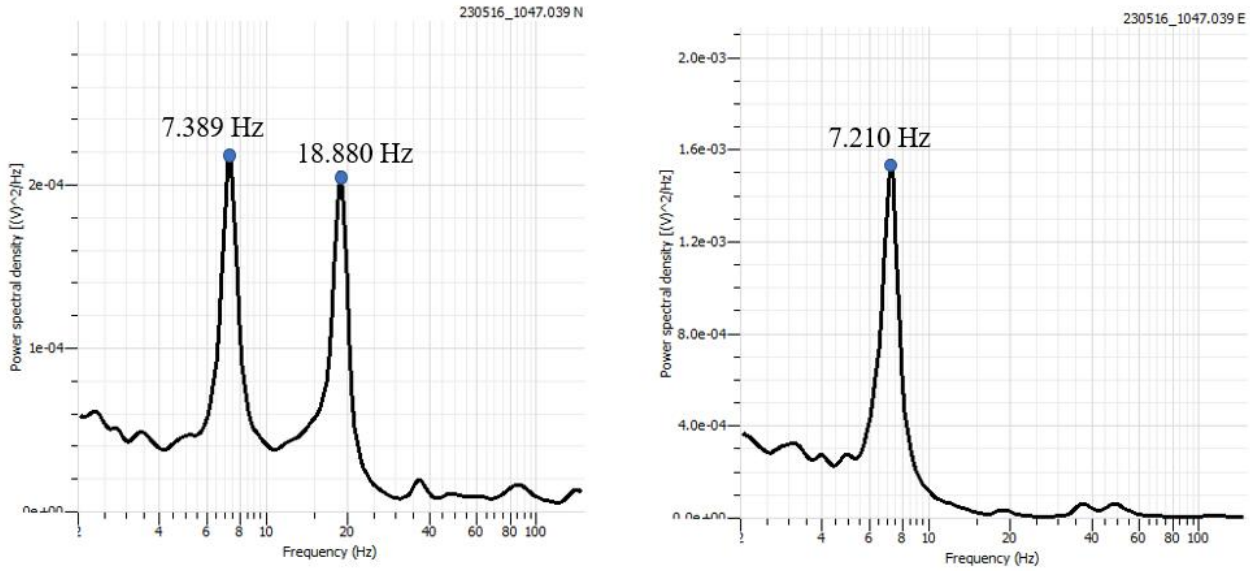

Figure 4.11: The measured Fourier spectrum curves of the wall.

The analysis of the results reveals that the wall exhibits dominant vibration modes in the north (N) and east (E) directions. Two peaks were observed in the north direction, while a single peak was observed in the east direction. Notably, the first peak in the north direction closely resembles the peak in the east direction, indicating a similar mode shape. However, it is important to note that the amplitude of vibrations in the east direction is larger than in the north direction, despite both peaks having the same frequency. This suggests that the first mode shape corresponds to a flexural vibration in the east direction, with a frequency of 7.210 Hz. The second mode shape corresponds to a flexural vibration in the north direction, with a frequency of 18.880 Hz. These findings provide valuable insights into the dynamic behavior of the wall and the distribution of vibrations in different directions.

4.4.2.3 The arches

The figure below illustrates the spectrum response curves for the arches, specifically in the north (N) and east (E) directions.

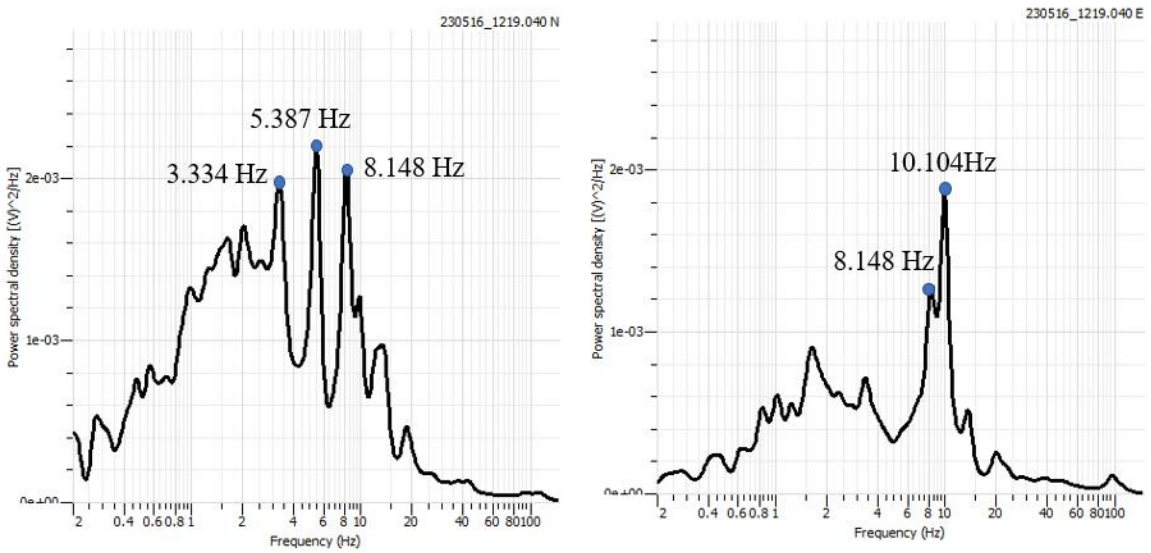

Figure 4.12: The measured Fourier spectrum curves of the arches.

In the case of the arches, the observation of frequencies was initiated after 2 Hz, considering that the peaks before this range were likely caused by the wind's impact on the sensor. Upon analyzing the obtained spectrum response curves, it was observed that there are three peaks in the north (N) direction and two peaks in the east (E) direction. Among these peaks, one particular peak with a value of 8.148 Hz was observed in both directions. However, it was determined that this peak is considered part of the north direction due to its larger amplitude compared to the corresponding peak in the east direction. The frequencies identified in the north direction are 3.334 Hz, 5.387 Hz, and 8.148 Hz, while in the east direction, a frequency of 10.104 Hz was observed.

The table 4.1 provided below displays the experimental frequencies obtained for each structure.

Table 4.1: The experimental natural frequencies of each structure

	Column		**Wall**		**Arches**	
Mode	**Freq (Hz)**	**Direction**	**Freq (Hz)**	**Direction**	**Freq(Hz)**	**Direction**
1	16.285	(N)	7.210	(E)	3.334	(N)
2	30.947	(E)	18.880	(N)	5.387	(N)
3	103.37	Torsion	—	—	8.148	(N)
4	—	—	—	—	10.104	(E)

4.5 Scanned model process description

To acquire a detailed scanned model of the selected structures from the Tipaza historical site, we will employ the photogrammetry process.

4.5.1 Data Acquisition

Starting of the digitizing process of the historic chosen specimens, with the image data acquisition, the same approach as mentioned in chapter 2 was followed to get as much details out of the objects as possible, taking as much photos as needed per object at different angles and elevations, and adjusting the camera settings accordingly to match the lighting across the hole data set.

4.5.1.1 Column:

For the column specimen a dataset of 49 images was taken and used by the alignment program.

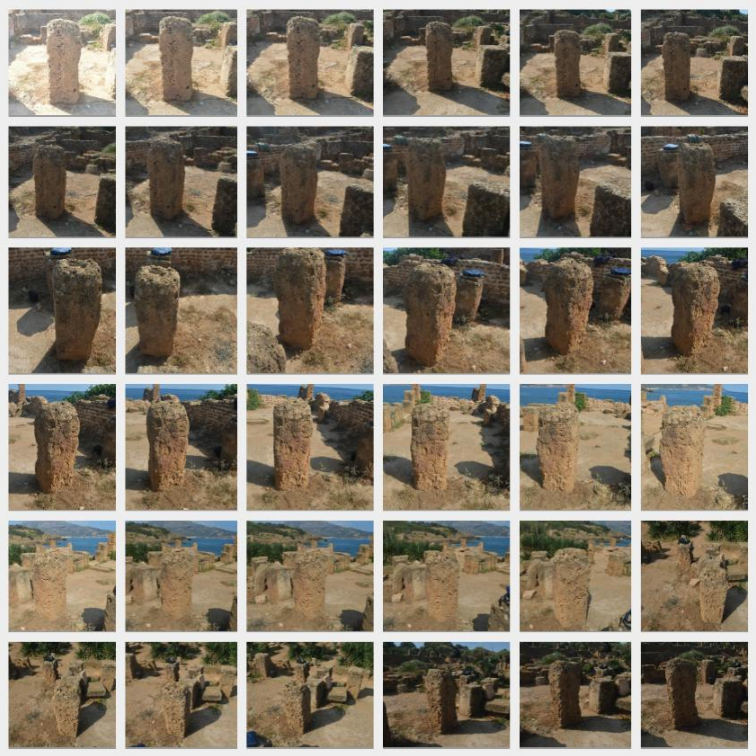

Figure 4.13: Captured image dataset of column.

4.5.1.2 Wall:

For the wall specimen a dataset of 279 images was taken and only 273 was used by the alignment program.

Figure 4.14: Captured images dataset of wall.

4.5.1.3 Arches:

For the Arches specimen a dataset of 478 images was taken and only 458 was used by the alignment program.

Figure 4.15: Captured images dataset of Arches.

NB: It is worth noting that some of the problems mentioned in the photogrammetry process chapter were encountered such as the strong lighting produced by the sun that caused some difficulties while taking pictures when the camera is pointing upwards as well as hard shadows that can compromise the quality of the final model, one other problem is the existence of some vegetation with the scanned objects which added more work in the processing phase.

4.5.2 Alignment and meshing

4.5.2.1 Column:

For the column an automatic alignment was used and it produced a total of 244350 points cloud

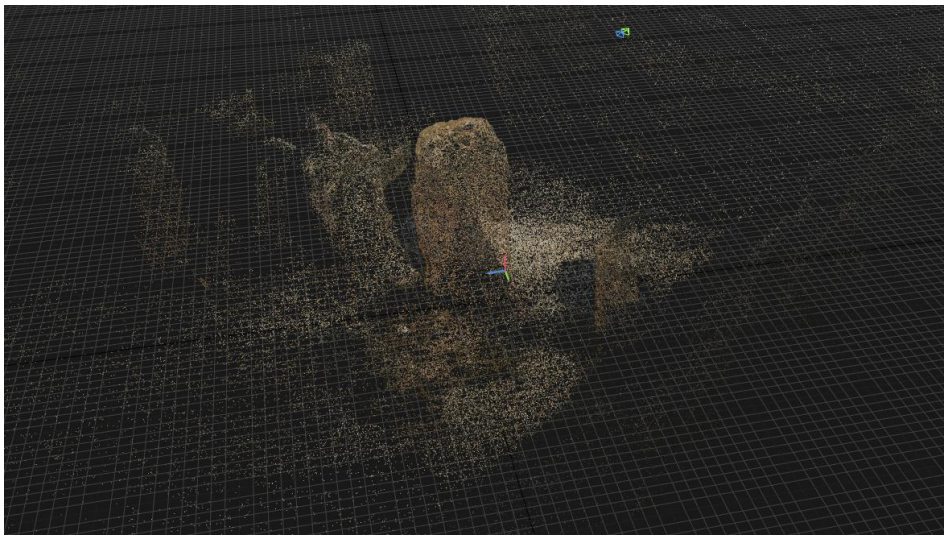

Figure 4.16: Point Cloud of the column model.

Figure 4.17: Calculated mesh of the column model.

4.5.2.2 Wall:

For the wall specimen on the other hand a manual alignment was required as the automatic one produced two different components, this was a result of missing image data from the top part, and to resolve that control points were created to merge the different components into one and give a single meshes model at the end, a point cloud of 933925 points was produced.

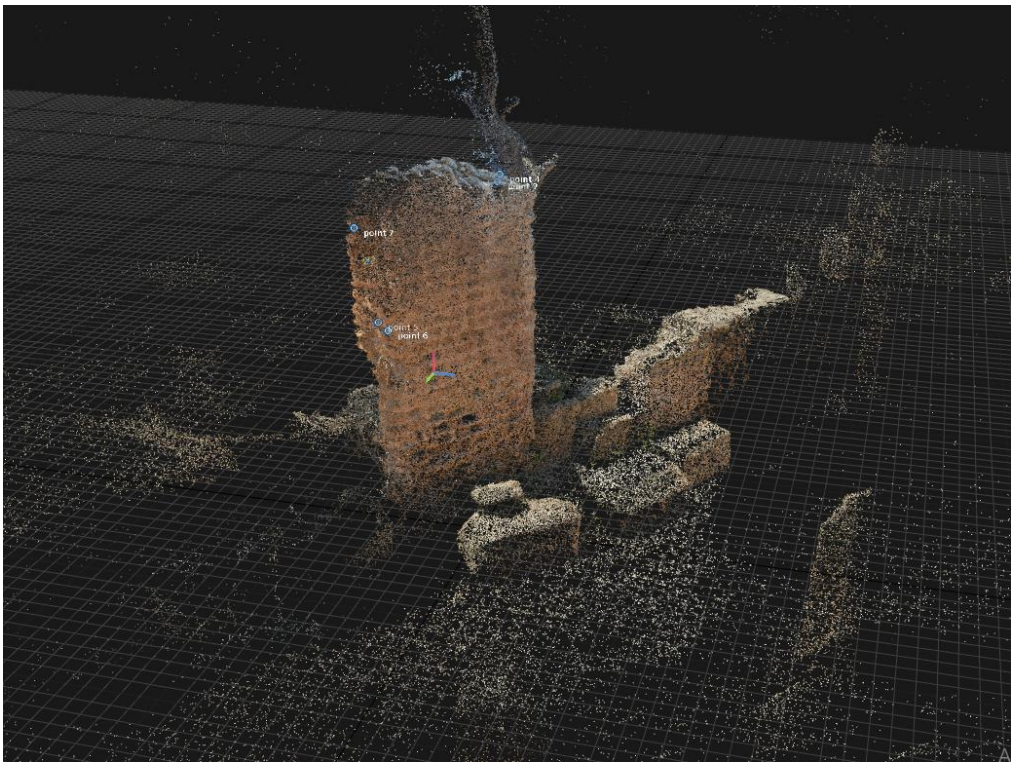

Figure 4.18: Point Cloud of the wall model.

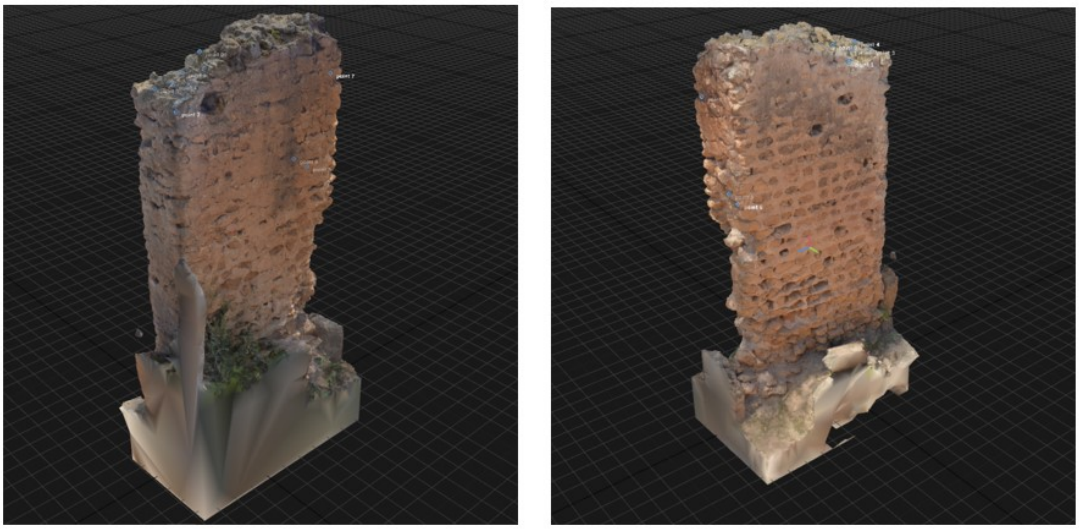

Figure 4.19: Calculated mesh of the wall model.

4.5.2.3 Arches:

The manual alignment was not needed in the arches model thanks to the large number of images taken and the amount of angles covered, a point cloud of 1455321 points was produced.

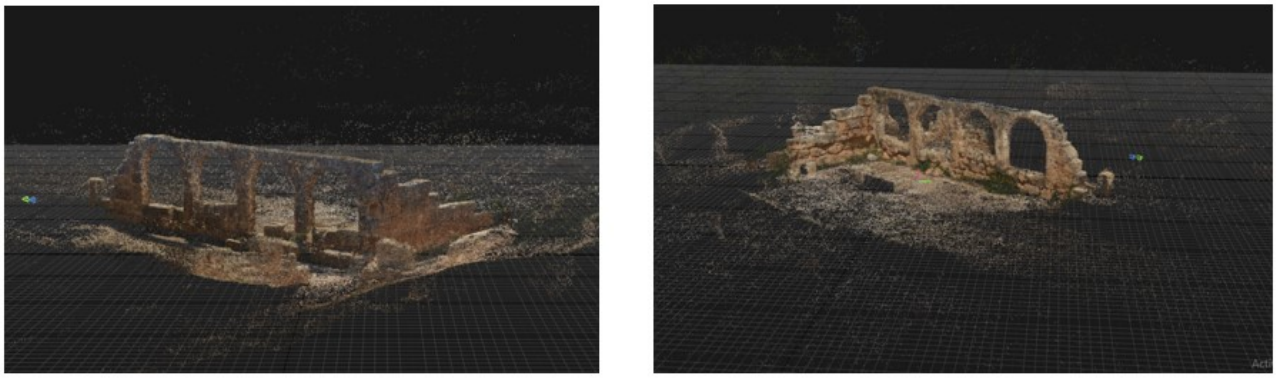

Figure 4.20: Point Cloud of the arches model.

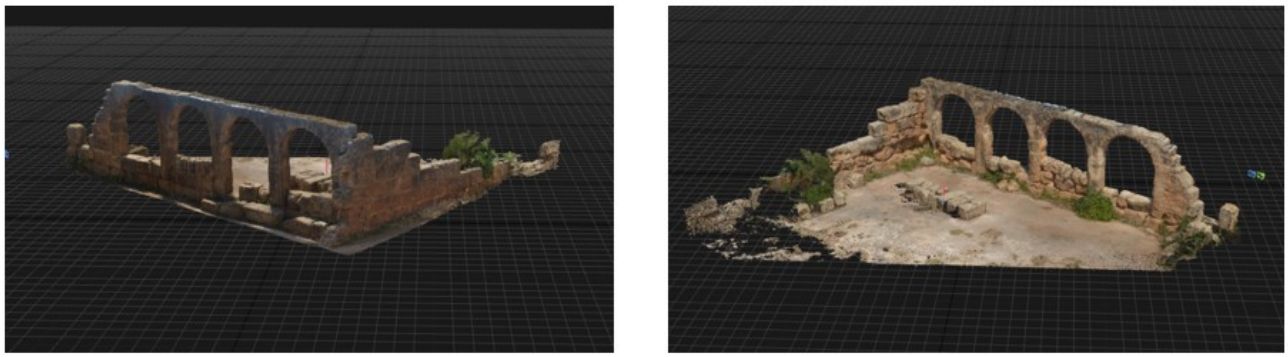

Figure 4.21: Calculated mesh of the arches model.

4.5.3 Processing

For processing the historic specimens after meshing them in RealityCapture roughly the same method described prior was used, simple Boolean operations were used to remove unwanted mesh parts, and smoothing as well as reducing the number of mesh elements was performed, resizing and calibration were taken into consideration as well so the models can be exported to Comsol for analysis.

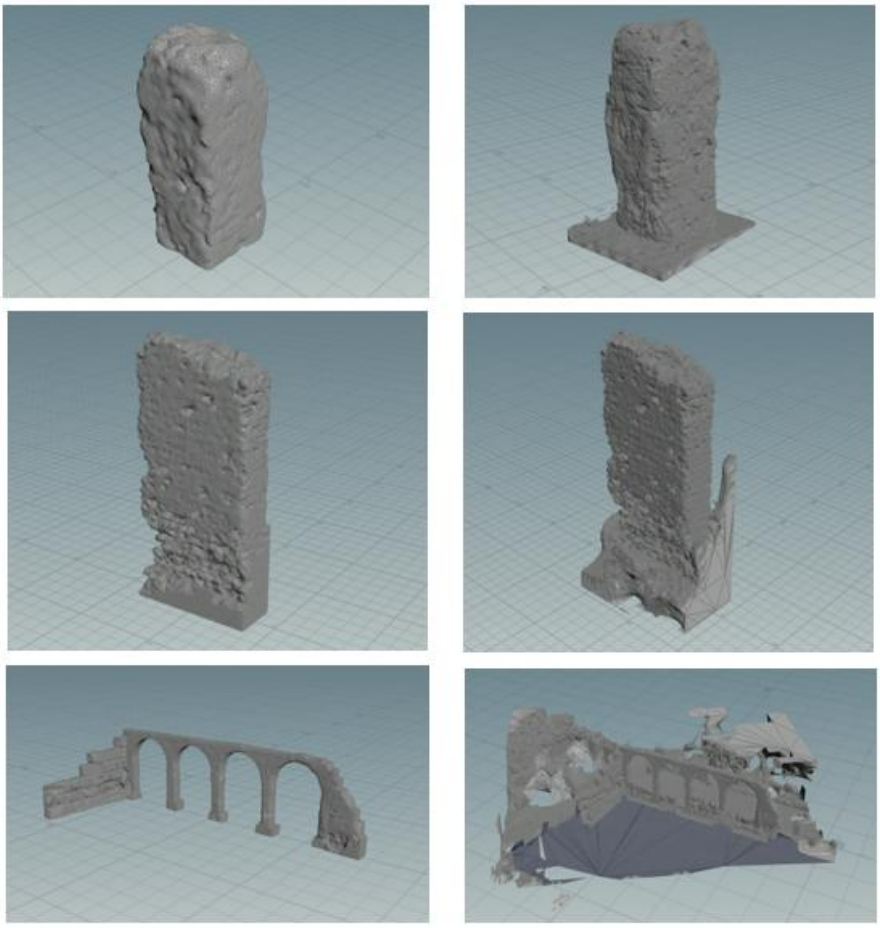

Figure 4.22: Models before (right) and after (left) processing.

4.5.4 FE Model

Unlike the RC beam and the steel column where we used the geometry import in Comsol, here we used the mesh import to directly import the Houdini surface mesh and add a tetrahedral node after that to mesh the volume of the objects.

4.5.4.1 Column:

The generated column mesh had 50310 tetrahedral elements and 238302 DoFs.

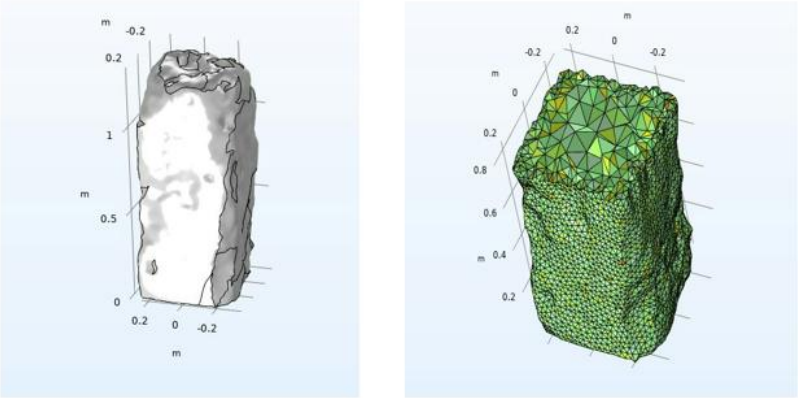

Figure 4.23: Comsol Column model and Tetrahedral Mesh.

4.5.4.2 Wall:

The generated wall mesh had 126283 tetrahedral elements and 599025 DoFs.

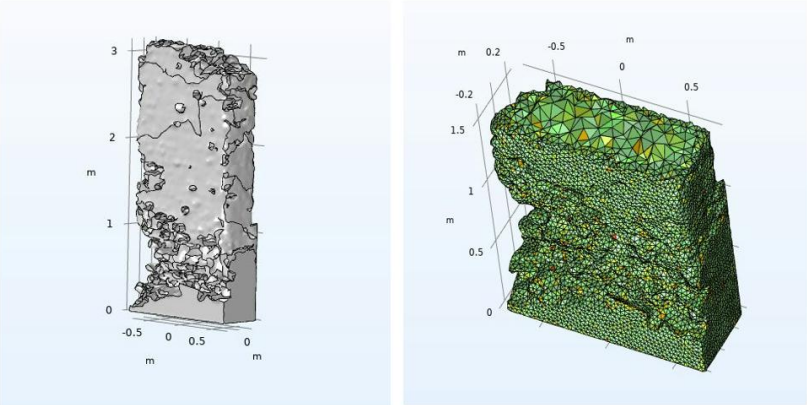

Figure 4.24: Comsol wall model and Tetrahedral Mesh.

4.5.4.3 Arches:

The generated arches mesh had 107929 tetrahedral elements and 533151 DoFs.

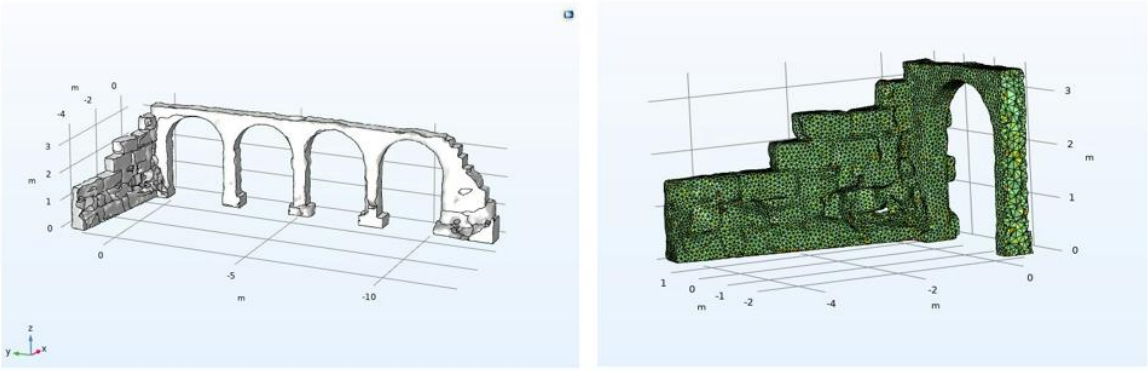

Figure 4.25: Comsol arches model and Tetrahedral Mesh.

4.6 Material properties optimization

4.6.1 Definition of Genetic Algorithm (GA)

Genetic algorithms (GAs) are optimization techniques that draw inspiration from genetics, natural selection, and evolution. These algorithms find applications in various fields such as finance, function optimization, and planning, among others. GAs is favored for their simplicity and efficiency. The core principle of a genetic algorithm involves manipulating potential solutions to a given problem iteratively, with the ultimate goal of reaching an optimal or satisfactory solution. To understand the workings of a genetic algorithm, it is important to familiarize oneself with certain fundamental terms which are [23]:

- **Individual:** represents a potential solution to the problem.
- **Chromosome:** represents a potential solution to the problem encoded as a sequence or string of characters.
- **Population:** is a finite collection of individuals or solutions.
- **Gene:** refers to a non-divisible elementary part or character of a chromosome.
- **Fitness:** is the evaluation function of an individual, which is linked to the objective function to be optimized. The fitness function determines the performance level of an individual (and thus a solution) relative to the problem.

4.6.2 The concept of the Genetic Algorithm (GA)

The genetic algorithm is derived from Darwin's theory of evolution, where the principles of natural selection and genetic inheritance are applied to solve optimization problems. By mimicking the mechanisms of natural selection, genetic algorithms iteratively improve potential solutions in a population, leading to the emergence of fitter individuals over generations. This approach allows for the exploration and exploitation of solution spaces, eventually converging towards optimal or satisfactory solutions [23].

Genetic algorithms employ several key operators that are essential to their functioning and evolution, these operators can be categorized into three main types [23]:

- **Selection:** The selection operator in genetic algorithms serves a similar purpose to natural selection, adhering to the fundamental principle of Darwinian theory that favors the survival of the fittest individuals. It determines the individuals that will continue to the next generation and those that will be eliminated, based on their fitness functions. The selected individuals form the subsequent population that will undergo further genetic operations.
- **Crossover:** The crossover operator facilitates the exchange of genetic information, specifically genes, between a pair of selected individuals. This process involves taking two individuals, referred to as parents, and combining their genetic material to

generate new individuals that inherit a combination of their traits. Various techniques can be utilized for crossover, such as one-point crossover, two-point crossover, or uniform crossover, depending on the specific problem domain. The goal is to introduce diversity and explore different genetic combinations in the population.

- **Mutation:** The mutation operator enables the exploration of new points within the search space and prevents the algorithm from getting trapped in local optima. By randomly modifying genes within an individual, mutation introduces small changes that allow for the exploration of different regions of the solution space. The mutation rate determines the probability of a gene being altered, controlling the extent of exploration. Through mutation, the algorithm can potentially discover better solutions that may have been overlooked through other operators like selection and crossover.

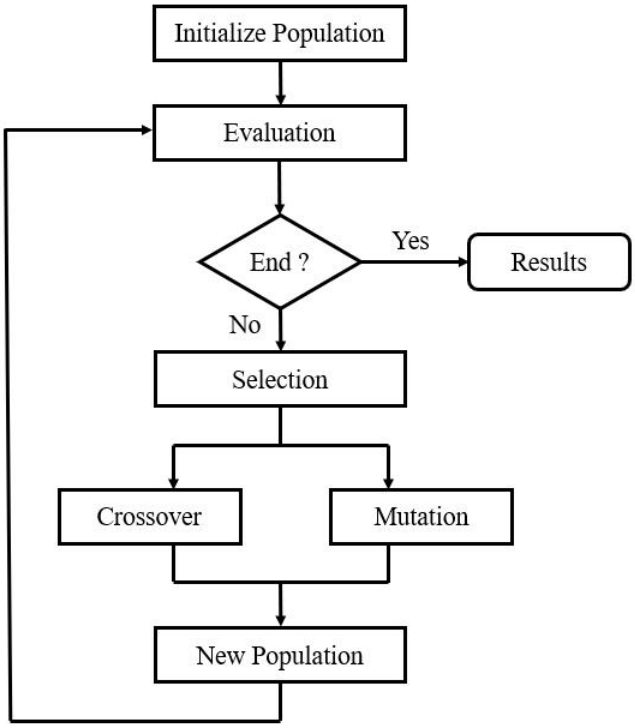

Figure 4.26: Flowchart of a simple genetic algorithm [23].

4.6.3 Optimization process

The primary objective of our work is to enhance the accuracy of the scanned model by comparing its predicted modal characteristics with the experimental data. This is accomplished by evaluating unknown structural parameters using an optimization process that minimizes the error between observed data and numerical predictions. In this particular case, the two key properties influencing the model frequencies, namely Young's modulus and density, were selected for prediction. To achieve this, a genetic algorithm was employed with an objective function that quantifies the sum of squared difference between experimental and simulated frequencies. The fitness function was defined as the inverse of

the objective function, transforming the problem into a minimization task, where the aim is to maximize fitness. The optimization procedure requires careful selection of suitable parameters and strategies to achieve effective convergence and accurate estimation of the desired structural properties.

4.6.3.1 Population Initialization

To initiate the genetic algorithm, a population of individuals is generated, with each individual representing a potential solution. These individuals are encoded with values for Young's modulus and density. In this case, an initial population of 40 individuals is created. The values for Young's modulus and density are assigned randomly within the specified ranges of 1 to 3 GPa and 1400 to 2400 kg/m^3, respectively. This ensures a diverse set of initial solutions for further evolution and optimization.

4.6.3.2 Fitness evaluation

After the creation of the initial population, our next step is to select the most promising individuals who will contribute to the improvement of our population. To accomplish this, we evaluate each individual's fitness by calculating the objective function. The objective function quantifies the discrepancy between the experimental and simulated frequencies, incorporating the participation ratio of each mode. By calculating the sum of squared differences and considering the mode participation, we obtain a fitness score for each individual. By ranking the individuals based on their fitness scores, we can pinpoint the most promising individuals within the population who exhibit superior performance.

The equation of the objective function can be expressed as follows:

$$\text{Objective Function} = \sum_i \alpha_i \cdot \left| \frac{f_{\text{num}_i} - f_{\text{exp}_i}}{f_{\text{exp}_i}} \right| \tag{4.1}$$

In this equation, the objective function is calculated by summing the absolute differences between the simulated frequency (f_{num_i}) and the experimental frequency (f_{exp_i}), normalized by the experimental frequency. The weights (α_i) are used to assign importance to each frequency component.

The coefficients (α_i) represent the weights proportional to the amplitude of relative peaks of the selected number of correlated modes. The sum of all α_i coefficients is equal to 1, i.e.,

$$\sum \alpha_i = 1. \tag{4.2}$$

4.6.3.3 Creating New Individuals

- **Selection:**

  Selection plays a crucial role in the genetic algorithm by determining which individuals from the current population will have the opportunity to reproduce. Its purpose is to evaluate the performance of each individual using the objective function and

make decisions regarding their survival, reproduction, or elimination. There are various selection methods available, including roulette wheel selection, rank-based selection and tournament selection [23].

In our specific case, we have opted for rank-based selection to choose the individuals for crossover. This method involves two stages. Firstly, the individuals are arranged in either ascending or descending order based on their performance. Then, a selection procedure similar to roulette wheel selection is applied, where each individual is assigned a probability of selection based on their rank. This approach reduces the likelihood of selecting the same individual multiple times, which can occur with other selection methods like roulette wheel selection. By assigning probabilities according to relative performance, individuals that are well-adapted to their environment gain a natural advantage and are more likely to contribute to the reproduction process.

- **Crossover:**

  Crossover involves the exchange of genetic information between selected individuals to create offspring. In our genetic algorithm, we employ a single-point crossover technique. This means that a random crossover point is selected along the chromosome, and the genetic material before and after that point is exchanged between two parent individuals.

  Example: Let's consider two parent individuals from the population:

  Parent 1: [1.8 GPa, 1600 kg/m^3]

  Parent 2: [2.5 GPa, 2000 kg/m^3]

  A random crossover point is selected, let's say at index 1. After crossover, the offspring individuals are formed:

  Offspring 1: [1.8 GPa, 2000 kg/m^3]

  Offspring 2: [2.5 GPa, 1600 kg/m^3]

- **Mutation:**

  Mutation introduces random changes to the genetic material of an individual. It helps to explore new solutions by adding small variations to the existing ones. In our genetic algorithm, we use a random mutation approach, where a randomly selected gene is modified within an individual.

  Example: Consider an individual from the population:

  Individual: [1.9 GPa, 1800 kg/m^3]

  A random gene is selected, let's say the density gene at index 1. After mutation, a small random change is applied to the selected gene:

  Mutated Individual: [1.9 GPa, 1850 kg/m^3]

By applying selection, crossover and mutation operations, the genetic algorithm creates new individuals that possess a combination of genetic information from the parent individuals and introduce random variations. This process allows for the exploration of different solutions and increases the chances of finding optimal or satisfactory solutions to our problem.

4.6.4 Termination criterion

After generating new individuals through crossover and mutation, we proceed to select the individuals who will contribute to the improvement of our population. This selection process ensures that the fittest individuals, those with higher fitness values, are chosen to continue in the optimization process.

As in any iterative algorithm, it is necessary to define a termination criterion. In our problem, we have several options for the termination criterion [23]:

- Termination when a satisfactory solution is reached: The algorithm stops when the result meets a predefined criterion of satisfaction. This criterion could be, for example, reaching a specific threshold of accuracy or meeting certain performance requirements.
- Termination if there is no improvement for a certain number of generations: If there is no improvement in the fitness of the individuals for a specified number of generations, the algorithm stops. This helps prevent the algorithm from running indefinitely without making progress.
- Termination after a certain number of generations: The algorithm stops after a predefined number of generations have been completed. This ensures that the optimization process has sufficient iterations to explore different solutions and converge towards an optimal or satisfactory result.

In our problem, we have chosen to terminate the algorithm after 6 generations. Once these generations have been completed, the optimization process concludes. The best individual in terms of fitness, which represents the estimated values of Young's modulus and density for the Tipaza structures, is identified. This individual provides the most optimal and satisfactory solution for our problem.

4.7 Results and discussions

Using the genetic algorithm (GA) as part of our optimization process, we aimed to estimate the Young's modulus (E) and density values for different structural components such as the column, wall, and arches. To evaluate the accuracy of our estimations, we compared the simulated frequencies, which were obtained by applying the estimated properties, with the experimental frequencies. This comparison enabled us to assess the reliability of our predictions. The GA implementation was carried out using the Python programming language. Based on our GA optimization, we obtained the following results:

Table 4.2: Estimated Material Properties for Each Element Obtained from GA.

Component	**Young modulus (GPa)**	**Density (Kg/m^3)**
Column	1.79	2370
Wall	1.96	1800
Arches	1.17	2150

Table 4.3: Comparison of Simulated and Experimental Frequencies for Different structures.

	Mode 1	Mode 2	Mode 3	Mode 4
	Column			
Experimental Frequency (Hz)	—	30.947	103.37	—
Simulated Frequency (Hz)	37.110	37.408	101.610	—
Error (%)	—	20.88	1.70	—
	Wall			
Experimental Frequency (Hz)	7.210	18.880	—	—
Simulated Frequency (Hz)	7.435	19.030	—	—
Error (%)	3.12	0.80	—	—
	Arches			
Experimental Frequency (Hz)	3.334	5.387	8.148	10.104
Simulated Frequency (Hz)	3.588	5.706	8.846	9.300
Error (%)	7.61	5.92	8.57	7.96

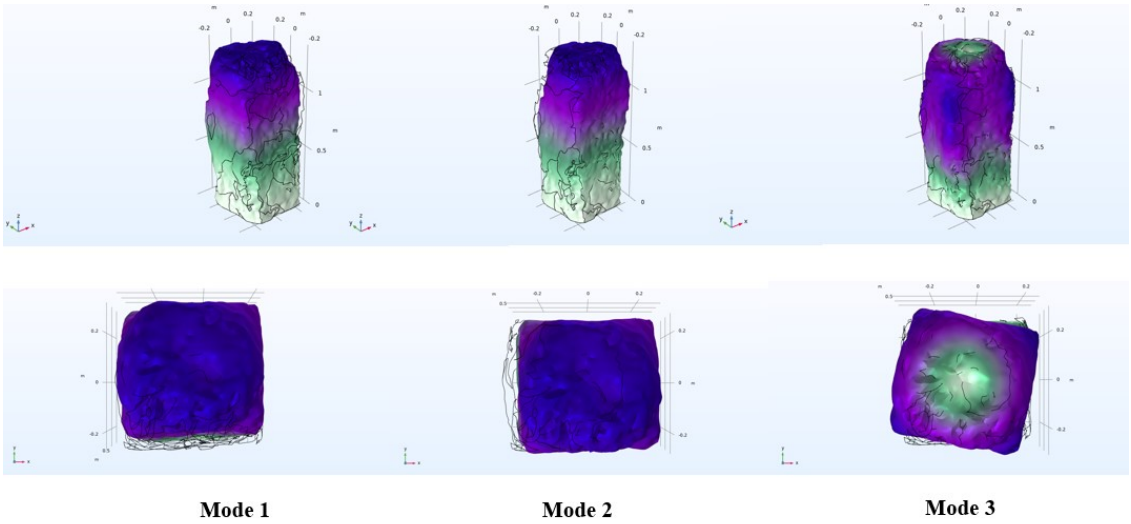

Figure 4.27: Shape modes of column.

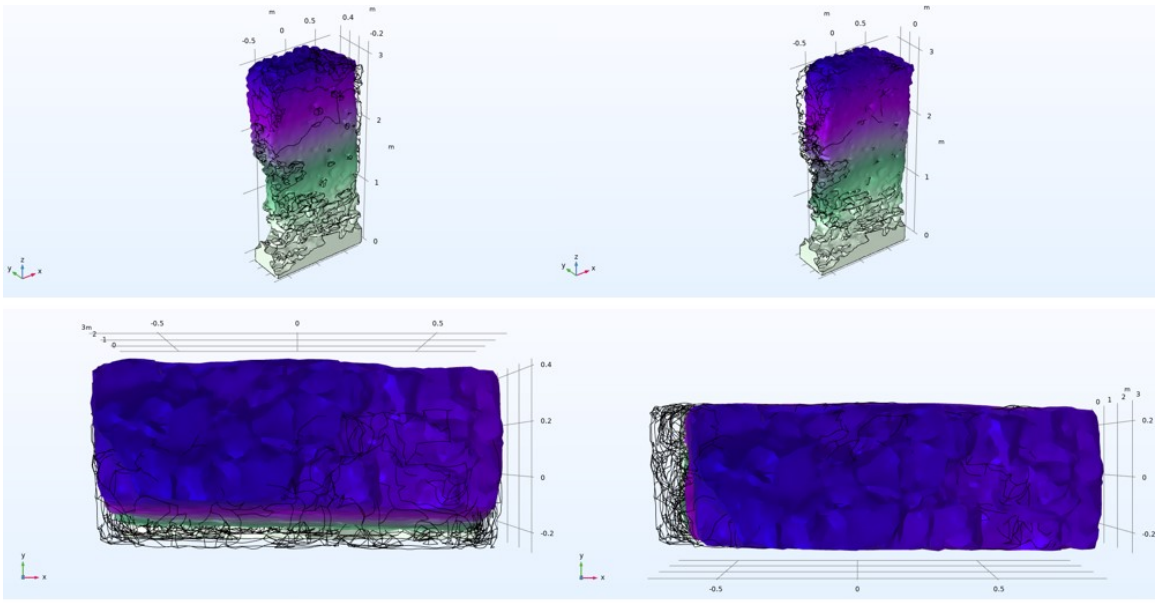

Figure 4.28: Shape modes of wall.

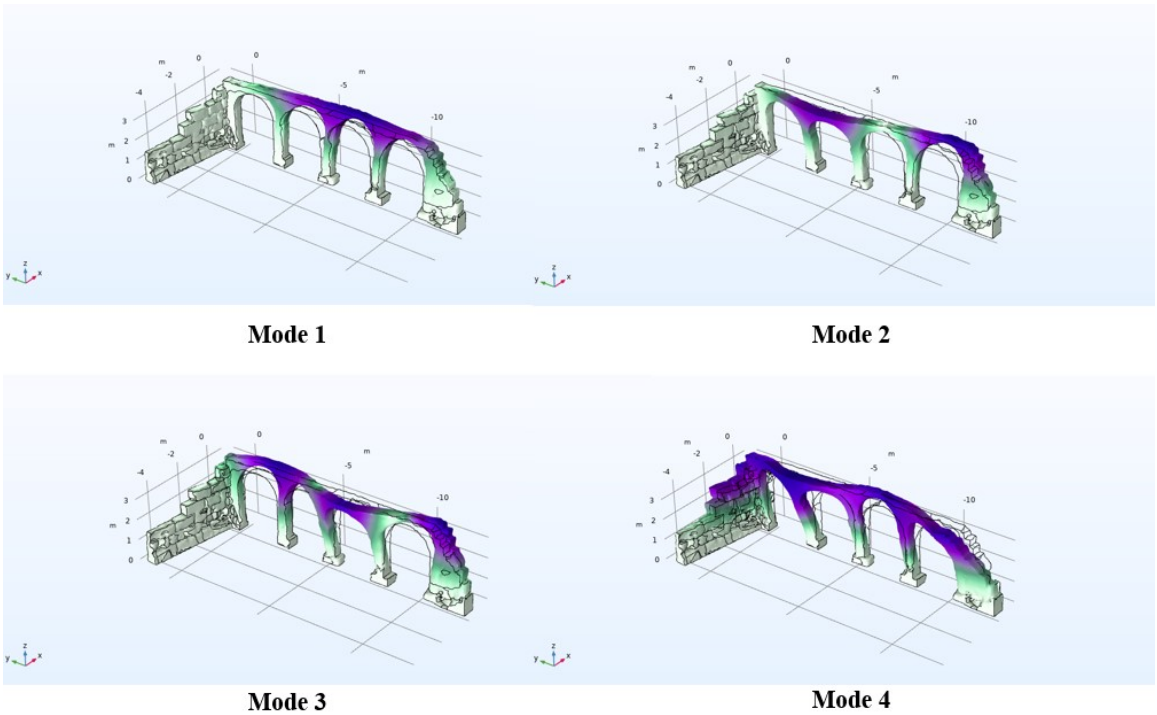

Figure 4.29: Shape modes of arches.

For the **column**, the disparities between the simulated and experimental frequencies can be ascribed to multiple factors. Notably, the existence of voids in the real column structure deviates from the idealized assumptions employed in the simulation. Furthermore, the boundary conditions in reality may not precisely correspond to the assumed complete fixation in the simulation. These imperfections in the actual column play a substantial role in affecting its frequencies and account for the observed discrepancies.

Regarding the **wall**, our optimization process yielded a reasonable estimation of the material properties, with relative errors of 3.12% and 0.8% in frequencies. It is important to consider the presence of imperfections such as cracks and voids in the actual wall, as these can contribute to the observed errors. However, even with these imperfections, the results obtained are in the range of common similar historical materials.

For the **arches** , the Young's modulus and density of the arches were estimated as 1.17 GPa and 2150 kg/m3, respectively. The matching procedure yields relative errors for the frequencies ranged from 6% to 8.6% which justify the obtained values of the density and Young's modulus. The low values of the latter is attributed to the presence of imperfections, variations in material composition, and the effects of cracks and voids. The differences in material properties among the three elements confirm the variability in the observed condition of these elements.

4.8 Conclusion

In conclusion, the obtained estimations contribute to a better understanding of the structural characteristics of the column, wall, and arches, providing valuable insights for the photogrammetry process. Despite the complexities and challenges associated with accurately estimating material properties, our approach utilizing photogrammetry has proven to be a viable and effective technique. This study demonstrates the utility of photogrammetry, especially when dealing with complex forms of sections and elements, as well as large-scale structures, albeit with certain limitations. The successful application of photogrammetry in this study validates its potential as a valuable tool for future investigations and assessments of similar structures. The integration of photogrammetry, AVT, and AI-based optimization genetic algorithm provides a robust and reliable approach for determining material properties in existing structures. The combined utilization of these techniques contributes to a better understanding of the structural behavior, aiding in expert analysis, and facilitating the preservation of historical monuments.

It is important to acknowledge the limitations and areas for improvement, such as further refinement of the estimation process and considering additional factors that influence structural behavior.

Conclusion and Perspectives

The main objective of the study is to explore the potential uses and benefits of photogrammetry in capturing and modeling existing structures. Through a comprehensive examination of the principles, advancements, and limitations of photogrammetry, valuable insights have been obtained.

The study highlighted the significance of photogrammetry in generating simulation-ready 3D models. It emphasized the importance of this technique in the civil engineering domain and its potential to enhance various aspects of the construction industry.

The limitations inherent to photogrammetry were thoroughly discussed, and potential solutions were explored to overcome these challenges. The integration of photogrammetry with Building Information Modeling (BIM) and Historic Building Information Modeling (HBIM) was also examined, showcasing how it can contribute to these fields.

In first instance, the study presented a step-by-step procedure for the 3D digitization of photogrammetry, and this process was accomplished successfully. The study provided comprehensive guidelines that encompassed various stages of the procedure, such as obtaining data, aligning images, reconstructing mesh, processing mesh, calibration, and creating finite element model. To effectively showcase the process, a laboratory column specimen was utilized, and the study offered detailed explanations regarding the tools and software employed in the process.

The major focus of the study provided valuable insights into the dynamic behavior of the investigated structures. By determining the natural frequencies of each structural element, AVT enhanced our understanding of their fundamental modes of vibration.It is important to note that the accuracy and precision of AVT results can be influenced by various factors, including the complexity and size of the structural elements. The primary focus of the present study is to propose a hybrid technique that utilizes photogrammetry to create 3D models and control deformations under loading conditions, along with ambient vibration testing for experimental modal analysis. To achieve this objective, a small-scale reinforced concrete (RC) beam was employed in the laboratory. The modal characteristics of the beam were initially determined, and the displacement was continuously monitored until failure. Additionally, a finite element (FE) model was developed and validated against the experimental results.

Furthermore, the proposed technique has been applied to identify the global material properties of historic monuments. Three elements of increasing complexity were selected from the Tipaza historic site and subjected to testing. A genetic algorithm was employed to identify the global material characteristics by comparing the experimentally obtained frequencies with the 3D finite element (FE) models based on photogrammetric data.

Finally, the report represents a significant contribution to the field by expanding our understanding of photogrammetry and its applications in structural analysis. The findings highlight the remarkable potential of photogrammetry as a powerful tool for investigating and evaluating existing structures, driving advancements in the field and promoting the development of digital technologies in the construction and preservation sectors. The

outcomes of this study contribute to the existing body of knowledge in photogrammetry and establish a solid foundation for future research and practical applications in the field of structural engineering.

Bibliographie

[2] Albertz, Jörg and Wiedemann, Albert. "From analogue to digital close-range photogrammetry". *First Turkish-German Joint Geodetic Days* (1995), pp. 245–253.

[4] American Society of Photogrammetry. *Manual of photogrammetry*. 4th ed. Falls Church, VA: Chester C, 1980. ISBN: 978-0-935-403-00-2.

[5] AMIRTHARAJAH Meninger S. Mur-Miranda JO et JH, R. Chandrakasan A. Lang. "Vibration-to-electric energy conversion". *IEEE Transactions on Very Large Scale Integration (VLSI) Systems* 9.1 (2001), p. 64.

[6] Asgarian, A and McClure, G. "Using ambient vibration measurements to generate experimental floor response spectra and inter-story drift curves of reinforced concrete (RC) buildings". *Procedia engineering* 199 (2017), pp. 92–97.

[8] Belbut Gaspar, M. "Small scale 3D scanning: an assessment of capabilities and limitations of photogrammetry technique". *Proceedings of ICDDMAP 2021*. 2021. DOI: 10.13140/RG.2.2.10146.71367.

[9] BENALI AOUDIA, L. and CHENNAOUI, Y. "The Archaeological Site of Tipasa, Algeria: What Kind of Management Plan?" *Conservation and Management of Archaeological Sites* 19.3 (2017), pp. 173–196. (Accessed on: [Accessed on: 06/03/2023]). https://doi.org/10.1080/13505033.2017.1348853.

[10] Birtharia, A and Jain, SK. "Applications of ambient vibration testing: An overview". *Int. Res. J. Eng. Technol* 2 (2015), pp. 845–852.

[11] Conde, Antonio J Loredo, García-Sanz-Calcedo, Justo, and Rodríguez, Antonio M Reyes. "Use of BIM with photogrammetry support in small construction projects. Case study for commercial franchises". *Journal of Civil Engineering and Management* 26.6 (2020), pp. 513–523.

[12] Demirtas, B, Bayraktar, Alemdar, and Dumanoglu, A. "Model updating effects on the seismic behavior of tall buildings under far and near-fault ground motions". *Research on Engineering Structures & Materials* 3.2 (2017), pp. 99–112.

[14] Douglass, Matthew, Lin, Sam, and Chodoronek, Michael. "The application of 3D photogrammetry for in-field documentation of archaeological features". *Advances in Archaeological Practice* 3.2 (2015), pp. 136–152. ISSN: 2326-3768. DOI: 10.7183/2326-3768.3.2.136.

[15] Ebert, James I. "Photogrammetry, photointerpretation, and digital imaging and mapping in environmental forensics". *Introduction to environmental forensics*. Elsevier, 2015, pp. 39–64.

[16] Eldar, Yonina C. "Fourier analysis". *Sampling Theory: Beyond Bandlimited Systems*. Cambridge University Press, 2015, pp. 67–93. DOI: 10.1017/CBO9780511762321.004.

[18] fib. *fib Model Code for Concrete Structures 2010*. Wiley-VCH, 2013. ISBN: 978-3-433-03061-5. https://onlinelibrary.wiley.com/doi/book/10.1002/9783433604090.

[20] Gilvear, David and Bryant, Robert. "Analysis of remotely sensed data for fluvial geomorphology and river science". *Tools in fluvial geomorphology* (2016), pp. 103–132.

[22] González-Jorge, H et al. "Photogrammetry and laser scanner technology applied to length measurements in car testing laboratories". *Measurement* 45.3 (2012), pp. 354–363.

[23] HELLAL, A. "Métaheuristiques Algorithmes Génétiques". National Polytechnic School, 2020-2021, p. 27.

[24] Ivanovic, Sanja S, Trifunac, Mihailo D, and Todorovska, MI. "Ambient vibration tests of structures-a review". *ISET Journal of earthquake Technology* 37.4 (2000), pp. 165–197.

[26] Kalinichenko, M Yu et al. "Optimization of the regeneration of the sodium-cation ion-exchange filter". *IOP Conference Series: Materials Science and Engineering*. Vol. 905. 1. IOP Publishing. 2020, p. 012034.

[27] Kent, Jake and Burt, Aidan. "Photogrammetry as a finite element modelling geometry builder". *Proceedings of Meetings on Acoustics ICUA2022*. Vol. 47. 1. Acoustical Society of America. 2022, p. 022001.

[29] Konecny, Gottfried. "The International Society for Photogrammetry and Remote Sensing-75 years old, or 75 years young". *Photogrammetric Engineering and Remote Sensing* 51.7 (1985), pp. 919–933.

[30] KRSTEVSKA, Lidija, RUNEVSKI, Kristijan, and NAUMOVSKI, Nikola. "Ambient vibration testing of historical monuments within monastery complex "TRESKAVEC" NEAR PRILEP" ().

[32] Linder, Wilfried. *Digital photogrammetry*. Berlin/Heidelberg, Germany: Springer, 2009. ISBN: 978-3-540-89464-9.

[34] Luhmann, Thomas et al. *Close-Range Photogrammetry and 3D Imaging*. Berlin, Boston: De Gruyter, 2020. DOI: 10.1515/9783110607253.

[35] Martínez-Carricondo, Patricio et al. "Combination of HBIM and UAV photogrammetry for modelling and documentation of forgotten heritage. Case study: Isabel II dam in Níjar (Almería, Spain)". *Heritage Science* 9.1 (2021), pp. 1–15.

[39] Mugabo, Ignace et al. "Ambient vibration measurement data of a four-story mass timber building". *Frontiers in Built Environment* 5 (2019), p. 67.

[40] Multiphysics, COMSOL. "Introduction to comsol multiphysics®". *COMSOL Multiphysics, Burlington, MA, accessed Feb* 9.2018 (1998), p. 32.

[41] Obst, Maciej, Wasilewicz, Piotr, and Adamiec, Jarosław. "Experimental investigation of four-point bending of thin walled open section steel beam loaded and set in the shear center". *Scientific Reports* 12.1 (2022), p. 7275.

[42] Ottosen, N. S. *Nonlinear finite element analysis of concrete structures*. Tech. rep. Risø-R-411. DK-4000 Roskilde, Denmark: Risø National Laboratory, May 1980.

[43] Ottosen, Niels Saabye. "A failure criterion for concrete". *Journal of the Engineering Mechanics Division* 103.4 (1977), pp. 527–535.

[44] Ottosen, Niels Saabye and Ristinmaa, Matti. *The mechanics of constitutive modeling*. Elsevier, 2005.

[47] Rashdi, Rabia et al. "Scanning Technologies to Building Information Modelling: A Review". *Infrastructures* 7.4 (2022), p. 49.

[49] Saif, W. "A Brief Historical Overview" (2022). DOI: 10.13140/RG.2.2.27518.87369.

[52] SEKER, Dursun Z and DURAN, Res Asist Zaide. "TERRESTRIAL & NUMERICAL PHOTOGRAMMETRY". *Lecture Note. Istanbul Technic Universities* (2001).

[54] Stojaković, Vesna. "Terrestrial photogrammetry and application to modeling architectural objects". *Facta universitatis-series: Architecture and Civil Engineering* 6.1 (2008), pp. 113–125.

[55] Tsoraeva, EN et al. "Application of photogrammetric methods in architecture, construction and land management". *IOP Conference Series: Materials Science and Engineering*. Vol. 1083. 1. IOP Publishing. 2021, p. 012052.

[58] Valentine, Daniel T and Hahn, Brian H. *Essential MATLAB for engineers and scientists*. Academic Press, 2022.

[61] Yang, Xiucheng et al. "Review of built heritage modelling: Integration of HBIM and other information techniques". *Journal of Cultural Heritage* 46 (2020), pp. 350–360.

Webographie

[1] 3D Sourced. *Photogrammetry Guide [Online]*. [Accessed: 15/05/2023]. Available at: https://www.3dsourced.com/guides/photogrammetry-guide/.

[3] All the Science. *What is Aerial Photogrammetry? [Online]*. [Accessed: 24 April 2023]. Available at: https://www.allthescience.org/what-is-aerial-photogrammetry.htm.

[7] Autodesk. *Building Information Modeling (BIM) [Online]*. [Accessed: 04/05/2023]. Available from: https://www.autodesk.com/industry/aec/bim.

[13] DIY Drones. *Aerial Photogrammetry vs. Terrestrial Photogrammetry [Online]*. [Accessed: 24 April 2023]. Available at: https://diydrones.com/profiles/blogs/aerial-photogrammetry-vs-terrestrial-photogrammetry.

[17] Epic Developer Community. *Learning Library [Online]*. [Accessed: 22/02/2023]. Available at: https://dev.epicgames.com/community/unreal-engine/learning.

[19] Geodetic Systems. *Basics of Photogrammetry – Geodetic Systems, Inc [Online]*. [Accessed: 24 April 2023]. Available at: https://www.geodetic.com/basics-of-photogrammetry/.

[21] GIS Lounge. *A Brief Introduction to Photogrammetry and Remote Sensing [Online]*. [Accessed: 25/04/2023]. Available at: https://www.gislounge.com/a-brief-introduction-to-photogrammetry-and-remote-sensing/.

[25] Jobsite Editorial Staff. *Reality Capture: Using Photogrammetry in Construction [Online]*. [Accessed: 17/04/2023]. Available at: https://www.procore.com/jobsite/reality-capture-using-photogrammetry-in-construction/.

[28] Koeva, M. *Photogrammetry: Recent Developments and the Way Forward [Online]*. In: GIM International. [Accessed: 17/04/2023]. Available: https://www.gim-international.com/content/article/photogrammetry-recent-developments-and-the-way-forward.

[31] LEADR-MSU. *Photogrammetry - Data Collection Tutorial [Online]*. [Accessed: 25/02/2023]. Available at: https://leadr-msu.github.io/photogrammetry-data-collection/.

[33] Luhmann, T. *Recent Developments in Close-Range Photogrammetry [Online]*. In: GIM International. [Accessed: 17/04/2023]. Available: https://www.gim-international.com/content/article/recent-developments-in-close-range-photogrammetry.

[36] MaxCloudOn. *The best photogrammetry software - 2019 [Online]*. [Accessed 15 December 2022]. Available at: https://photogrammetry.maxcloudon.com/the-best-photogrammetry-processing-software-2019/.

[37] MDPI. *BIM and HBIM: Principles, Applications, and Standardization/Interoperability Issues [Online]*. [Accessed: 07/05/2023]. Available from: https://www.mdpi.com/journal/applsci/special_issues/BIM_HBIM.

[38] MDPI. *Heritage Building Information Modeling (BIM) [Online]*. [Accessed: 07/05/2023]. Available from: https://www.mdpi.com/journal/heritage/special_issues/heritage_BIM.

[45] Pijaudier-Cabot, Gilles and Mazars, Jacky. *Damage models for concrete*. 2001.

[46] Planning Tank. *Applications, Advantages, Disadvantages of Photogrammetry [Online]*. [Accessed: 07/05/2023]. Available from: https://planningtank.com/geographic-information-system/applications-advantages-disadvantages-of-photogrammetry.

[48] ResearchGate. *What are the limitations of photogrammetry? [Online]*. [Accessed: 07/05/2023]. Available from: https://www.researchgate.net/post/What-are-the-limitations-of-photogrammetry.

[50] Satpalda Geospatial Services. *Concepts of Photogrammetry [Online]*. [Accessed: 25/04/2023]. Available at: https://www.satpalda.com/blogs/concepts-of-photogrammetry.

[51] Sebago Technics. *What is Photogrammetry? [Online]*. [Accessed: 24 April 2023]. Available at: https://www.sebagotechnics.com/blog/what-is-photogrammetry/.

[53] SideFX. *Houdini Documentation [Online]*. [Accessed: 03/03/2023]. Available at: https://www.sidefx.com/docs/.

[56] UNESCO. *Tipasa [Online]*. Accessed: 2023-06-03. Available at: https://whc.unesco.org/en/list/193/maps/.

[57] University of British Columbia (UBC). *History of Photogrammetry [Online]*. [Accessed: 16/04/2023]. Available at: https://ibis.geog.ubc.ca/courses/geob373/lectures/Handouts/History_of_Photogrammetry.pdf.

[59] Vedantu. *Photogrammetry [Online]*. [Accessed: 25/04/2023]. Available at: https://www.vedantu.com/geography/photogrammetry.

[60] XYHT. *Close Range Terrestrial Photogrammetry [Online]*. [Accessed: 25/04/2023]. Available at: https://www.xyht.com/tag/close-range-terrestrial-photogrammetry/.

Appendices

Appendix A

Interaction Python-COMSOL Multiphysics software and optimization using a genetic algorithm.

Importing necessary libraries

```
import mph
import pygad
import numpy as np
```

COMSOL Multiphysics integration

```
path = r'C:\Users\user\Desktop\Higoun_Amamra\API & Optimization\model.mph'
study_name = 'Study 1'

client = mph.start()
model = client.load(path)
def run_analysis():
    model.solve(study_name)

simulation_frequencies = model.evaluate('freq')
```

Define objective function

```
experimental_frequencies = [3.334, 5.387, 8.148, 10.104] # Arches's frequencies
weights = [0.6, 0.2, 0.1, 0.1]  #

def compute_objective(X):
    diff = (simulation_frequencies - experimental_frequencies) / experimental_frequencies
    objective_value = np.sum(np.abs(diff) * weights)
    return objective_value
```

Genetic Algorithm parameter

```
num_generations = 6
num_parents_mating = 4
sol_per_pop = 6
num_genes = 2
parent_selection_type = "sss"
keep_parents = 1
crossover_type = "single_point"
mutation_type = "random"
mutation_percent_genes = 40

# Fitness Function
def fitness_func(ga_instance, solution, solution_idx):
    output = compute_objective(solution)
    fitness = 1 / output
    return fitness

# Create Population
youngs_modulus = np.random.uniform(1, 2.5, size=(sol_per_pop,))
density = np.random.uniform(1500, 2400, size=(sol_per_pop,))
initial_population = np.c_[youngs_modulus, density]
```

Genetic Algorithm Configuration and Running

```
ga_instance = pygad.GA(num_generations=num_generations,
                       num_parents_mating=num_parents_mating,
                       fitness_func=fitness_func,
                       sol_per_pop=sol_per_pop,
                       num_genes=num_genes,
                       parent_selection_type=parent_selection_type,
                       keep_parents=keep_parents,
                       crossover_type=crossover_type,
                       mutation_type=mutation_type,
                       mutation_percent_genes=mutation_percent_genes,
                       initial_population=initial_population)

# Running the Genetic Algorithm
ga_instance.run()
```

Retrieving the Best Solution

```
solution, solution_fitness, solution_idx = ga_instance.best_solution()
print("Parameters of the best solution:", solution)
print("Fitness value of the best solution:", solution_fitness)
```